doi.org/10.26434/chemrxiv.8204159.v2

Ab Initio Prediction of Metal-Organic Framework Structures

James P. Darby, Mihails Arhangelskis, Athanassios D. Katsenis, Joseph Marrett, Tomislav Friscic, Andrew J. Morris

Submitted date: 10/06/2019 • Posted date: 10/06/2019

Citation information: Darby, James P.; Arhangelskis, Mihails; Katsenis, Athanassios D.; Marrett, Joseph; Friscic, Tomislav; Morris, Andrew J. (2019): Ab Initio Prediction of Metal-Organic Framework Structures. ChemRxiv. Preprint.

Metal-organic frameworks (MOFs) have emerged as highly versatile materials with applications in gas storage and separation, solar light energy harvesting and photocatalysis. The design of new MOFs, however, has been hampered by the lack of computational methods for ab initio crystal structure prediction, which could be used to direct experimental synthesis. Here we report the first ab intio method for MOF structure prediction, and test it against a diverse set of MOFs, with differences in topology, metal coordination geometry and ligand binding sites. In all cases our calculations produced structures which match experiment, proving the versatility of our procedure for MOF structure prediction. With our new methodology for ab initio structure prediction, current approaches to MOF design are set to change towards a more sustainable theory-driven materials development.

File list (2)

Supplementary Information

AB INITIO PREDICTION OF METAL-ORGANIC FRAMEWORK STRUCTURES

James P. Darby,[1†] Mihails Arhangelskis,[2†] Athanassios D. Katsenis,[2] Joseph M. Marrett,[2] Tomislav Friščić,[2] and Andrew J. Morris[3]*

[1]TCM Group, Cavendish Laboratory, 19 JJ Thomson Avenue, Cambridge, CB3 0HE, UK.
[2]Department of Chemistry, McGill University, 801 Sherbrooke Street W., Montreal H3A 0B8, Canada.
[3]School of Metallurgy and Materials, University of Birmingham, Edgbaston, Birmingham B15 2TT, UK.

[†]These authors contributed equally to this work

Corresponding author:

*Dr. Andrew J. Morris, E-mail: a.j.morris@bham.ac.uk

Table of contents

1. Computational methods 3
1.1. Theoretical description of WAM method 3
1.2. Structure generation with WAM method 5
1.3. Periodic DFT geometry optimization of generated structures 5
1.4. Analysis and clustering of optimized crystal structures 6
1.5. Water coordination to open metal sites in Zn_2(DHTA) structures 6
1.6. Topology analysis 7
2. Experimental synthesis and characterization 8
2.1. Synthesis of $Zn(trz)_2$ frameworks 8
2.2. Powder X-ray diffraction (PXRD) measurements 8
2.3. Crystal structure determination and Rietveld refinement 9
2.4. Thermal analysis 11
2.5. Solid-state infrared spectroscopy 12
3. Predicted MOF energy landscapes 13
3.1. Crystal structure prediction of $Zn(pyr)_2SiF_6$ framework 13
3.2. Crystal structure prediction of $Zn(trz)_2$ framework 15
3.3. Crystal structure prediction of $Zn(ttz)_2$ framework 19
3.4. Crystal structure prediction of Zn_2DHTA framework 25
4. References 54

1. Computational methods

1.1. Theoretical description of WAM method

In the main text we discussed the idea of placing molecules onto Wyckoff sites and the advantages of doing so. Here we outline our approach.

We start by using the symmetry analyser tool from the Pymatgen[1,2] package to detect the point group **M** of the molecule. Next we find the site symmetry group **S**. This is a subgroup of the full space group which consists of all operators which map the site onto itself. We obtained the space group operators and Wyckoff site coordinates from the Bilbao crystallographic server.[3–5] Many sites have variable coordinates e.g. the y in the site (0,y, 0.5). When determining **S** we replace variables with irrational numbers to allow for easy numerical manipulations.

Having found **M** and **S** we determine how many symmetry distinct ways there are of orienting the molecule on the site, such that the symmetry is preserved. We treat orientations as symmetry distinct if it is not possible to move smoothly between them without disrupting the site symmetry.

For clarity the rest of the approach is described stepwise.

For all $\mathbf{s} \in \mathbf{S}$:

1. Decompose **s** into a rotation and inversion component, $\mathbf{s} = \mathbf{R}\ (-\mathbb{1})^{\mathbf{n}}$ where n=0 for pure rotations and 1 for roto-inversions.
2. Assign all operators with a Hermann-Maguin symbol. We use -n (instead of $\bar{n}$) to represent an n-fold roto-inversion so that symbols can be assigned as **sign(det(m))·order(R)**. These symbols reflect the geometric action of the operator and are independent of orientation.
3. Find the eigenvector of **R**. All rotation matrices, bar the identity, have one unique eigenvector which describes the symmetry axis of the molecule. If **R** is the identity it has no preferred orientation so we do not assign it an eigenvector.

Repeat for all $\mathbf{m} \in \mathbf{M}$ then verify that **M** has at least as many operators of each type as **S** e.g. if **S** contains seven 2 fold rotation operators then **M** must have seven or more. Next form the set **E** of all unique site eigenvectors; eigenvectors $\vec{\boldsymbol{\lambda}}_\mathbf{i}$ and $\vec{\boldsymbol{\lambda}}_\mathbf{j}$ are equivalent if $\left|\vec{\boldsymbol{\lambda}}_\mathbf{i} \times \vec{\boldsymbol{\lambda}}_\mathbf{j}\right| = 0$. The set **E** will then contain either 0, 1 or 2+ eigenvectors and we treat these cases separately.

Case 1: $|\mathbf{E}| = \mathbf{0}$

If there are no unique directions in **E** then the site is either P1 or $P\bar{1}$. As there are no unique directions any orientation of the molecule on the site will do. We count this as 1 symmetry distinct orientation with 3 rotational degrees of freedom.

Case 2: $|\mathbf{E}| \geq \mathbf{2}$

Aligning two of the molecules eigenvectors with two eigenvectors in **E** is sufficient to rigidly fix the molecule. We denote the two chosen site eigenvectors as $\vec{\boldsymbol{\lambda}}_\mathbf{a}$ and $\vec{\boldsymbol{\lambda}}_\mathbf{b}$ where **a** and **b** are the symbols of the corresponding operators. We then loop over all combinations of molecule eigenvectors with the same symbols which we denote as $\vec{\boldsymbol{\mu}}_\mathbf{a}$ and $\vec{\boldsymbol{\mu}}_\mathbf{b}$**.** For a given $\vec{\boldsymbol{\mu}}_\mathbf{a}$ and $\vec{\boldsymbol{\mu}}_\mathbf{b}$ we attempt four alignments, $\left(\pm\vec{\boldsymbol{\mu}}_\mathbf{a} : \vec{\boldsymbol{\lambda}}_\mathbf{a}\right), \left(\pm\vec{\boldsymbol{\mu}}_\mathbf{b} : \vec{\boldsymbol{\lambda}}_\mathbf{b}\right)$. Many alignments are not possible as the angle

between the pairs must be the same. The alignments that are possible define a unique rotation matrix **P**, so that **P** acting on the molecules original orientation recovers the aligned orientation. For each alignment we then check if all site operators are matched by a corresponding molecule operator. At this stage we have a complete list of allowed **P** matrices, many of which will correspond to symmetry equivalent orientations. Two orientations $\mathbf{P_i}$ and $\mathbf{P_j}$ are equivalent if there is an $\mathbf{m} \in \mathbf{M}$ such that $\mathbf{P_i m P_i^{-1} = P_j}$ which can be re-written as $\mathbf{P_i^{-1} P_j P_i} \in \mathbf{M}$. After reducing the list in this way we arrive at our desired result. Note that because the molecule is rigidly fixed all of these orientations have no rotational degrees of freedom.

Case 3: $|\mathbf{E}| = \mathbf{1}$

As the site only has 1 unique symmetry axis aligning the molecule with this axis will not fix it rigidly. Instead each orientation option will have a rotational degree of freedom, rotation about the sites symmetry axis. Consequently there is not a unique rotation matrix associated with each option and a different approach is needed.

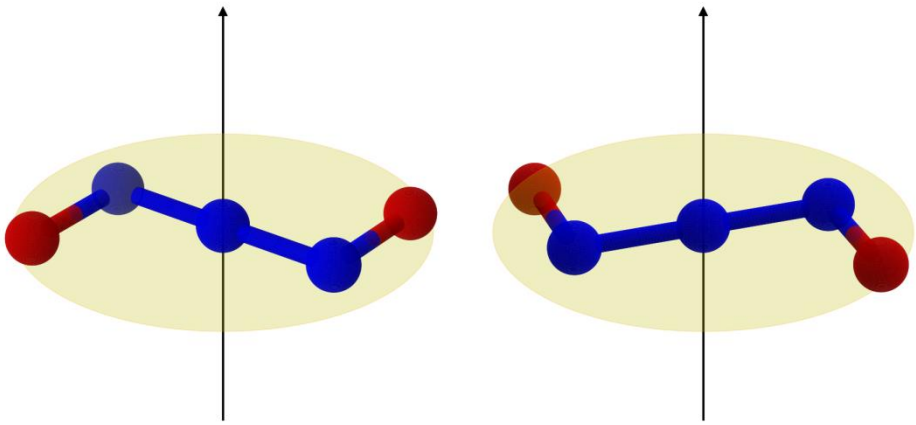

Figure S1. Two distinct orientations of a hypothetical molecule with point group 2/m on a site with point group 2/m. The two-fold rotation axis is shown as the black arrow whilst the mirror plane is shown in yellow.

Consider a site eigenvector $\vec{\boldsymbol{\lambda}}_\mathbf{a}$ and all molecule operators of the same type. Take the eigenvectors $\vec{\boldsymbol{\mu}}_\mathbf{a}$ of these molecule operators and form the set **F** containing $\pm\vec{\boldsymbol{\mu}}_\mathbf{a}$ for each operator, Figure S1 illustrates why both directions are required. Next find the subgroup $\mathbf{M_R} = \{\mathbf{m} \in \mathbf{M} \mid \mathbf{m} \in \mathbf{R^3}\}$ which contains only the rotations from **M**. For two eigenvectors $\vec{\boldsymbol{\mu}}_\mathbf{a}^\mathbf{i}$ and $\vec{\boldsymbol{\mu}}_\mathbf{a}^\mathbf{j}$ within **F** they are symmetry equivalent directions if $\mathbf{m_r}\vec{\boldsymbol{\mu}}_\mathbf{a}^\mathbf{i} = \vec{\boldsymbol{\mu}}_\mathbf{a}^\mathbf{j}$ for some $\mathbf{m_r} \in \mathbf{M_R}$. Next reduce **F** so that it contains no symmetry equivalent duplicates and align each eigenvector in **F** with $\vec{\boldsymbol{\lambda}}_\mathbf{a}$. Finally, for each alignment check that the other site symmetry operators are preserved and discard the alignments which break the site symmetry.

In addition to being simple to implement the method outlined above has proven to be robust and well suited for use in high throughput structure generation. In practice we do not go through this entire procedure for every alignment. We do it once per site and store the eigenvector

alignments for future use. When generating structures we randomise over both the orientation options and any rotational degrees of freedom they may have.

1.2. Structure generation with WAM method

The geometries of the organic linkers were specified with the highest possible point group symmetry. Geometric restraints in terms of minimum interatomic distances were utilized to prevent overlap of molecular fragments in the generated structures.

The structure generation was performed for 1, 2, 3 and 4 formula units per primitive unit cell (numbers vary for different MOF types), with gradually increasing number of trial structures for each additional formula unit. The details of WAM calculations are summarized in Table S1.

Table S1. Summary of search parameters used in WAM calculations.

Structure	Composition of formula unit	Point group symmetry of the linker(s)	Number of generated structures			
			1 formula unit per primitive cell	2 formula units per primitive cell	3 formula units per primitive cell	4 formula units per primitive cell
Zn(**pyr**)$_2$**SiF$_6$**	1 x Zn 2 x **pyr** 1 x SiF_6	**pyr** - D_{2h} **SiF$_6$** - O_h	2000	-	-	-
Zn(**trz**)$_2$	1 x Zn 2 x **trz**	**trz** - C_{2v}	1978	6267	6544	5093
Zn(**ttz**)$_2$	1 x Zn 2 x **ttz**	**ttz** - C_{2v}	2000	2000	3000	4000
Zn$_2$**DHTA**	2 x Zn 1 x **DHTA**	**DHTA** - C_{2h}	2000	4000	6000	-

1.3. Periodic DFT geometry optimization of generated structures

Crystal structures generated in WAM, were geometry-optimized using plane-wave DFT code CASTEP 19.1.[6] Initial calculations were performed using LDA functional (Zn(**pyr**)$_2$**SiF$_6$**, Zn(**trz**)$_2$ and Zn(**ttz**)$_2$) or PBE[7] functional combined with Grimme D2[8] dispersion correction (Zn$_2$**DHTA**). The plane-wave cut-off was set to 400 eV and the ultrasoft pseudopotentials from CASTEP internal QC5 library were used. The Brillouin zone was sampled with a 0.07 $Å^{-1}$ Monkhorst-Pack k-point grid. The following convergence criteria were applied for geometry optimization: maximum energy change $2x10^{-5}$ eV/atom, maximum force on atom 0.05 eV/Å, maximum atom displacement 0.001 Å and residual stress 0.1 GPa.

The optimized structures were ranked by energy. The set of structures falling within a certain energy window above the global minimum (50 kJ mol^{-1} per formula unit for Zn(**pyr**)$_2$**SiF$_6$**, Zn(**trz**)$_2$ and Zn(**ttz**)$_2$; 200 kJ mol^{-1} for Zn$_2$**DHTA**) were selected for further analysis. First duplicate

structures were removed (see section 1.4 for details), then the remaining structures were once again geometry-optimized using a more reliable energy model and more stringent convergence criteria. This time we used PBE functional combined with many body dispersion (MBD*) correction scheme. Convergence testing with respect to plane wave cutoff and k-point sampling was performed for each MOF system, and the following parameters were established:

Zn(**pyr**)$_2$**SiF$_6$**: 650 eV plane wave cutoff and 0.1 Å^{-1} k-point grid

Zn(**trz**)$_2$: 700 eV plane wave cutoff and 0.08 Å^{-1} k-point grid

Zn(**ttz**)$_2$: 700 eV plane wave cutoff and 0.08 Å^{-1} k-point grid

Zn$_2$**DHTA**: 800 eV plane wave cutoff and 0.09 Å^{-1} k-point grid

1.4. Analysis and clustering of optimized crystal structures

Presence of duplicates within the set of predicted structures is a major indication that the structure search had converged. In the case when the majority of structures had only been found once, it is likely that continuing the search will reveal additional structures.

While having duplicate structures during the search process is desirable, it is necessary to remove the redundant data at the end of the calculation. In order to remove the duplicate structures, we have used the COMPACK[9] as implemented in the CCDC Mercury software and Python API. Since the COMPACK algorithm is geared towards comparison of molecular rather than polymeric crystal structures, the connectivity between metal atoms and organic linkers in our predicted MOF structures had to be broken. This was achieved by changing the **Zn** atom type to **He** in all structures, while preserving all atom positions. Structures were deemed identical when an overlay of 15 fragments had been found with default convergence criteria (20% distance tolerance, 20º angle tolerance).

Finally, packing coefficient and solvent-accessible void volume was calculated for all remaining structures using the program PLATON.[10] In addition, PLATON was used to convert from primitive unit cell representation used in CASTEP to the conventional crystallographic unit cell parameters.

1.5. Water coordination to open metal sites in Zn$_2$(DHTA) structures

Predicted structures of Zn$_2$**DHTA** were analysed for the presence of open coordination sites, that could potentially interact with solvent molecules. First, structures were examined for the presence of solvent-accessible voids. For this purpose, we used a probe of 0.9 Å radius, smaller than the conventionally used 1.2 Å probe. The rationale for using a small probe is that structures undergo reorganisation upon insertion of water molecules. Thus, anhydrous structures, which lack sufficient void space to accommodate a standard probe, may expand once the water molecules is inserted, and the structure is allowed to optimise.

Among those structures, 19 structures containing unsaturated metal coordination polyhedra were selected. Water molecules were than manually added to produce a structure with saturated coordination environment. For example, for the structure with 5-coordnate square-pyramidal metal atom, one water molecule was added to yield octahedral coordination. When inserting the water molecules, steric limitations were taken into account, avoiding unrealistically short interatomic contacts.

The resulting hydrated structures were geometry-optimized in CASTEP using PBE+MBD* energy model and the same calculation parameters used for optimizing anhydrous structures (see section 1.4). The packing coefficient and solvent-accessible void volume for the hydrated structures was then calculated in PLATON.

In order to compare the energies of the hydrated structures to their corresponding anhydrous analogues, we had to account for the differences in atomic composition. In order to do that, we had to subtract the energy of an isolated gas phase water molecule from the total electronic energy of the hydrated structures. The resulting energy would define the stability of the hydrated structure in the atmosphere of water vapor. Since, in practice, we are interested in the interaction with liquid water we have further corrected the energies with the experimental value of water enthalpy of vaporization ($\Delta H_{vap,\,exp}$=40.65 kJ mol^{-1}):

$$E_{corrected} = E(Zn_2DHTA \cdot nH_2O) - nE\left(H_2O_{(g)}\right) + n\Delta H_{vap,exp}$$

The corrected energies were used to place the hydrated structures in the energy plots alongside the anhydrous structures of Zn_2**DHTA**.

1.6. Topology analysis

ToposPro[11] was used to obtain network topologies of all the reported structures. For the automatic classification of the structures, the "standard representation" of the program ToposPro was used. This method takes each individual organic ligand and each individual metal ion as a separate node. In cases of new topologies, the total point symbol for the whole net is reported. For subnets and subnets transformations we use the notation as described in ToposPro manual.[12]

2. Experimental synthesis and characterization

2.1. Synthesis of Zn(trz)$_2$ frameworks

Synthesis of the target Zn(**trz**)$_2$ framework was performed mechanochemically, by placing 1 mmol of zinc oxide (Sigma-Aldrich) and 2.3 mmol of 1,2,4-triazole (Sigma-Aldrich, 15% excess) into a stainless steel milling jar of 15 mL internal volume, along with two 1.3 g stainless steel ball bearings as milling media. The reaction mixture was milled for 60 minutes at a frequency of 30 Hz, affording a phase-pure sample of *int-dia*-Zn(**trz**)$_2$. The product was then suspended in 20 ml of 95% ethanol and stirred for 24 hours. The product was collected by centrifugation and dried under vacuum at 80 ˚C for 24 hours to remove any remaining solvent.

The *int-dia* Zn(**trz**)$_2$ framework was also observed over a wide range of liquid-assisted grinding (LAG)[13] and ion- and liquid-assisted grinding (ILAG)[14] milling conditions, some of them illustrated in Figure **S2** below. Note that all patterns shown include features which correspond to the Bragg reflections for the *int-dia* framework, without or without crystalline impurities of 1,2,4-triazole and zinc oxide starting materials.

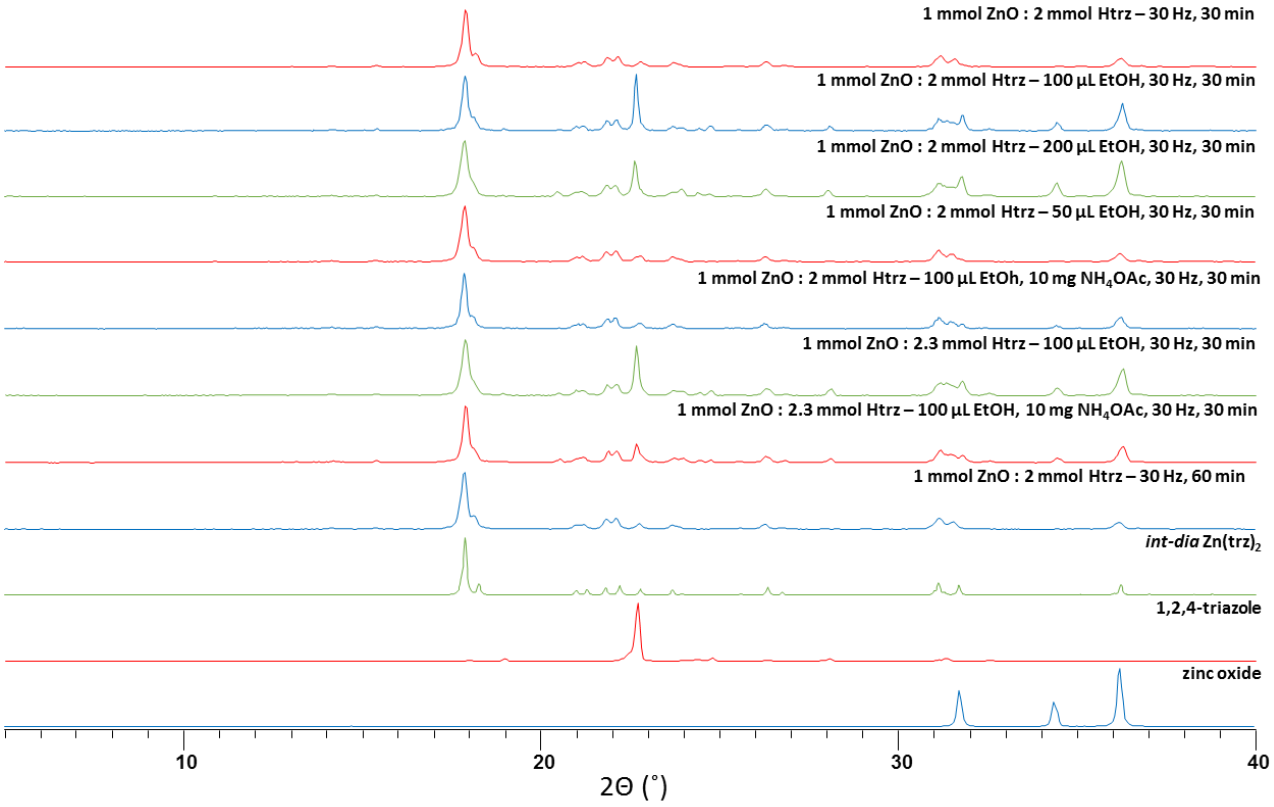

Figure **S2**: Comparison of selected powder X-ray diffractograms for mechanochemical screening of reactions of zinc oxide and 1,2,4-triazole.

2.2. Powder X-ray diffraction (PXRD) measurements

Powder X-ray diffraction data was collected on a Bruker D2 PHASER benchtop powder x-ray diffractometer using Ni-filtered CuKα radiation and equipped with a LynxEye linear position-sensitive detector. Data for structure solution was collected on the washed and dried sample with

a step size of 0.01 degrees 2 (theta) and a collection time of 5 second per step from 3 to 70 degrees 2 (theta). Data for reaction screening was collected from 4 to 40 degrees 2 (theta) with a step size of 0.05 degrees 2 (theta) and a collection time per step of 0.5 seconds.

2.3. Crystal structure determination and Rietveld refinement

The crystal structure of the *int-dia* polymorph of Zn(**trz**)$_2$ framework was solved from powder X-ray diffraction (PXRD) data. The unit cell was determined using the N-TREOR[15] algorithm, with peak selection performed via the interface of EXPO2014.[16] The indexing procedure located an orthorhombic cell, similar to that of the reported *int-dia* structure of Zn(**ttz**)$_2$ (CSD WAQRAI).[17] Diffraction peak intensities, extracted via Le Bail method,[18] were used for space group determination. The space group search resulted in a *Pbca* space group as the most probable option, also matching the space group of WAQRAI structure.

Simulated annealing structure solution was performed in EXPO2014, with one Zn atom and two **ttz** fragments in the crystallographic asymmetric unit. During the structure solution process all three fragments were given independent translational degrees of freedom, while rotations were allowed for the two **ttz** fragments. The structure solution procedure was repeated 10 times, and the structure with the lowest R_{wp} value was selected for Rietveld refinement.

Rietveld refinement was performed in the program TOPAS Academic 6. Position of the Zn atom was refined independently, while the **ttz** linkers were modelled as rigid body fragments with refineable translational and rotational degrees of freedom. In addition, soft bond length restraints were placed on the Zn-N bonds. The diffraction peak shape was modelled with a pseudo-Voigt function, while the background was described by a 10th order polynomial function. Atomic vibrational motion was modelled isotropically, with C, H and N atoms assigned one Debye-Waller factor (DWF), while a separate DWF was assigned to the Zn atom.

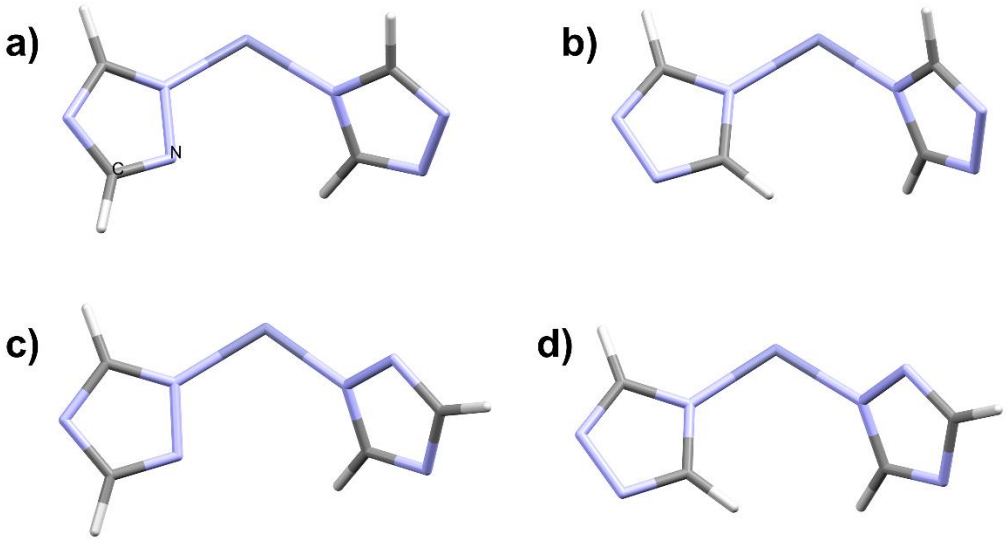

Figure **S3**. The four possible orientation of **ttz** linkers in Zn(**ttz**)$_2$ structure. The lowest energy arrangement is shown in (d), this arrangement was used for Rietveld refinement.

Final ambiguity that had to be resolved, regarding the structure solution from powder data, concerned the orientation of **ttz** linkers in the structures. Since the nitrogen at 2-position and the C-H group at 3-position of the **ttz** ring both have 7 electrons, the two moieties are essentially indistinguishable by Rietveld refinement. Since there are two **ttz** linkers in the asymmetric unit, this gives rise to four crystallographically distinct arrangements (Figure S3). In order to determine the most likely atomic arrangement, we have optimized all four structures using periodic DFT calculations (PBE+MBD*, for details see section 1.3). The lowest energy arrangement was then used for Rietveld refinement (Figure S4). The refinement parameters are summarized in Table S2.

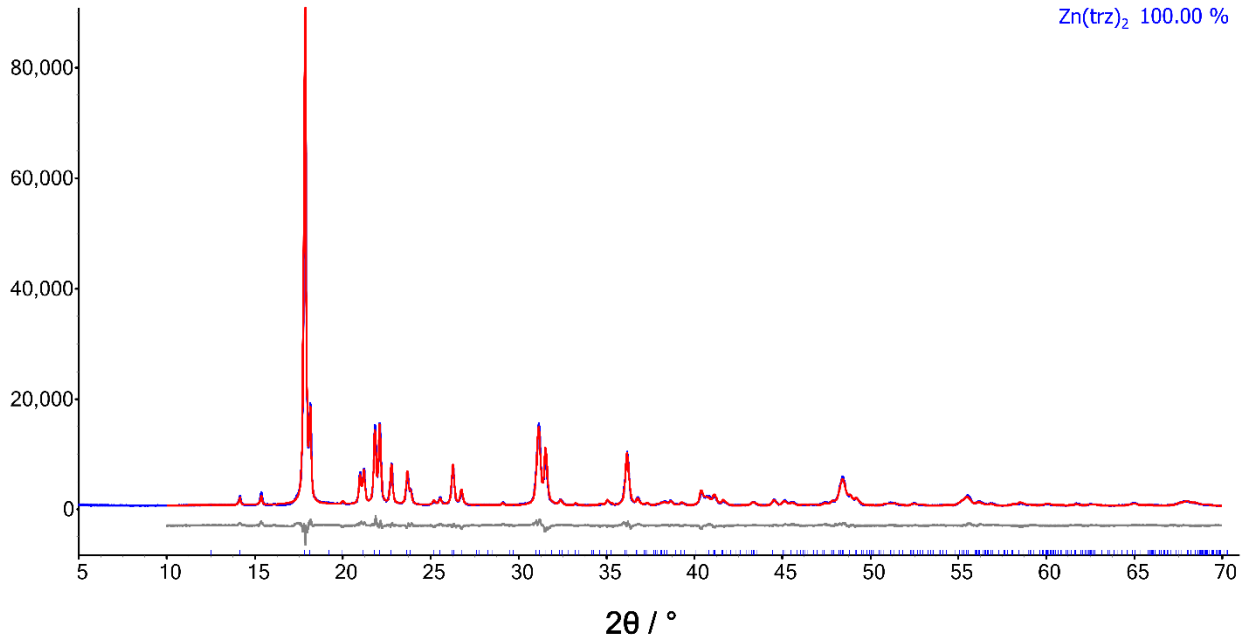

Figure **S4**. Rietveld refinement of Zn(**ttz**)$_2$ *int-dia* structure. The calculated profile is shown in red, the experimental profile is shown in blue, and the difference curve is shown in grey.

Table **S2**. Summary of crystallographic and Rietveld refinement parameters.

Material	*int-dia* Zn(**trz**)$_2$
chemical formula	$Zn(C_2H_2N_3)_2$
M_r / g mol^{-1}	201.50
Crystal system	orthorhombic
a / Å	9.9588(3)
b / Å	9.7770(3)
c / Å	14.1456(4)
α / °	90
β / °	90
γ / °	90

V / Å^3	1377.33(7)
Space group	*P b c a*
Density / g cm^{-3}	1.9437(1)
Radiation type	Cu Kα
F(000)	800
R_{wp}	0.067
R_p	0.051
R_{Bragg}	0.032
χ^2	2.807
CCDC number	1911841

2.4. Thermal analysis

Thermogravimetric analysis (TGA) and differential scanning calorimetry (DSC) were measured simultaneously using a TGA/DSC 1 instrument (Mettler-Toledo) on approximately 10 mg of the washed and dried sample. The sample was heated from 25 to 900 ºC at a rate of 10 ºC min^{-1} under a 60 mL min^{-1} stream of air.

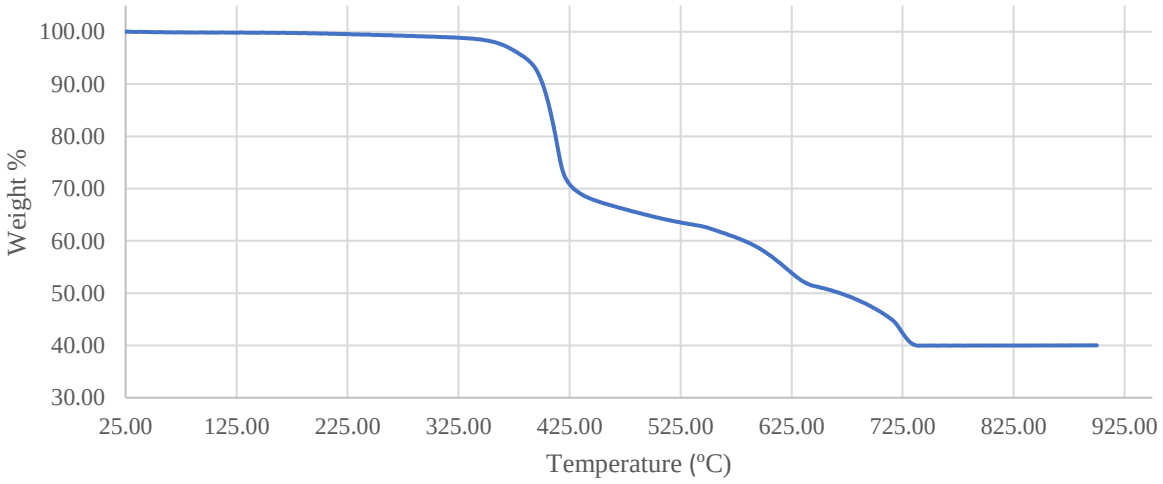

Figure **S5.** A TGA thermogram for *int-dia*-Zn(**trz**)$_2$, recorded in a dynamic air atmosphere. Experimental residue: **40.0%**; Calculated residue for ZnO: **40.4%.**

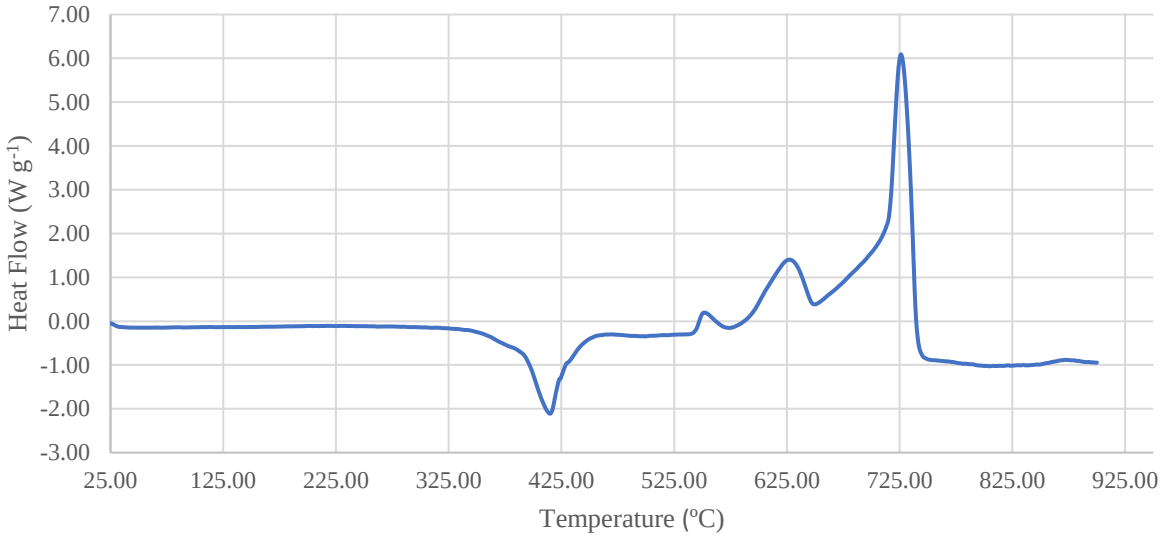

Figure **S6.** A DSC thermogram for *int-dia*-Zn(**trz**)$_2$ recorded in a dynamic atmosphere of air.

2.5. Solid-state infrared spectroscopy

Fourier-transform infrared attenuated total reflectance (FTIR-ATR) spectra were collected using a Bruker Vertex 70 FTIR spectrometer fitted with the Platinum ATR unit.

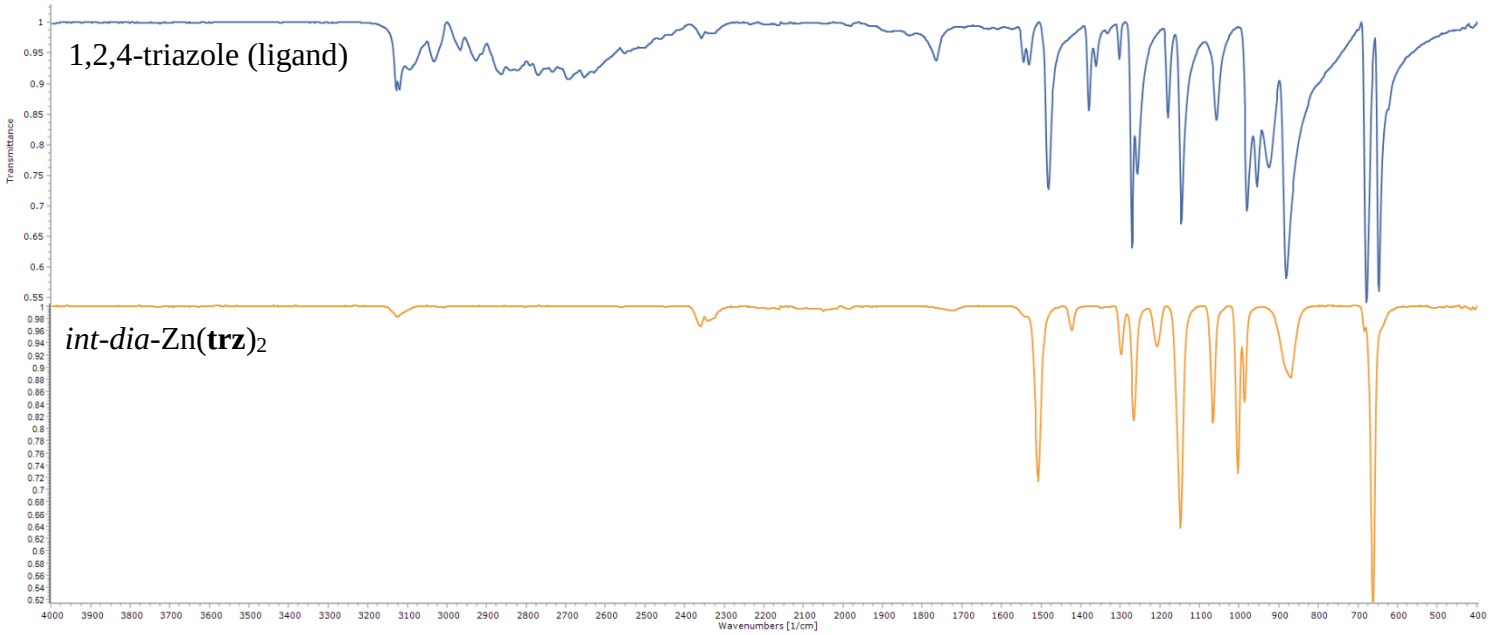

Figure **S7.** Overlay of the FTIR-ATR spectra for the 1,2,4-triazole ligand and the purified *int-dia*-Zn(**trz**)$_2$.

3. Predicted MOF energy landscapes

3.1. Crystal structure prediction of $Zn(pyr)_2SiF_6$ framework

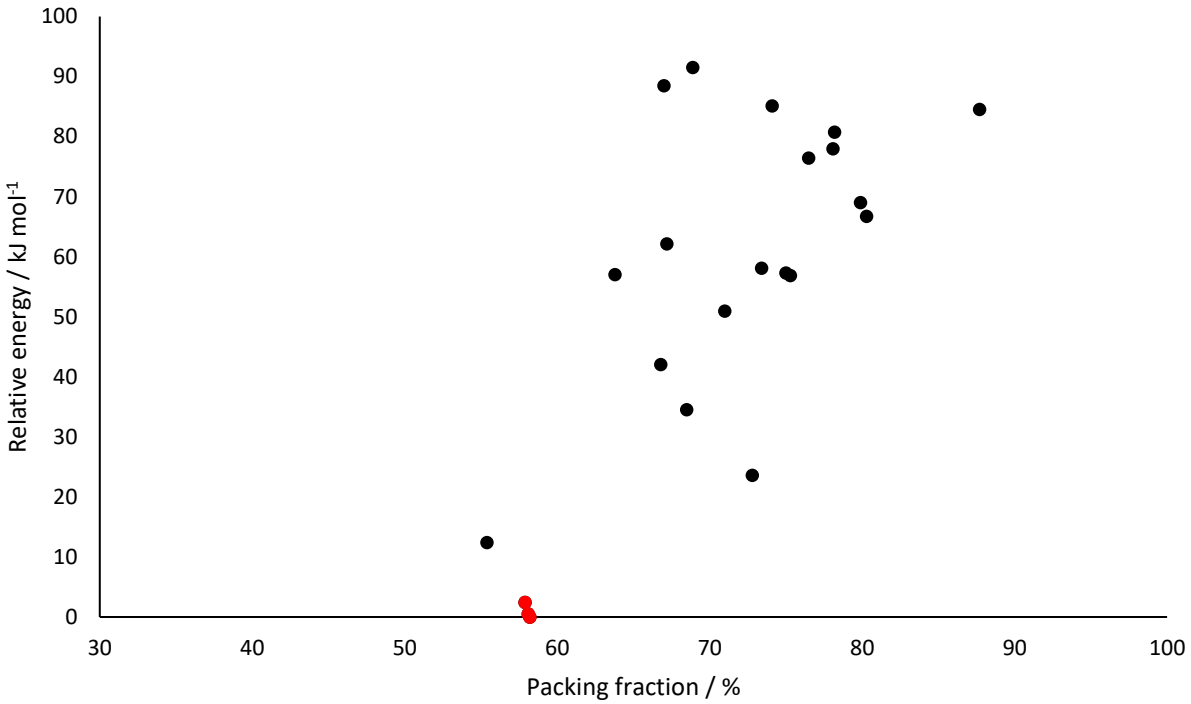

Figure **S8.** Relative energies of predicted Zn(**pyr**)$_2$**SiF$_6$** plotted against packing fraction. The experimentally observed structure matches the structures shown with red dots (disordered and ordered configuration).

Table **S3.** Calculated parameters for the predicted structures of Zn(**pyr**)$_2$**SiF$_6$** after geometry optimization with PBE+MBD* method.

Structure name	Density / g cm^{-3}	Packing coefficient / %	Energy per f. u. / eV	Relative energy / kJ mol^{-1}	Topology
SiF6_2_P-1_VEaLoEMd	1.570	58.2	-8434.48	0.000	pcu; 6/4/c1; sqc1
SiF6_12_C2_m_z5l30oMk	1.568	58.1	-8434.48	0.506	pcu; 6/4/c1; sqc1
SiF6_123_P4_mmm_G7PkBocG	1.556	57.9	-8434.46	2.402	pcu; 6/4/c1; sqc1
SiF6_123_P4_mmm_iCVEA3Rx	1.509	55.4	-8434.35	12.417	pcu; 6/4/c1; sqc1
SiF6_2_P-1_Sr3WuGec	1.947	72.8	-8434.24	23.573	sql
SiF6_107_I4mm_mei29khC	1.802	68.5	-8434.12	34.499	sql
SiF6_121_I-42m_UuBsXhdU	1.798	66.8	-8434.05	42.040	sql
SiF6_2_P-1_H1ATQfXV	1.869	71	-8433.95	50.961	1D
SiF6_2_P-1_Dk25U952	1.982	75.3	-8433.89	56.880	sql
SiF6_107_I4mm_9jxG6AIk	1.692	63.8	-8433.89	57.022	sql

Structure name	Density / g cm^{-3}	Packing coefficient / %	Energy per f. u. / eV	Relative energy / kJ mol^{-1}	Topology
SiF6_2_P-1_sj1bJsMy	1.974	75	-8433.89	57.282	sql
SiF6_2_P-1_3BSfPu5P	1.936	73.4	-8433.88	58.090	1D
SiF6_5_C2_z2fPTo8P	1.767	67.2	-8433.84	62.111	sql
SiF6_12_C2_m_sqyauBWJ	2.175	80.3	-8433.79	66.726	sql
SiF6_23_I222_BDZIKCHH	2.139	79.9	-8433.77	69.008	sql
SiF6_65_Cmmm_AcBNsSBi	2.072	76.5	-8433.69	76.411	sql
SiF6_12_C2_m_70xnL3aV	2.090	78.1	-8433.67	77.966	sql
SiF6_12_C2_m_Ag8xy9vC	2.094	78.2	-8433.65	80.743	sql
SiF6_82_I-4_AS4YM4oZ	2.316	87.7	-8433.61	84.531	sql
SiF6_12_C2_m_CfisGJd4	2.012	74.1	-8433.60	85.091	sql
SiF6_10_P2_m_0cuNUyPt	1.761	67	-8433.56	88.496	sql
SiF6_38_Amm2_WhUMokgh	1.818	68.9	-8433.53	91.525	sql
SiF6_119_I-4m2_DvEzBLTQ	2.203	82.8	-8433.29	114.841	sql
SiF6_12_C2_m_9tfIaCKo	1.765	68.1	-8433.28	115.957	1D
SiF6_12_C2_m_6LbXPsOr	1.777	68.2	-8433.20	123.209	1D
SiF6_5_C2_Y2hxiJYk	1.810	69.9	-8433.17	126.149	sql
SiF6_12_C2_m_YcsIEtMU	2.158	80.3	-8432.74	167.974	1D
SiF6_47_Pmmm_S8M7rAwi	1.968	76.2	-8432.72	170.021	sql

3.2. Crystal structure prediction of Zn(trz)$_2$ framework

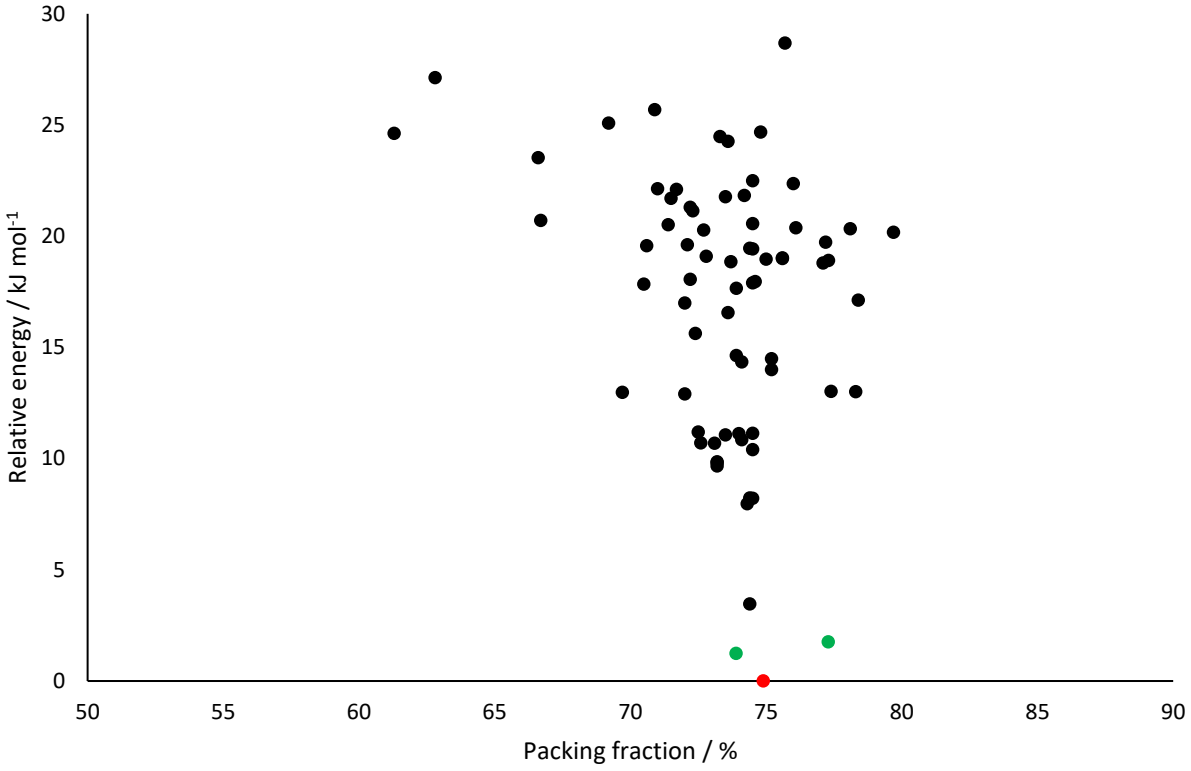

Figure **S9.** Relative energies of predicted Zn(**trz**)$_2$ plotted against packing fraction. Experimental structures (CSD JINRIK and LIHQUP) are marked green, lowest energy predicted structure is marked red. The calculated global minimum is 1.240 kJ mol^{-1} lower in energy than experimental structure JINRIK.

Table **S4.** Calculated parameters for the predicted and experimental (CSD JINRIK and LIHQUP) structures of Zn(**trz**)$_2$ after geometry optimization with PBE+MBD* method.

Structure name	Density / g cm^{-3}	Packing coefficient / %	Energy per f. u. / eV	Relative energy / kJ mol^{-1}	Topology
ZnTri2_70_Fddd_vTNfvZSw	1.941	74.9	-4142.80	0.000	dia; 4/6/c1; sqc6
JINRIK	1.971	73.9	-4142.78	1.241	tsa
LIHQUP	1.995	77.3	-4142.78	1.757	dia; 4/6/c1; sqc6
ZnTri2_110_I41cd_tIzMHYhm	1.928	74.4	-4142.76	3.466	dia; 4/6/c1; sqc6
ZnTri2_88_I41_a_qfRwDRKe	1.930	74.3	-4142.71	7.960	dia; 4/6/c1; sqc6
ZnTri2_110_I41cd_Et1n5UZr	1.925	74.5	-4142.71	8.204	dia; 4/6/c1; sqc6
ZnTri2_110_I41cd_e2O4ekUU	1.927	74.4	-4142.71	8.218	dia; 4/6/c1; sqc6
ZnTri2_122_I-42d_DnY6KdnE	1.895	73.2	-4142.70	9.670	dia; 4/6/c1; sqc6
ZnTri2_82_I-4_9jN3lqse	1.894	73.2	-4142.70	9.803	dia; 4/6/c1; sqc6
ZnTri2_9_Cc_cPAZe595	1.905	73.2	-4142.69	9.857	cds; 4/6/t4; sqc5

Structure name	Density / g cm^{-3}	Packing coefficient / %	Energy per f. u. / eV	Relative energy / kJ mol^{-1}	Topology
ZnTri2_77_P42_9b8Mg1g9	1.933	74.5	-4142.69	10.396	1D
ZnTri2_72_Ibam_4HuypDTd	1.893	73.1	-4142.69	10.691	1D
ZnTri2_46_Ima2_0shzhgjn	1.885	72.6	-4142.69	10.700	1D
ZnTri2_45_Iba2_ii9FX6hZ	1.925	74.1	-4142.68	10.842	1D
ZnTri2_60_Pbcn_KOWchzEn	1.914	73.5	-4142.68	11.067	1D
ZnTri2_50_Pban_2aDt6ZbQ	1.931	74	-4142.68	11.120	1D
ZnTri2_7_Pc_V2z5EN9d	1.925	74.5	-4142.68	11.135	dia; 4/6/c1; sqc6
ZnTri2_56_Pccn_JBxf2DwA	1.882	72.5	-4142.68	11.185	1D
ZnTri2_12_C2_m_h3zVkhK7	1.924	72.0	-4142.66	12.907	tsa
ZnTri2_14_P21_c_byIfSWZO	1.812	69.7	-4142.66	12.972	sql
ZnTri2_2_P-1_ufP8ynFb	2.035	78.3	-4142.66	13.011	1D
ZnTri2_2_P-1_dIu05Zd0	2.014	77.4	-4142.66	13.019	1D
ZnTri2_7_Pc_k8M8D66b	1.947	75.2	-4142.65	13.998	dia; 4/6/c1; sqc6
ZnTri2_14_P21_c_82mUBdZ0	1.922	74.1	-4142.65	14.350	sql
ZnTri2_7_Pc_o8aJqlkd	1.946	75.2	-4142.65	14.490	dia; 4/6/c1; sqc6
ZnTri2_7_Pc_JDEbts5U	1.917	73.9	-4142.65	14.634	sql
ZnTri2_9_Cc_G0vVNH8t	1.879	72.4	-4142.64	15.619	cds; 4/6/t4; sqc5
ZnTri2_4_P21_l2YA5PBA	1.906	73.6	-4142.63	16.561	sql
ZnTri2_88_I41_a_MpHbC1t9	1.863	72	-4142.62	16.993	dia; 4/6/c1; sqc6
ZnTri2_14_P21_c_woutrT2p	2.037	78.4	-4142.62	17.124	sql
ZnTri2_88_I41_a_ld3jo3Vl	1.905	73.9	-4142.61	17.650	dia; 4/6/c1; sqc6
ZnTri2_40_Ama2_SUdEo90c	1.842	70.5	-4142.61	17.847	1D
ZnTri2_12_C2_m_VtSmJzEk	1.984	74.5	-4142.61	17.900	{3.6.7}4{3^2.4.6^2.7}2{3^4.4^2.8^6.9^3}{6^4.8^8.11^3}
ZnTri2_34_Pnn2_KxZH8Lot	1.945	74.6	-4142.61	17.956	dia; 4/6/c1; sqc6
ZnTri2_2_P-1_gHUoZD7x	1.869	72.2	-4142.61	18.050	1D
ZnTri2_18_P21212_YyyYGxDU	1.999	77.1	-4142.60	18.790	sql
ZnTri2_4_P21_uUaVGtra	1.918	73.7	-4142.60	18.852	sql
ZnTri2_18_P21212_edQWWrw3	2.005	77.3	-4142.60	18.910	sql
ZnTri2_29_Pca21_eNK82w99	1.947	75	-4142.60	18.964	dia; 4/6/c1; sqc6
ZnTri2_4_P21_ZhE1f40d	1.968	75.6	-4142.60	18.993	sql
ZnTri2_2_P-1_XFmbevaz	1.965	75.6	-4142.60	19.017	1D

Structure name	Density / g cm^{-3}	Packing coefficient / %	Energy per f. u. / eV	Relative energy / kJ mol^{-1}	Topology
ZnTri2_4_P21_y4lZUk0R	1.895	72.8	-4142.60	19.092	sql
ZnTri2_4_P21_jIFdM2ci	1.932	74.5	-4142.60	19.420	sql
ZnTri2_4_P21_lRbdtpz8	1.926	74.4	-4142.60	19.449	sql
ZnTri2_88_I41_a_0vvqm97m	1.832	70.6	-4142.59	19.574	dia; 4/6/c1; sqc6
ZnTri2_32_Pba2_pqYdpAbi	1.871	72.1	-4142.59	19.613	dia; 4/6/c1; sqc6
ZnTri2_114_P-421c_navvc727	2.003	77.2	-4142.59	19.726	sql
ZnTri2_2_P-1_O0KyNkNT	2.079	79.7	-4142.59	20.172	sql
ZnTri2_41_Aba2_tg0pOcCE	1.885	72.7	-4142.59	20.279	sql
ZnTri2_14_P21_c_xlogpfzg	2.040	78.1	-4142.59	20.332	fes
ZnTri2_33_Pna21_zqSzFcAp	1.972	76.1	-4142.59	20.380	sql
ZnTri2_110_I41cd_t1gO87GF	1.858	71.4	-4142.58	20.513	dia; 4/6/c1; sqc6
ZnTri2_4_P21_72C6mRDc	1.935	74.5	-4142.58	20.568	sql
ZnTri2_33_Pna21_QfLyjW3W	1.734	66.7	-4142.58	20.706	sql
ZnTri2_2_P-1_pW2uu9Ce	1.881	72.3	-4142.58	21.139	1D
ZnTri2_9_Cc_82bFZjPn	1.869	72.2	-4142.58	21.296	sql
ZnTri2_12_C2_m_70KW8sJs	1.919	71.5	-4142.57	21.692	{4.5^2.6^2.7}2{4.5^2}4{4^2.5^4.8^6.9.10^2}{5^2.6^4.7^4.8^2.9^2.10}
ZnTri2_144_P31_XkaJzM0w	1.911	73.5	-4142.57	21.777	1D
ZnTri2_144_P31_0diA6Wvc	1.931	74.2	-4142.57	21.822	1D
ZnTri2_7_Pc_SUEwkJjA	1.866	71.7	-4142.57	22.105	sql
ZnTri2_15_C2_c_qoNrLPuI	1.839	71	-4142.57	22.135	sql
ZnTri2_41_Aba2_X2mk81R6	1.976	76	-4142.57	22.365	hcb
ZnTri2_15_C2_c_B8XtA8lN	1.926	74.5	-4142.56	22.486	sql
ZnTri2_4_P21_PpwWgPGt	1.728	66.6	-4142.55	23.522	sql
ZnTri2_92_P41212_up9qHblG	1.907	73.6	-4142.55	24.254	dia; 4/6/c1; sqc6
ZnTri2_12_C2_m_gIVfDBb1	1.973	73.3	-4142.54	24.476	{4.5^2.6^2.7}2{4.5^2}4{4^2.5^4.8^6.9.10^2}{5^2.6^4.7^4.8^2.9^2.10}
ZnTri2_14_P21_c_KKvgGRgC	1.599	61.3	-4142.54	24.623	sql
ZnTri2_29_Pca21_uFEtAjWb	1.957	74.8	-4142.54	24.681	sql
ZnTri2_180_P6222_6aMxXxfb	1.796	69.2	-4142.54	25.083	1D
ZnTri2_34_Pnn2_Fe80ZjQV	1.845	70.9	-4142.53	25.684	dia; 4/6/c1; sqc6
ZnTri2_82_I-4_TYtKJgkp	1.638	62.8	-4142.52	27.129	sql

Structure name	Density / g cm^{-3}	Packing coefficient / %	Energy per f. u. / eV	Relative energy / kJ mol^{-1}	Topology
ZnTri2_130_P4_ncc_zqqvcsWV	1.164	44.7	-4142.51	27.783	1D
ZnTri2_120_I-4c2_MEWXRRbO	1.160	44.6	-4142.51	27.957	1D
ZnTri2_146_H3_xkkHY7je	1.983	75.7	-4142.50	28.679	1D
ZnTri2_152_P3121_DZbx1oFY	1.250	48.4	-4142.50	28.733	qtz; 4/6/h1

3.3. Crystal structure prediction of Zn(ttz)$_2$ framework

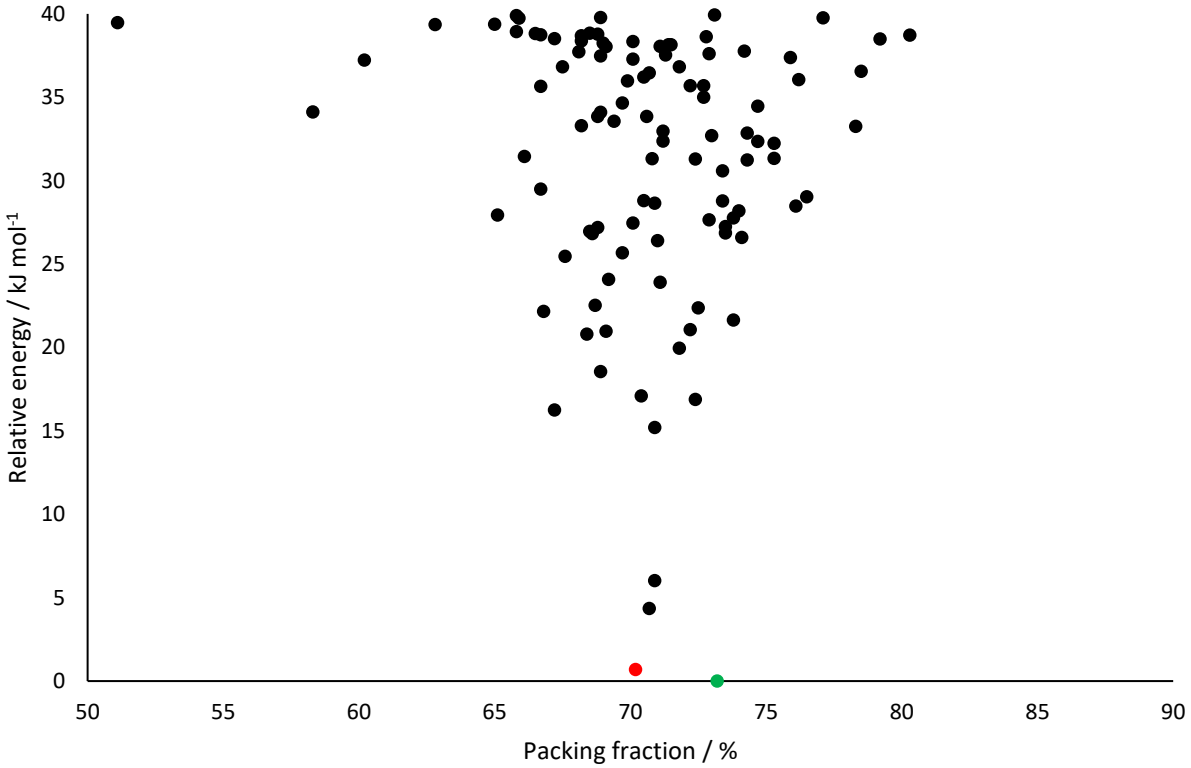

Figure **S10.** Relative energies of predicted Zn(**ttz**)$_2$ plotted against packing fraction. Experimental structure (CSD WAQRAI) is marked green, lowest energy predicted structure is marked red. The experimental structure is 0.680 kJ mol^{-1} lower in energy than the theoretical global minimum.

Table **S5.** Calculated parameters for the predicted structures of Zn(**ttz**)$_2$ after geometry optimization with PBE+MBD* method.

Structure name	Density / g cm^{-3}	Packing coefficient / %	Energy per f. u. / eV	Relative energy / kJ mol^{-1}	Topology
WAQRAI	2.048	73.2	-4346.45	0.000	dia; 4/6/c1; sqc6
Zntet2_110_I41cd_ExiJsl8J	1.964	70.2	-4346.45	0.680	dia; 4/6/c1; sqc6
Zntet2_70_Fddd_kLn6BbJ0	1.997	70.7	-4346.41	4.356	dia; 4/6/c1; sqc6
Zntet2_122_I-42d_sxuvDQFc	1.997	70.9	-4346.39	6.021	dia; 4/6/c1; sqc6
Zntet2_102_P42nm_0Zjq2qqd	2.021	70.9	-4346.29	15.201	dia; 4/6/c1; sqc6
Zntet2_80_I41_onL7lbpf	1.898	67.2	-4346.28	16.258	dia; 4/6/c1; sqc6
Zntet2_94_P42212_hZNwyYHc	2.028	72.4	-4346.28	16.892	dia; 4/6/c1; sqc6
Zntet2_91_P4122_fr6m9p4D	1.974	70.4	-4346.28	17.104	dia; 4/6/c1; sqc6
Zntet2_12_C2_m_nUEQGmwC	2.000	68.9	-4346.26	18.559	tsa

Structure name	Density / g cm^{-3}	Packing coefficient / %	Energy per f. u. / eV	Relative energy / kJ mol^{-1}	Topology
Zntet2_76_P41_3KUMCQ16	2.014	71.8	-4346.25	19.956	dia; 4/6/c1; sqc6
Zntet2_39_Abm2_GzGWynnc	1.929	68.4	-4346.24	20.815	dia; 4/6/c1; sqc6
Zntet2_12_C2_m_Z1JwmcUK	2.002	69.1	-4346.23	20.988	tsa
Zntet2_9_Cc_Y1awGVpo	2.023	72.2	-4346.23	21.069	cds; 4/6/t4; sqc5
Zntet2_110_I41cd_CTVPRGZK	2.061	73.8	-4346.23	21.658	dia; 4/6/c1; sqc6
Zntet2_33_Pna21_EEs2ty3s	1.879	66.8	-4346.22	22.170	dmp
Zntet2_33_Pna21_9IeZaasu	2.027	72.5	-4346.22	22.380	cds; 4/6/t4; sqc5
Zntet2_12_C2_m_ybDG7qIL	1.995	68.7	-4346.22	22.529	tsa
Zntet2_29_Pca21_t7bIWbLW	1.990	71.1	-4346.20	23.926	dia; 4/6/c1; sqc6
Zntet2_113_P-421m_Rxi1BBs9	1.949	69.2	-4346.20	24.092	sql
Zntet2_91_P4122_7QYTvAtf	1.911	67.6	-4346.19	25.462	dia; 4/6/c1; sqc6
Zntet2_122_I-42d_K4Z8QrwJ	1.950	69.7	-4346.19	25.689	dia; 4/6/c1; sqc6
Zntet2_76_P41_1dbHdnKU	1.987	71	-4346.18	26.418	dia; 4/6/c1; sqc6
Zntet2_12_C2_m_ZKWY6vNf	2.150	74.1	-4346.18	26.603	{3.6.7}4{3^2.4.6^2.7}2{3^4.4^2.8^6.9^3}{6^4.8^8.11^3}
Zntet2_12_C2_m_JKf0IK9X	1.999	68.6	-4346.17	26.830	tsa
Zntet2_4_P21_Qw5hHQuW	2.062	73.5	-4346.17	26.878	sql
Zntet2_14_P21_c_q3NCBQsY	1.927	68.5	-4346.17	26.972	sql
Zntet2_12_C2_m_axfWZQSM	1.994	68.800	-4346.17	27.202	{4.5^2.6^2.7}2{4.5^2}4{4^2.5^4.8^6.9.10^2}{5^2.6^4.7^4.8^2.9^2.10}
Zntet2_12_C2_m_8Ufo2DWB	2.131	73.50	-4346.17	27.259	{3.6.7}4{3^2.4.6^2.7}2{3^4.4^2.8^6.9^3}{6^4.8^8.11^3}
Zntet2_7_Pc_RONmxrf0	1.962	70.1	-4346.17	27.460	dia; 4/6/c1; sqc6
Zntet2_9_Cc_u5rEkJBm	2.050	72.9	-4346.17	27.661	sql
Zntet2_33_Pna21_TYpaxyrT	2.079	73.8	-4346.16	27.776	sql
Zntet2_88_I41_a_4yESX0pK	1.840	65.1	-4346.16	27.947	dia; 4/6/c1; sqc6
Zntet2_19_P212121_X6nKl0fY	2.082	74	-4346.16	28.205	sql
Zntet2_147_P-3_WKVFQkKZ	2.280	76.1	-4346.16	28.493	3,6,6T20
Zntet2_7_Pc_qODgrxVL	2.002	70.9	-4346.16	28.654	dia; 4/6/c1; sqc6
Zntet2_29_Pca21_oetfKgEo	2.068	73.4	-4346.15	28.796	dia; 4/6/c1; sqc6
Zntet2_29_Pca21_xnzN6YB8	1.985	70.5	-4346.15	28.820	dia; 4/6/c1; sqc6
Zntet2_60_Pbcn_JkpbKtfs	2.270	76.5	-4346.15	29.042	apo

Structure name	Density / g cm^{-3}	Packing coefficient / %	Energy per f. u. / eV	Relative energy / kJ mol^{-1}	Topology
Zntet2_14_P21_c_gS3BNDFT	1.909	66.7	-4346.15	29.493	sql
Zntet2_70_Fddd_VzeX1W9t	2.062	73.4	-4346.14	30.603	dia; 4/6/c1; sqc6
Zntet2_88_I41_a_5ydhHF1b	2.074	74.3	-4346.13	31.239	dia; 4/6/c1; sqc6
Zntet2_29_Pca21_AIk66CkA	2.031	72.4	-4346.13	31.307	sql
Zntet2_9_Cc_i6aSHOuq	1.988	70.8	-4346.13	31.333	cds; 4/6/t4; sqc5
Zntet2_12_C2_m_XZYgxK1s	2.193	75.3	-4346.13	31.341	{3.6.7}4{3^2.4.6^2.7}2{3^4.4^2.8^6.9^3}{6^4.8^8.11^3}
Zntet2_14_P21_c_kffwufDc	1.872	66.1	-4346.13	31.459	1D
Zntet2_143_P3_6HarzTsM	2.257	75.3	-4346.12	32.246	3,6,6T20
Zntet2_29_Pca21_2iqOaqHr	2.086	74.7	-4346.12	32.359	dia; 4/6/c1; sqc6
Zntet2_34_Pnn2_mYOHMmvb	2.011	71.2	-4346.12	32.376	dia; 4/6/c1; sqc6
Zntet2_4_P21_IS0tOvgf	2.050	73	-4346.11	32.699	sql
Zntet2_94_P42212_llcoF2VK	2.082	74.3	-4346.11	32.865	dia; 4/6/c1; sqc6
Zntet2_4_P21_T9PRqoVP	2.006	71.2	-4346.11	32.979	sql
Zntet2_114_P-421c_TdIxazTE	2.190	78.3	-4346.11	33.266	sql
Zntet2_9_Cc_JMXJm4h9	1.907	68.2	-4346.11	33.311	cds; 4/6/t4; sqc5
Zntet2_12_C2_m_cfiKtC2B	2.015	69.4	-4346.10	33.567	tsa
Zntet2_146_H3_eeugur7m	2.102	70.6	-4346.10	33.867	{4.6.8}{4^2.6}{4^6.6^5.8^3.10}
Zntet2_76_P41_Iv0rjs0y	1.928	68.8	-4346.10	33.869	cds; 4/6/t4; sqc5
Zntet2_29_Pca21_tKCsnjRj	1.929	68.9	-4346.10	34.115	sql
Zntet2_114_P-421c_i2lHbQMZ	1.645	58.3	-4346.10	34.120	sql
Zntet2_19_P212121_1TVODW9k	2.106	74.7	-4346.10	34.469	dia; 4/6/c1; sqc6
Zntet2_29_Pca21_PYjy87Aa	2.012	69.7	-4346.09	34.669	3,5L2
Zntet2_19_P212121_6u3SQsr4	2.038	72.7	-4346.09	35.005	dia; 4/6/c1; sqc6
Zntet2_55_Pbam_PUGZ9SsS	1.927	66.7	-4346.08	35.663	fet; fsc-3,5-P4/mbm
Zntet2_57_Pbcm_u3mj7LXG	2.034	72.7	-4346.08	35.695	sql
Zntet2_18_P21212_8m6kUYjE	2.027	72.2	-4346.08	35.710	sql
Zntet2_29_Pca21_bvlvcp7Z	2.019	69.9	-4346.08	35.982	3,5L2
Zntet2_19_P212121_ckio5PjR	2.136	76.2	-4346.08	36.071	sql
Zntet2_17_P2221_oqYBSMlT	1.976	70.5	-4346.08	36.217	sql
Zntet2_29_Pca21_YZ9f8B8C	1.982	70.7	-4346.07	36.467	sql

Structure name	Density / g cm^{-3}	Packing coefficient / %	Energy per f. u. / eV	Relative energy / kJ mol^{-1}	Topology
Zntet2_19_P212121_6cROg7Fb	2.269	78.5	-4346.07	36.556	seh-3,5-P43212
Zntet2_76_P41_WxZv7l8l	2.022	71.8	-4346.07	36.826	cds; 4/6/t4; sqc5
Zntet2_6_Pm_6FWp2gH4	1.902	67.5	-4346.07	36.831	sql
Zntet2_82_I-4_ih3datm8	1.688	60.2	-4346.07	37.240	sql
Zntet2_14_P21_c_nBqJY3N3	1.984	70.1	-4346.07	37.304	fes
Zntet2_19_P212121_LtiHBS7r	2.161	75.9	-4346.06	37.393	sql
Zntet2_41_Aba2_eGx1r1l5	1.938	68.9	-4346.06	37.480	sql
Zntet2_14_P21_c_ivI1Qh9o	2.060	71.3	-4346.06	37.545	seh-3,5-P21/c
Zntet2_122_I-42d_UlCJ1PlW	2.063	72.9	-4346.06	37.627	dia; 4/6/c1; sqc6
Zntet2_15_C2_c_eFDuUtoy	1.908	68.1	-4346.06	37.736	sql
Zntet2_19_P212121_ZpDc0MaD	2.088	74.2	-4346.06	37.781	dia; 4/6/c1; sqc6
Zntet2_20_C2221_CobHO4cD	1.933	69.1	-4346.06	38.040	sql
Zntet2_92_P41212_L105k1TV	1.997	71.1	-4346.06	38.061	sql
Zntet2_5_C2_C3R3gYEL	2.012	71.4	-4346.06	38.150	sql
Zntet2_60_Pbcn_r5GiScaJ	2.020	71.5	-4346.06	38.155	1D
Zntet2_12_C2_m_0PKPMzRr	1.998	69.00	-4346.06	38.249	{4.5^2.6^2.7}2{4.5^2}4{4^2.5^4.8^6.9.10^2}{5^2.6^4.7^4.8^2.9^2.10}
Zntet2_33_Pna21_nTpbCDUr	1.974	70.1	-4346.05	38.355	dmp
Zntet2_14_P21_c_3AT0wxYu	1.914	68.2	-4346.05	38.391	hcb
Zntet2_146_H3_OnniqSjq	2.374	79.2	-4346.05	38.511	{4.6^2}3{4^2.6}3{4^3.6^3.8^6.10^3}{4^3.6^6.8^6}{4^6.6^9}
Zntet2_19_P212121_42gOzZqX	1.935	67.2	-4346.05	38.517	3,5T1
Zntet2_14_P21_c_z9P7jVPj	2.104	72.8	-4346.05	38.640	3,5L66
Zntet2_5_C2_jL3wZstO	1.910	68.2	-4346.05	38.694	sql
Zntet2_19_P212121_IuYU0dDl	2.317	80.3	-4346.05	38.727	3,5T25
Zntet2_33_Pna21_So1RxwD7	1.927	66.7	-4346.05	38.756	3,5L2
Zntet2_7_Pc_t5QGyX9E	1.925	68.8	-4346.05	38.797	lfm; tcj-4,4-Imma-1
Zntet2_98_I4122_lQO0CRvh	1.862	66.5	-4346.05	38.826	dia; 4/6/c1; sqc6
Zntet2_29_Pca21_HGxYi7O0	1.921	68.5	-4346.05	38.847	sql
Zntet2_19_P212121_fsPwdHy1	1.898	65.8	-4346.05	38.939	3,5L2
Zntet2_29_Pca21_mYwNBrX7	1.761	62.8	-4346.04	39.368	sql

Structure name	Density / g cm^{-3}	Packing coefficient / %	Energy per f. u. / eV	Relative energy / kJ mol^{-1}	Topology
Zntet2_120_I-4c2_653nyGE2	1.842	65	-4346.04	39.392	dia; 4/6/c1; sqc6
Zntet2_19_P212121_htgszOSz	1.436	51.1	-4346.04	39.486	sql
Zntet2_2_P-1_5EZ2SZ62	1.845	65.9	-4346.04	39.759	sql
Zntet2_19_P212121_lUYGfrZJ	2.231	77.1	-4346.04	39.778	seh-3,5-P43212
Zntet2_52_Pnna_RopiN8ep	1.934	68.9	-4346.04	39.783	sql
Zntet2_19_P212121_bPpwuEvt	1.900	65.8	-4346.04	39.913	3,5L2
Zntet2_7_Pc_lgFJbvVT	2.065	73.1	-4346.04	39.939	sql
Zntet2_41_Aba2_0w15IwZs	1.956	69.6	-4346.03	40.353	sql
Zntet2_45_Iba2_9FcQ0Qyo	1.997	70.8	-4346.03	40.423	1D
Zntet2_29_Pca21_7ckoi6DP	1.532	54.5	-4346.03	40.548	sql
Zntet2_43_Fdd2_CZV43Vrk	1.928	68.4	-4346.03	40.700	dia; 4/6/c1; sqc6
Zntet2_33_Pna21_7GDS6Mmh	1.992	70.8	-4346.03	40.965	cds; 4/6/t4; sqc5
Zntet2_14_P21_c_iRPuMKxQ	2.104	72.6	-4346.03	41.004	dmc
Zntet2_76_P41_XmqQPgyJ	1.960	69.7	-4346.03	41.078	sql
Zntet2_114_P-421c_lrvyesrw	2.059	73.80	-4346.03	41.170	sql
Zntet2_60_Pbcn_hIC5wQhP	2.230	74.8	-4346.02	41.320	apo
Zntet2_33_Pna21_u4zPVWQ3	1.978	70.5	-4346.02	41.329	cds; 4/6/t4; sqc5
Zntet2_19_P212121_Bmqg7xqw	1.841	64.2	-4346.02	41.776	dia; 4/6/c1; sqc6
Zntet2_14_P21_c_P2kqVhNL	2.344	79	-4346.02	41.882	rtl
Zntet2_152_P3121_KrzEqfEz	1.331	47.5	-4346.02	41.965	qtz; 4/6/h1
Zntet2_88_I41_a_YCrEf7ak	2.035	72.3	-4346.01	42.603	dia; 4/6/c1; sqc6
Zntet2_144_P31_gdQWIepU	2.243	77.5	-4346.01	42.609	1D
Zntet2_33_Pna21_gaucfWLs	1.873	66.7	-4346.01	42.791	sql
Zntet2_121_I-42m_EdVZ0yXw	1.858	66	-4346.01	42.808	sql
Zntet2_76_P41_d0ibDAsb	1.943	69.2	-4346.01	42.849	cds; 4/6/t4; sqc5
Zntet2_33_Pna21_zBQzOD15	1.881	65.3	-4346.01	42.984	3,5T1
Zntet2_13_P2_c_pAzD0xF7	1.923	68.3	-4346.00	43.356	sql
Zntet2_80_I41_iH1tBaQ2	1.923	68.3	-4346.00	43.476	1D
Zntet2_144_P31_JlDDUqpO	1.321	47.2	-4346.00	43.509	qtz; 4/6/h1
Zntet2_33_Pna21_UvWUmemW	2.109	75.2	-4346.00	43.532	sql
Zntet2_122_I-42d_OjUYUg4S	2.036	72.5	-4345.99	44.123	dia; 4/6/c1; sqc6

Structure name	Density / g cm^{-3}	Packing coefficient / %	Energy per f. u. / eV	Relative energy / kJ mol^{-1}	Topology
Zntet2_19_P212121_ZCMttq8A	2.333	81.1	-4345.99	44.542	3,5T25
Zntet2_171_P62_RUqHMAQl	2.344	83.6	-4345.99	44.686	qtz; 4/6/h1
Zntet2_33_Pna21_D715tlmg	1.220	43.6	-4345.99	44.718	dia; 4/6/c1; sqc6
Zntet2_9_Cc_kDJveihE	2.292	78.9	-4345.98	45.092	kdd; seh-3,5-Cmc21
Zntet2_19_P212121_C65x1wax	1.171	41.8	-4345.98	45.495	dia; 4/6/c1; sqc6
Zntet2_33_Pna21_XPb8Yvum	1.112	39.6	-4345.98	45.570	sql
Zntet2_60_Pbcn_0ABj00OS	2.231	74.4	-4345.98	45.910	apo
Zntet2_14_P21_c_RUj9CvPw	2.082	72	-4345.98	46.038	3,5L66
Zntet2_14_P21_c_llQRu5UU	1.880	67	-4345.97	46.067	hcb
Zntet2_19_P212121_eEXwtqnF	1.709	60.9	-4345.97	46.479	dia; 4/6/c1; sqc6
Zntet2_33_Pna21_CPEiY3sJ	2.028	70.2	-4345.96	47.133	3,5T1
Zntet2_14_P21_c_sf3myU5y	2.366	79.8	-4345.96	47.812	rtl
Zntet2_144_P31_GDxyRRjt	2.358	84	-4345.94	48.973	qtz; 4/6/h1
Zntet2_146_H3_sKZwcpRm	2.345	78.4	-4345.88	55.216	{4.6^2}3{4^2.6}3{4^3.6^3.8^6.10^3}{4^3.6^6.8^6}{4^6.6^9}
Zntet2_85_P4_n_jbwvyQ3r	1.787	64.3	-4345.31	110.003	sql
Zntet2_147_P-3_KH56reG9	1.787	64.7	-4345.21	119.838	kgm

3.4. Crystal structure prediction of Zn_2DHTA framework

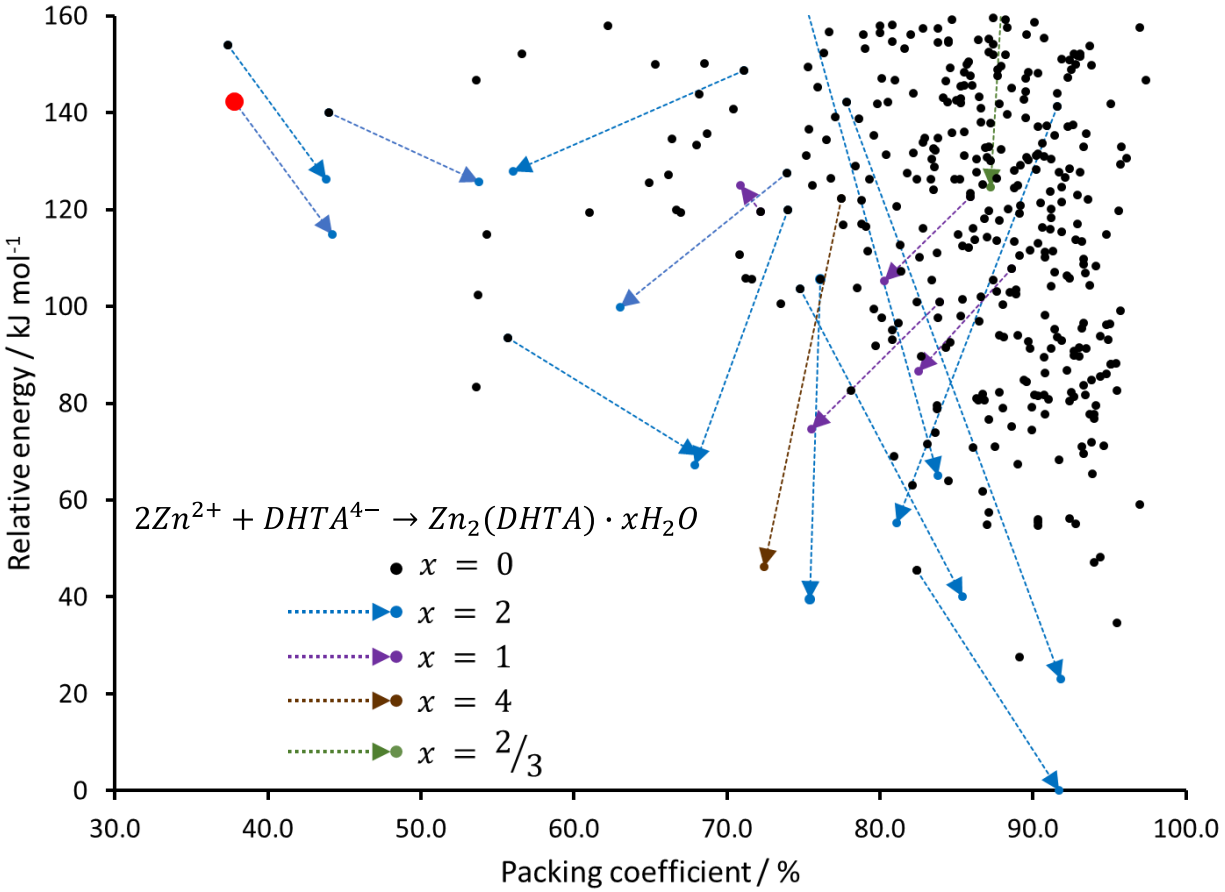

Figure **S11.** Relative energies of predicted Zn_2**DHTA** plotted against packing fraction. The anhydrous structures are shown in black, while the hydrated structures are shown in blue. The arrows connect the anhydrous structures with their corresponding hydrated structures. The structure matching MOF-74 is shown in red.

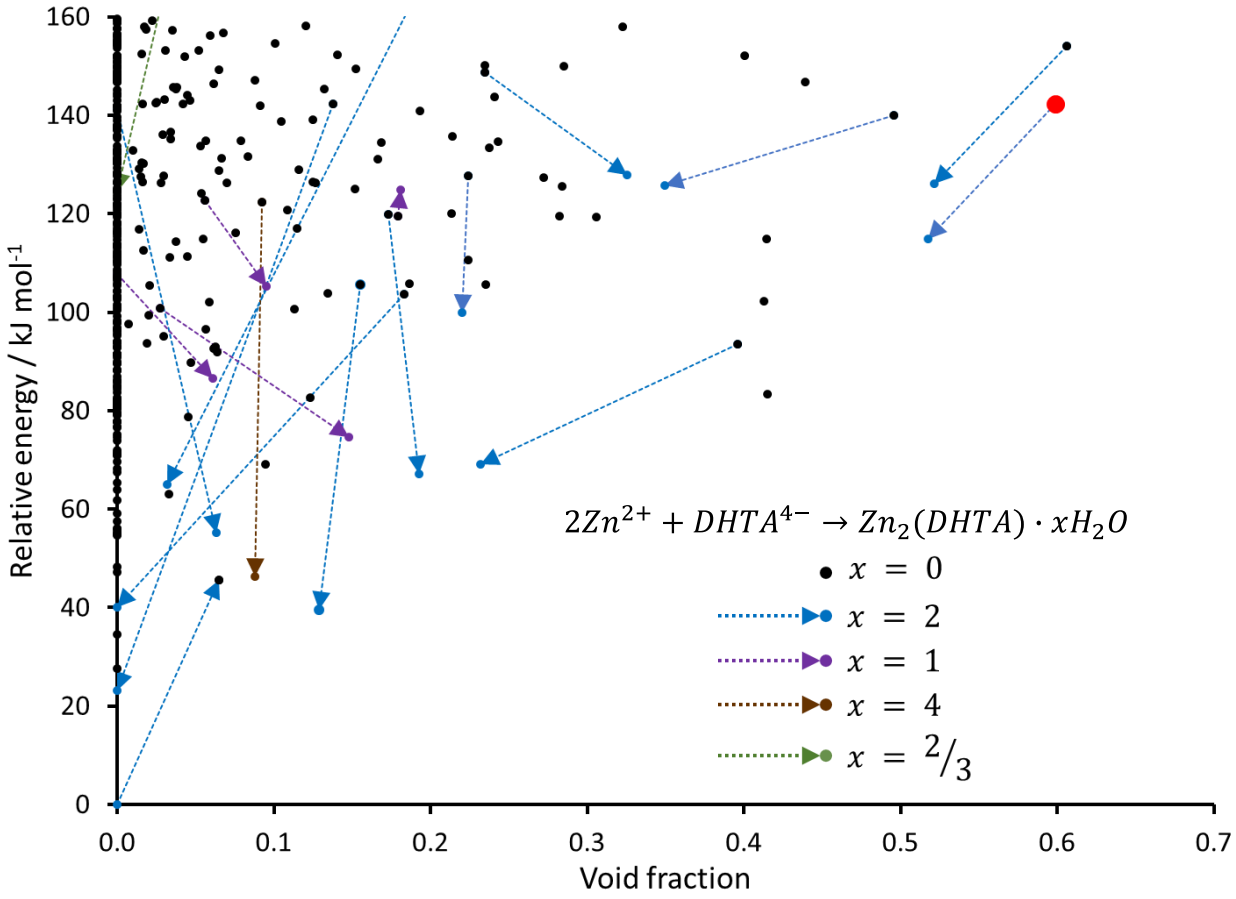

Figure **S12.** Relative energies of predicted Zn_2**DHTA** plotted against solvent-accessible void fraction. The anhydrous structures are shown in black, while the hydrated structures are shown in blue. The arrows connect the anhydrous structures with their corresponding hydrated structures. The structure matching MOF-74 is shown in red.

Table **S7.** Calculated parameters for the predicted anhydrous structures of Zn_2**DHTA** after geometry optimization with PBE+MBD* method. The relative energies are provided with respect to lowest energy hydrated structure (see section 1.5 for details).

Structure name	Density / g cm^{-3}	Packing coefficient / %	Void fraction	Energy per f. u. / eV	Relative energy / kJ mol^{-1}	Topology
MOF74_14_P21_c_y3O60Gin	2.863	89.1	0.00	-7507.010	27.669	alb-3,6-P42/mnm
MOF74_14_P21_c_5EkmwhNL	3.291	95.5	0.00	-7506.938	34.591	5,10T32
MOF74_14_P21_c_8ykFjmN5	2.605	82.4	0.07	-7506.825	45.538	rtl
MOF74_14_P21_c_AF7bMYJw	3.072	94	0.00	-7506.807	47.231	alb-4,8-P21/c-1
MOF74_14_P21_c_I6WOIMVX	3.210	94.4	0.00	-7506.797	48.205	alb-4,8-P21/c-1
MOF74_14_P21_c_eXRO4yzP	2.939	90.3	0.00	-7506.729	54.757	flu; sqc169
MOF74_14_P21_c_SwAbBdS9	2.843	87	0.00	-7506.728	54.858	alb-4,8-P21/c-1
MOF74_2_P-1_2qPtWxsU	3.019	92.8	0.00	-7506.726	55.075	flu; sqc169
MOF74_14_P21_c_OrMa3Tzf	2.928	90.3	0.00	-7506.723	55.403	alb-4,8-Cmce
MOF74_14_P21_c_07jkXqcu	2.916	90.3	0.00	-7506.717	55.987	alb-4,8-Cmce
MOF74_2_P-1_7eNoOOeC	3.003	92.4	0.00	-7506.715	56.108	flu; sqc169
MOF74_2_P-1_6lcSol80	2.820	87.1	0.00	-7506.700	57.551	flu; sqc169
MOF74_14_P21_c_WuF3bkRZ	3.317	97	0.00	-7506.684	59.166	alb-5,10-P21/c-1
MOF74_2_P-1_dcWszn63	2.694	86.7	0.00	-7506.656	61.810	alb-3,6-C2/c
MOF74_2_P-1_0UhkX99L	2.631	82.1	0.03	-7506.643	63.087	flu; sqc169
MOF74_14_P21_c_WAanLGb4	2.740	84.5	0.00	-7506.633	64.005	flu; sqc169

Structure name	Density / g cm^{-3}	Packing coefficient / %	Void fraction	Energy per f. u. / eV	Relative energy / kJ mol^{-1}	Topology
MOF74_2_P-1_0iuTdyUW	3.098	93.9	0.00	-7506.619	65.375	flu; sqc169
MOF74_14_P21_c_8m6V7CWK	2.910	89	0.00	-7506.598	67.445	alb-4,8-Cmce
MOF74_7_Pc_xOeHXnu7	2.999	91.7	0.00	-7506.589	68.255	alb/P 6/m m m->P b c n (a+b,-a+b,2c; 0,0,1/2);Bond sets: 2,3,5,6:alb
MOF74_14_P21_c_CveZ5oy7	2.653	80.9	0.09	-7506.581	69.032	flu; sqc169
MOF74_15_C2_c_upHIhxaX	3.063	93.3	0.00	-7506.575	69.615	alb-4,8-Fddd
MOF74_4_P21_OHsuQb1j	2.743	86.1	0.00	-7506.562	70.899	3,4,7T146
MOF74_9_Cc_d5nmEYg9	3.037	93.2	0.00	-7506.561	70.990	flu; sqc169
MOF74_2_P-1_8cHDxV8C	2.819	87.5	0.00	-7506.561	71.019	{4^11.6^11.8^6}2{4^2.6}2{4^4.6^2.8^9}{4^5.6}4
MOF74_14_P21_c_C24DAWIr	3.173	94.6	0.00	-7506.559	71.227	flu; sqc169
MOF74_14_P21_c_2RAqvngR	2.661	83.1	0.00	-7506.554	71.632	rtl
MOF74_5_C2_x13kMMCs	3.145	93.8	0.00	-7506.552	71.864	alb/P 6/m m m->C 2 (a-b,a+b,c);Bond sets: 2,4,5,6:alb
MOF74_14_P21_c_B8hxKBUU	2.738	83.6	0.00	-7506.530	73.986	alb-4,8-P21/c-1
MOF74_2_P-1_2XSj2oIj	2.908	89.9	0.00	-7506.524	74.537	flu; sqc169
MOF74_2_P-1_Mm0aQHhn	2.857	88.6	0.00	-7506.518	75.175	flu; sqc169
MOF74_9_Cc_Gt2otiB3	2.837	87.1	0.00	-7506.502	76.669	alb/P 6/m m m->C 2/c (a-b+2c,-a-b,-2c);Bond sets: 2,4,5,6:alb
MOF74_15_C2_c_3GlZKr6g	3.131	94	0.00	-7506.500	76.847	flu; sqc169
MOF74_4_P21_ae4b7EZz	3.087	93.7	0.00	-7506.492	77.653	alb-4,8-Cmce
MOF74_15_C2_c_10JUcH30	2.985	90.8	0.00	-7506.491	77.749	alb/P 6/m m m->P n m a (-a-b,2c,-a+b; 0,0,1/2);Bond sets: 2,3,4,6:alb

Structure name	Density / g cm^{-3}	Packing coefficient / %	Void fraction	Energy per f. u. / eV	Relative energy / kJ mol^{-1}	Topology
MOF74_15_C2_c_nm2Er9Nl	3.124	94	0.00	-7506.491	77.793	flu; sqc169
MOF74_14_P21_c_8iYA6x7a	2.691	83.7	0.05	-7506.481	78.753	flu; sqc169
MOF74_4_P21_bb3SwRfV	2.816	88	0.00	-7506.477	79.081	{4.6^2}{4^3.6^3}{4^4.6^13.8^4}
MOF74_15_C2_c_unDz87bk	2.908	89.9	0.00	-7506.476	79.211	flu; sqc169
MOF74_7_Pc_WwOrkYNB	3.114	94.1	0.00	-7506.473	79.491	{4^4.6^2}2{4^8.6^17.8^3}
MOF74_2_P-1_1tlVUObN	2.757	83.7	0.00	-7506.472	79.585	scu; sqc170
MOF74_14_P21_c_7sVDdTjI	2.928	92.4	0.00	-7506.464	80.374	flu; sqc169
MOF74_15_C2_c_husKzNcq	2.836	86.8	0.00	-7506.461	80.600	{4^14.6^12.8^2}{4^2.6^4}{4^4.6^2}
MOF74_43_Fdd2_KaVZAXtp	2.791	86.4	0.00	-7506.461	80.634	alb-4,8-Fddd
MOF74_5_C2_jD17wx25	2.833	91	0.00	-7506.460	80.770	flu; sqc169
MOF74_43_Fdd2_9VajiAqp	2.785	86.3	0.00	-7506.458	80.919	alb-4,8-Fddd
MOF74_2_P-1_nsCWAQgo	2.837	86.7	0.00	-7506.456	81.112	{3^2.4^10.5^2.6}{3^2.4^12.5^4.6^9.7}2{4^6}2
MOF74_14_P21_c_APDoVz8M	2.937	92.7	0.00	-7506.454	81.343	flu; sqc169
MOF74_7_Pc_AuTnZ4pg	2.950	90.3	0.00	-7506.451	81.599	{4^10.6^16.8^2}{4^4.6^2}{4^6}
MOF74_2_P-1_2QHGAiHH	3.013	90.1	0.00	-7506.450	81.715	{4^18.6^10}{4^24.6^20.8}{4^4.6^2}{4^5.6}{4^7.6^3}2
MOF74_9_Cc_iePZ5soU	3.079	93.4	0.00	-7506.450	81.739	4,8T6
MOF74_13_P2_c_pgOZE2sa	2.821	90.7	0.00	-7506.449	81.763	flu; sqc169
MOF74_14_P21_c_Nxh6KKVm	2.786	86.7	0.00	-7506.448	81.917	flu; sqc169
MOF74_9_Cc_M4hWSDLw	2.828	87.8	0.00	-7506.444	82.308	alb-4,8-C2/c

Structure name	Density / g cm^{-3}	Packing coefficient / %	Void fraction	Energy per f. u. / eV	Relative energy / kJ mol^{-1}	Topology
MOF74_14_P21_c_iSZojXqv	3.001	92.5	0.00	-7506.444	82.323	alb-4,8-Cmce
MOF74_43_Fdd2_0D8oU3BI	3.242	95.5	0.00	-7506.441	82.578	alb-4,8-Fddd
MOF74_41_Aba2_P9PvKoon	2.550	78.1	0.12	-7506.440	82.631	flu; sqc169
MOF74_148_H-3_2jPeD1Su	1.672	53.6	0.42	-7506.432	83.424	3,6T18
MOF74_43_Fdd2_kG8ZHEzh	2.975	93.3	0.00	-7506.429	83.751	alb-4,8-Fddd
MOF74_4_P21_N4MbqQ2B	2.846	89.6	0.00	-7506.421	84.460	alb-4,8-P21/c-1
MOF74_9_Cc_pwzpGdaA	2.973	93.8	0.00	-7506.417	84.870	alb/P 6/m m m->C 2/c (a-b+2c,-a-b,-2c);Bond sets: 2,4,5,6:alb
MOF74_2_P-1_WPTx8Aap	2.982	89.4	0.00	-7506.417	84.889	{4^14.6^12.8^2}{4^4.6^2}2
MOF74_5_C2_9x6n8tq0	3.225	94.4	0.00	-7506.410	85.588	{4^24.6^20.8}{4^8.6^2}2
MOF74_4_P21_qy40rpgO	3.036	94.8	0.00	-7506.405	86.061	{4^3.6^3}{4^5.6}{4^8.6^18.8^2}
MOF74_2_P-1_noErMKdE	2.998	90.8	0.00	-7506.403	86.258	{4^15.6^13}2{4^4.6^2}6{4^8.6^14.8^6}
MOF74_13_P2_c_GGgKTXWg	2.982	92.2	0.00	-7506.397	86.857	alb-4,8-P2/c
MOF74_14_P21_c_HZl0hD4e	3.031	95.1	0.00	-7506.383	88.136	alb-4,8-P21/c-1
MOF74_14_P21_c_4BJ6JfKz	3.148	95.1	0.00	-7506.383	88.141	flu; sqc169
MOF74_14_P21_c_9ye9fZri	3.160	95.4	0.00	-7506.382	88.300	flu; sqc169
MOF74_15_C2_c_bdDVByvg	2.977	90.7	0.00	-7506.369	89.520	alb-4,8-Fddd
MOF74_2_P-1_0g8CSh0n	3.048	93	0.00	-7506.368	89.632	6,8T13
MOF74_2_P-1_WRxaZOcA	2.663	82.7	0.05	-7506.367	89.734	{4.6^2}2{4^2.6^8.8^5}{4^4.6^14.8^9.10}{4^4.6^2}4{4^6.6^11.8^10.10}

Structure name	Density / g cm^{-3}	Packing coefficient / %	Void fraction	Energy per f. u. / eV	Relative energy / kJ mol^{-1}	Topology
MOF74_2_P-1_ROfKiAO9	3.041	92.7	0.00	-7506.365	89.929	6,8T13
MOF74_14_P21_c_cAExvWH2	3.028	92.7	0.00	-7506.356	90.789	alb-4,8-Cmce
MOF74_14_P21_c_5W11sC7m	2.837	89.8	0.00	-7506.350	91.329	alb-3,6-P42/mnm
MOF74_14_P21_c_KXleAFB8	2.953	91.2	0.00	-7506.350	91.339	alb-4,8-P21/c-1
MOF74_4_P21_4bMdmj8J	2.970	93.5	0.00	-7506.350	91.339	flu; sqc169
MOF74_2_P-1_3oiwdRH4	2.723	84.3	0.00	-7506.349	91.457	flu; sqc169
MOF74_7_Pc_qPcLm0DB	3.000	93	0.00	-7506.349	91.493	{4^5.6}2{4^7.6^20.8}
MOF74_152_P3121_1evpqUxl	2.482	79.7	0.06	-7506.344	91.905	{5^10.6^5}{5^4.6^2}
MOF74_18_P21212_CcpPjVwK	2.713	84.6	0.06	-7506.337	92.627	rtl
MOF74_2_P-1_GJfsAsgS	2.907	89.7	0.00	-7506.335	92.761	{4^12.6^11.8^5}2{4^3}2{4^5.6}2{4^6.6^6.8^3}{4^6}2
MOF74_41_Aba2_e8T0HC1Q	2.869	91.9	0.00	-7506.333	92.946	alb/P 6/m m m->C m c 21 (-a+b,-a-b,2c);Bond sets: 2,4,5,6:alb
MOF74_9_Cc_tVebk3T4	2.505	80.8	0.06	-7506.332	93.052	flu; sqc169
MOF74_14_P21_c_UzfLp3rL	3.044	94.9	0.00	-7506.332	93.056	alb/P 6/m m m->P b c n (a+b,-a+b,2c; 0,0,1/2);Bond sets: 2,3,5,6:alb
MOF74_147_P-3_6N8uMV7L	1.749	55.7	0.40	-7506.328	93.455	csq/P 6/m m m->P -3/Final structure;Bond sets: 2,3,4:csq
MOF74_4_P21_Al8THt7C	2.930	91.6	0.00	-7506.325	93.727	{4^2.6^4}{4^2.6}{4^4.6^15.8^2}
MOF74_23_I222_AXigtjI8	2.833	88.1	0.02	-7506.325	93.742	{4^11.6^12.8^5}2{4^2.6^4}2{4^4.6^2}{4^6}
MOF74_2_P-1_8f3ONqwR	3.130	94.4	0.00	-7506.323	93.939	flu; sqc169
MOF74_12_C2_m_FahIHdPL	2.784	89	0.00	-7506.322	94.035	flu; sqc169
MOF74_7_Pc_e5HrJg2h	2.838	87.8	0.00	-7506.322	94.074	alb/P 6/m m m->P 2/c (-a-2b,c,2b);Bond sets: 2,3,5,6:alb

Structure name	Density / g cm^{-3}	Packing coefficient / %	Void fraction	Energy per f. u. / eV	Relative energy / kJ mol^{-1}	Topology
MOF74_20_C2221_CfAyyRZn	2.677	80.8	0.03	-7506.311	95.112	flu; sqc169
MOF74_34_Pnn2_22VcfH6M	2.885	91.4	0.00	-7506.310	95.218	flu; sqc169
MOF74_14_P21_c_BZVAVR7s	2.945	93.2	0.00	-7506.306	95.555	alb-4,8-Cmce
MOF74_12_C2_m_EqEP5tYV	3.125	94.8	0.00	-7506.299	96.254	fit
MOF74_4_P21_ulNfNweh	3.169	95	0.00	-7506.297	96.448	{4^3.6^3}{4^3}{4^6.6^12.8^3}
MOF74_15_C2_c_zYOaoY7Y	2.634	81.2	0.06	-7506.296	96.559	alb/P 6/m m m->C 2/c (a-b+2c,-a-b,-2c);Bond sets: 2,4,5,6:alb
MOF74_7_Pc_GutenSBU	2.983	93.3	0.00	-7506.296	96.602	alb-4,8-Cmce
MOF74_4_P21_lBSRK8Eg	2.749	86.5	0.00	-7506.292	96.954	{4^3.6^3}{4^3}{4^6.6^12.8^3}
MOF74_5_C2_RSU3LRZO	2.586	80.1	0.01	-7506.285	97.659	flu; sqc169
MOF74_14_P21_c_daRINkKT	2.618	83.8	0.00	-7506.284	97.731	kgd
MOF74_14_P21_c_DDiYIlOc	2.697	85.3	0.00	-7506.282	97.934	flu; sqc169
MOF74_34_Pnn2_L9rjGAMJ	2.961	90.8	0.00	-7506.278	98.272	flu; sqc169
MOF74_13_P2_c_KkToTTDi	3.314	95.7	0.00	-7506.269	99.178	alb/P 6/m m m->P 2/c (a+b,-c,2b; 0,1/2,0);Bond sets: 2,3,4,5,6:alb
MOF74_4_P21_kcRhPNvZ	2.536	79.6	0.02	-7506.267	99.376	cml; flu-3,6-Cmc21
MOF74_2_P-1_PuYyZbT9	2.751	88	0.00	-7506.256	100.442	alb-3,6-C2/c
MOF74_148_H-3_AGn5T4Pj	2.298	73.5	0.11	-7506.254	100.634	3,6T18
MOF74_2_P-1_jHOzVFNo	2.724	83.9	0.03	-7506.251	100.877	{3.4^3.6^2}2{3^4.4^6.5^4.6^6.7^4.8^4}{4^4.6^2}{4^6.5.6^5.8^3}
MOF74_14_P21_c_gofWGjU7	2.607	82.4	0.00	-7506.251	100.934	rtl

Structure name	Density / g cm^{-3}	Packing coefficient / %	Void fraction	Energy per f. u. / eV	Relative energy / kJ mol^{-1}	Topology
MOF74_15_C2_c_8nBJEVlD	2.704	85.4	0.00	-7506.244	101.533	ant
MOF74_37_Ccc2_Lvr9XRJV	2.737	86.6	0.06	-7506.240	102.005	alb/P 6/m m m->C c c m (-a+b,-a-b,2c);Bond sets: 2,3:alb
MOF74_171_P62_OCDuaNBe	1.685	53.7	0.41	-7506.237	102.293	{4.6^2}2{4^2.6^10.8^3}
MOF74_9_Cc_2MvcXOvc	2.811	88.9	0.00	-7506.234	102.551	{4^3.6^3}{4^3}{4^6.6^12.8^3}
MOF74_4_P21_JDDGfAMT	2.823	88.5	0.00	-7506.230	102.956	{4^3.6^3}{4^3}{4^6.6^12.8^3}
MOF74_15_C2_c_3giee4p3	2.809	87.6	0.00	-7506.228	103.139	alb-4,8-Fddd
MOF74_2_P-1_JUcnsp57	2.875	88.9	0.00	-7506.225	103.380	alb-4,8-Fddd
MOF74_34_Pnn2_g64zCePU	2.362	74.8	0.18	-7506.223	103.607	rtl
MOF74_14_P21_c_fIri1Qvz	2.429	78.5	0.13	-7506.221	103.790	alb-4,8-Cmce
MOF74_2_P-1_2Estq5nH	3.028	91.2	0.00	-7506.216	104.244	fit
MOF74_4_P21_pA3EWE14	3.162	93.7	0.00	-7506.214	104.437	{4^17.6^18.8}{4^6}{4^8.6^2}
MOF74_148_H-3_LacD0oGM	2.670	83.4	0.02	-7506.204	105.394	{4^10.6^15.8^3}{4^5.6}2
MOF74_2_P-1_qMg9Zt7J	2.860	87.4	0.00	-7506.204	105.484	{4^4.5^2}2{4^4.6^2}{4^6.5^12.6^6.8^4}{4^6.5^6.7^3}
MOF74_9_Cc_ouBwFZkd	2.414	76.1	0.16	-7506.202	105.653	{4^3}{4^5.6}{4^8.6^9.8^4}
MOF74_2_P-1_xTGD0rRv	2.328	71.6	0.24	-7506.201	105.682	fit-4,8-P42/mmc
MOF74_43_Fdd2_WtfNLWqf	2.890	92.4	0.00	-7506.200	105.793	4,8T6
MOF74_144_P31_QIgj3zH5	2.223	71.2	0.19	-7506.200	105.847	flu/fluorite ;F m -3 m->P 32 2 1 (-1/2a+1/2b,-1/2b+1/2c,a+b+c; 2/3,0,1/3);Bond sets: 1,2,4:flu
MOF74_144_P31_6u98ezbg	3.012	92.2	0.00	-7506.194	106.416	{4^3.6^3}2{4^6.6^18.8^4}
MOF74_15_C2_c_6YjZpzvM	3.095	93.4	0.00	-7506.190	106.810	flu; sqc169

Structure name	Density / g cm^{-3}	Packing coefficient / %	Void fraction	Energy per f. u. / eV	Relative energy / kJ mol^{-1}	Topology
MOF74_7_Pc_eVXSed61	2.936	91.4	0.00	-7506.186	107.148	alb-4,8-P21/c-1
MOF74_41_Aba2_3s3S2cgV	2.694	81.4	0.00	-7506.186	107.211	flu; sqc169
MOF74_15_C2_c_wkeUitAg	2.936	88.6	0.00	-7506.179	107.828	{3^2.4^11.5^2}{3^4.4^8.5^8.6^7.8}
MOF74_4_P21_qiVWNnHg	3.130	94.1	0.00	-7506.174	108.354	{4^14.6^22}{4^6}{4^8.6^2}
MOF74_5_C2_O1EpgPH3	3.089	93.3	0.00	-7506.171	108.658	flu; sqc169
MOF74_20_C2221_HoADnQWr	3.022	93.3	0.00	-7506.160	109.719	fse
MOF74_4_P21_xGgnv0HH	2.857	90.8	0.00	-7506.155	110.192	{4^3.6^3}{4^3}{4^6.6^12.8^3}
MOF74_15_C2_c_6lE7nfB5	2.701	82.6	0.00	-7506.154	110.221	4,6T64
MOF74_2_P-1_YVxhfJ4A	2.872	89.1	0.00	-7506.151	110.583	{4.6^2}2{4^2.6^10.8^3}{4^4.6^10.8}{4^4.6^2}
MOF74_148_H-3_2LL1JxJs	2.288	70.8	0.22	-7506.150	110.630	4,8T3
MOF74_14_P21_c_CAuz3ebK	2.663	83.7	0.03	-7506.145	111.099	rtl
MOF74_4_P21_QmZ1MAMV	2.965	90.8	0.00	-7506.144	111.201	{4^2.6^4}{4^2.6}{4^4.6^15.8^2}
MOF74_148_H-3_SXoZkZWg	2.494	79.2	0.04	-7506.143	111.324	3,6T18
MOF74_14_P21_c_DzJfp4r4	2.888	91.3	0.00	-7506.143	111.355	alb-4,8-Cmce
MOF74_14_P21_c_BbXFBU0K	2.867	89.8	0.00	-7506.140	111.586	rtl
MOF74_14_P21_c_DPaIFbPA	2.707	85.8	0.00	-7506.135	112.054	rtl
MOF74_2_P-1_al16BsXc	2.706	85.4	0.00	-7506.131	112.440	{4^2.6}2{4^4.6^2}2{4^4.6^8.8^3}{4^8.6^14.8^6}
MOF74_160_H3m_evULgSr6	2.541	81.3	0.02	-7506.130	112.620	{4^10.6^15.8^3}{4^5.6}2
MOF74_13_P2_c_fa1fiaoz	2.968	90.3	0.00	-7506.125	113.077	alb-4,8-P2/c

Structure name	Density / g cm^{-3}	Packing coefficient / %	Void fraction	Energy per f. u. / eV	Relative energy / kJ mol^{-1}	Topology
MOF74_4_P21_3Bs4buNY	2.888	88.8	0.00	-7506.122	113.362	alb-4,8-Cmce
MOF74_5_C2_Y0z5sfSX	3.034	93.2	0.00	-7506.121	113.405	alb/P 6/m m m->C m c 21 (-a+b,-a-b,2c);Bond sets: 2,4,5,6:alb
MOF74_15_C2_c_cZS9BoPh	2.844	87.6	0.00	-7506.120	113.531	alb-4,8-Cmce
MOF74_2_P-1_2IqrYngC	2.681	86.2	0.00	-7506.118	113.756	{4^3}4{4^4.6^2}2{4^6.6^6.8^3}2{4^8.6^4.8^12.10^4}
MOF74_9_Cc_EtJPiW64	2.972	92.8	0.00	-7506.117	113.796	4,8T11
MOF74_15_C2_c_00aiEN33	2.818	87	0.04	-7506.112	114.360	alb/P 6/m m m->C 2/c (a-b+2c,-a-b,-2c);Bond sets: 2,4,5,6:alb
MOF74_4_P21_frhvhKmn	3.110	94.8	0.00	-7506.107	114.780	{4^17.6^18.8}{4^6}{4^8.6^2}
MOF74_32_Pba2_BcC7OOK1	2.746	85.1	0.05	-7506.107	114.809	scu/P 4/m m m->P 42 b c (a-b,a+b,2c; 1/2,1/2,1/2);Bond sets: 2,3,4:scu
MOF74_148_H-3_etxIwodc	1.717	54.3	0.41	-7506.107	114.817	3,6T18
MOF74_14_P21_c_8SSCEobr	3.006	91.9	0.00	-7506.101	115.378	{3^2.4^6.5^6.6}{3^4.4^8.5^8.6^7.8}
MOF74_2_P-1_qxoCdjiT	2.951	91.1	0.00	-7506.094	116.023	{4^10.6^14.8^3.10}{4^13.6^14.8}2{4^2.6}2{4^5.6}2{4^7.6^3}2
MOF74_14_P21_c_xcrhXajf	2.677	82.8	0.08	-7506.094	116.039	flu; sqc169
MOF74_5_C2_HFpZ9r8d	2.785	86.1	0.00	-7506.093	116.141	flu; sqc169
MOF74_2_P-1_akeMK7Sa	2.946	90.6	0.00	-7506.092	116.266	{4^13.6^13.8^2}2{4^4.6^2}{4^5.6}{4^6}2
MOF74_20_C2221_eoLMafmT	2.560	79.1	0.00	-7506.090	116.406	scu-3,6-C2221
MOF74_20_C2221_gVmcheO8	2.476	77.6	0.01	-7506.086	116.835	scu-3,6-C2221
MOF74_2_P-1_0XO6eVoc	2.509	78.8	0.11	-7506.084	116.975	{4^10.6^12.8^6}{4^3}2{4^5.6}2{4^6.6^6.8^3}
MOF74_4_P21_mh9nFNcW	3.012	92.9	0.00	-7506.083	117.081	alb/P 6/m m m->C m c 21 (-a+b,-a-b,2c);Bond sets: 2,4,5,6:alb

Structure name	Density / g cm^{-3}	Packing coefficient / %	Void fraction	Energy per f. u. / eV	Relative energy / kJ mol^{-1}	Topology
MOF74_14_P21_c_CsIySSci	2.752	87.8	0.00	-7506.076	117.757	alb-3,6-P42/mnm
MOF74_9_Cc_MqXLN1eW	2.793	86.8	0.00	-7506.073	118.056	{4^3.6^3}{4^3}{4^6.6^12.8^3}
MOF74_36_Cmc21_vrRxbpNN	2.868	91.2	0.00	-7506.070	118.321	{4^17.6^18.8}{4^6}{4^8.6^2}
MOF74_14_P21_c_40CEL7Zq	2.848	89.1	0.00	-7506.061	119.247	{5^10.6^3.7.8}{5^4.6^2}
MOF74_148_H-3_Y4OgZDbn	1.871	61	0.31	-7506.059	119.390	3,6T18
MOF74_15_C2_c_6XHtzB7s	2.144	67	0.28	-7506.059	119.435	fit-4,8-P42/mmc
MOF74_143_P3_pAlrmY1w	2.277	72.2	0.18	-7506.058	119.564	{4^3.6^18}{4^3.6^3}{4^3}
MOF74_15_C2_c_OgBs9ayP	3.192	95.6	0.00	-7506.056	119.735	{4^10.6^12.8^6}{4^5.6}2
MOF74_14_P21_c_gQ0dk11O	2.798	87.1	0.00	-7506.055	119.778	alb-4,8-P21/c-1
MOF74_147_P-3_5YRSbNhe	2.325	74	0.17	-7506.054	119.944	csq/P 6/m m m->P -3/Final structure;Bond sets: 2,3,4:csq
MOF74_14_P21_c_ImWR2fcH	2.034	66.7	0.21	-7506.053	119.995	rtl
MOF74_15_C2_c_1cQWcL0o	2.883	91.2	0.00	-7506.053	120.019	alb/P 6/m m m->I b a m (-a+b,-a-b,2c);Bond sets: 2,3:alb
MOF74_14_P21_c_ETUkQ0EL	2.883	88.4	0.00	-7506.052	120.106	flu; sqc169
MOF74_15_C2_c_ouKndAdv	2.741	81.1	0.11	-7506.046	120.675	4,4,8T74
MOF74_41_Aba2_Ydhfs4sF	2.871	89.2	0.00	-7506.045	120.757	flu-3,6-I41cd or kvh1 (All circuits for the 3-c vertex (up to 14): [(6(3),8(10),10(75),12(471),14(3345)).(6(3),8(10),10(75),12(471),14(3345)).(6(3),8(10),10(75),12(471),14(3341))])
MOF74_4_P21_jrloDTV5	2.844	90.5	0.00	-7506.039	121.312	alb-4,8-Cmce
MOF74_4_P21_joEt35Y9	2.895	91.9	0.00	-7506.036	121.611	{4^3.6^3}{4^3}{4^6.6^12.8^3}
MOF74_14_P21_c_oBH0vFd9	2.466	78.8	0.00	-7506.032	122.002	rtl

Structure name	Density / g cm^{-3}	Packing coefficient / %	Void fraction	Energy per f. u. / eV	Relative energy / kJ mol^{-1}	Topology
MOF74_14_P21_c_opuXvxFA	3.012	93.6	0.00	-7506.032	122.045	alb/P 6/m m m->P b c n (a+b,-a+b,2c; 0,0,1/2);Bond sets: 2,3,5,6:alb
MOF74_15_C2_c_JErmYMZW	2.372	77.5	0.09	-7506.029	122.301	flu-3,6-C2/c
MOF74_15_C2_c_LHGO4Cpr	2.738	85.9	0.06	-7506.025	122.697	4,6T5
MOF74_2_P-1_V4T9Stbm	3.073	92.9	0.00	-7506.022	122.957	urj
MOF74_15_C2_c_6neAMFKO	2.654	85.9	0.00	-7506.019	123.324	4,6L45
MOF74_18_P21212_Z4gFgBke	2.934	91.1	0.00	-7506.014	123.797	scu; sqc170
MOF74_2_P-1_0G4YMiP4	2.747	83.5	0.05	-7506.011	124.057	scu; sqc170
MOF74_2_P-1_2unOuYmV	2.845	88.8	0.00	-7506.007	124.432	flu; sqc169
MOF74_14_P21_c_yJbLplO9	2.966	91.9	0.00	-7506.006	124.564	flu; sqc169
MOF74_2_P-1_VC8joErq	2.869	89	0.00	-7506.002	124.906	3,4,7T3
MOF74_15_C2_c_0xOn5mVv	2.349	75.6	0.15	-7506.002	124.969	flu; sqc169
MOF74_2_P-1_0iMGmsuE	2.728	86.7	0.00	-7506.000	125.147	{4^3}2{4^4.6^2}2{4^6.6^6.8^3}{4^8.6^14.8^6}
MOF74_148_H-3_9gtjPJL8	1.991	64.9	0.28	-7505.996	125.527	3,6T18
MOF74_2_P-1_4JjXoS0Z	2.540	79.3	0.13	-7505.989	126.209	{4^2.5^2.6^6.7^4.8}{4^2.5^3.7}
MOF74_14_P21_c_mvPObjoz	2.618	83.3	0.00	-7505.989	126.223	alb-3,6-P42/mnm
MOF74_2_P-1_EQR8obYB	2.720	82.4	0.07	-7505.988	126.316	scu; sqc170
MOF74_2_P-1_vd5eIhR8	2.744	84.9	0.03	-7505.987	126.329	3,4,6T98
MOF74_9_Cc_59hOqijv	2.704	85.2	0.00	-7505.987	126.329	{4^3.6^3}{4^3}{4^6.6^11.8^4}
MOF74_144_P31_ChJmHFtw	2.397	76.8	0.12	-7505.986	126.453	{4^3.6^3}{4^3}{4^6.6^11.8^4}

Structure name	Density / g cm^{-3}	Packing coefficient / %	Void fraction	Energy per f. u. / eV	Relative energy / kJ mol^{-1}	Topology
MOF74_45_Iba2_EIUtPaPm	2.743	87.6	0.02	-7505.986	126.479	scu/P 4/m m m->I 4 c m (a-b,a+b,2c; 1/2,1/2,0);Bond sets: 2,3,4:scu
MOF74_32_Pba2_nYrFdHMh	2.918	92.1	0.00	-7505.984	126.696	alb/P 6/m m m->P b a 2 (-a+b,-a-b,c);Bond sets: 2,4,5,6:alb
MOF74_147_P-3_JXqcG5gi	2.037	66.2	0.27	-7505.978	127.254	csq/P 6/m m m->P -3/Final structure;Bond sets: 2,3,4:csq
MOF74_144_P31_XdeXIfNa	2.612	81.8	0.01	-7505.974	127.585	anh; flu-3,6-P6222
MOF74_148_H-3_7uDQl7X0	2.401	73.9	0.22	-7505.974	127.608	{4^16.6^12}{4^4.6^2}2
MOF74_15_C2_c_YOU9JtbR	2.739	86.3	0.03	-7505.974	127.632	flu-3,6-C2/c
MOF74_2_P-1_MAYm811p	3.053	93.1	0.00	-7505.974	127.657	flu; sqc169
MOF74_4_P21_GpUA4r2h	2.947	91.7	0.00	-7505.972	127.786	{4.6^2}2{4^2.6^10.8^3}
MOF74_15_C2_c_Zy4IO75K	2.856	88.8	0.00	-7505.969	128.143	fit-4,8-P42/mmc
MOF74_2_P-1_UZsTRd3f	2.959	90.2	0.00	-7505.968	128.206	urj
MOF74_3_P2_Fja2xuUq	3.008	92.4	0.00	-7505.966	128.360	alb/P 6/m m m->I m a 2 (a-b,-a-b,-2c; 1/2,0,1/2);Bond sets: 2,3,4,6:alb
MOF74_2_P-1_UNDlZCKm	2.779	83.6	0.07	-7505.964	128.624	{4^10.6^11.8^7}{4^14.6^13.8}{4^16.6^24.8^5}{4^4.6^2}{4^5.6}2{4^6}2{4^8.6^6.8}
MOF74_36_Cmc21_37Cpi3BM	2.585	78.4	0.12	-7505.960	128.988	flu; sqc169
MOF74_2_P-1_mKvIWmuM	2.941	89.2	0.01	-7505.959	129.119	{4^2.5^2.6^2}{4^2.6^2.8^2}{4^4.5^12.6^6.8^6}{4^4.5^3.6^2.7^5.8}{4^5.6}3{4^8.5^7.6^10.7^2.8}
MOF74_2_P-1_knTlFrzR	3.160	95.7	0.00	-7505.956	129.320	flu; sqc169
MOF74_14_P21_c_XCnsWrCC	2.791	87.2	0.00	-7505.948	130.107	rtl

Structure name	Density / g cm^{-3}	Packing coefficient / %	Void fraction	Energy per f. u. / eV	Relative energy / kJ mol^{-1}	Topology
MOF74_12_C2_m_RkIRCLsI	2.871	89.7	0.02	-7505.947	130.213	flu; sqc169
MOF74_15_C2_c_tGrfbWUW	2.785	83.4	0.02	-7505.946	130.343	alb-4,8-Imma (collisions)
MOF74_15_C2_c_EhW1rQNK	3.064	91.2	0.00	-7505.946	130.353	alb/P 6/m m m->I b a m (-a+b,-a-b,2c);Bond sets: 2,3:alb
MOF74_9_Cc_cPqjxdzl	2.728	86.3	0.00	-7505.945	130.454	{4^3.6^3}{4^3}{4^6.6^11.8^4}
MOF74_18_P21212_6Qxd0KFM	3.192	96.1	0.00	-7505.943	130.642	fit
MOF74_2_P-1_3ocCNq9q	2.968	89.6	0.00	-7505.942	130.701	scu; sqc170
MOF74_15_C2_c_OJx5rK7U	2.785	87	0.00	-7505.941	130.850	{4^12.6^16}{4^4.6^2}{4^5.6}
MOF74_9_Cc_k85ikFDZ	2.889	90.7	0.00	-7505.939	130.970	{4^3.6^3}{4^3}{4^6.6^11.8^4}
MOF74_4_P21_5RewDCeF	2.768	85.5	0.00	-7505.938	131.139	{4^12.6^14.8^2}{4^3}{4^6.6^4}
MOF74_148_H-3_5jpXYP7O	2.477	75.2	0.17	-7505.938	131.142	{4^10.6^15.8^3}{4^5.6}2
MOF74_14_P21_c_zfBcDCzy	2.845	90.2	0.00	-7505.937	131.158	kgd
MOF74_41_Aba2_A9yVlUIg	2.523	80.4	0.07	-7505.936	131.289	flu-3,6-I41cd or kvh1 (All circuits for the 3-c vertex (up to 14): [(6(3),8(10),10(75),12(471),14(3345)).(6(3),8(10),10(75),12(471),14(3345)).(6(3),8(10),10(75),12(471),14(3341))])
MOF74_20_C2221_8YDCDRfV	2.945	90.3	0.00	-7505.934	131.453	{4^12.6^16}{4^4.6^2}{4^5.6}
MOF74_14_P21_c_31OipNUp	2.708	82.2	0.08	-7505.933	131.617	{4^12.6^15.8}{4^2.6^3.8}{4^4.6^2}
MOF74_15_C2_c_GwvWTXLM	2.613	83.6	0.00	-7505.927	132.186	fsc; sqc11
MOF74_4_P21_1ISfgLnF	2.787	87.9	0.00	-7505.925	132.326	{4^3.6^3}{4^3}{4^6.6^12.8^3}
MOF74_15_C2_c_5GFIRkX3	2.622	83.5	0.00	-7505.923	132.562	seh-4,6-C2/c
MOF74_15_C2_c_ezoGnNSx	2.772	86.9	0.00	-7505.921	132.755	{4^10.6^16.8^2}{4^3.6^2.8}{4^4.6^2}

Structure name	Density / g cm^{-3}	Packing coefficient / %	Void fraction	Energy per f. u. / eV	Relative energy / kJ mol^{-1}	Topology
MOF74_22_F222_W3fzjOCg	2.784	87.1	0.01	-7505.919	132.924	{4^17.6^11}{4^2.6^4}{4^3.6^3}
MOF74_31_Pmn21_Cl813Esx	2.970	93.3	0.00	-7505.919	132.943	fit
MOF74_2_P-1_DtpNtlyD	3.108	95.8	0.00	-7505.918	132.990	flu; sqc169
MOF74_146_H3_iLzdEPB7	2.133	68	0.24	-7505.915	133.316	{4^3.6^18}{4^3.6^3}{4^3}
MOF74_15_C2_c_s0L1yI0n	2.881	90.6	0.00	-7505.911	133.706	flu; sqc169
MOF74_13_P2_c_dVKvd7YI	2.707	82.8	0.05	-7505.910	133.788	4,6T46
MOF74_9_Cc_ywyCFt7h	2.423	76.5	0.17	-7505.904	134.376	5,10T3;F d d d->F d d 2 (b,c,a;0,3/8,3/8);Bond sets: 2,3,5
MOF74_148_H-3_FF3ALQeF	2.071	66.4	0.24	-7505.902	134.619	{4.6^2}2{4^2.6^6.8^5.10^2}
MOF74_15_C2_c_CtEAqr9H	2.756	83.8	0.06	-7505.900	134.752	{4^14.6^12.8^2}{4^2.6^4}{4^4.6^2}
MOF74_2_P-1_w6iDzAeK	2.694	82.9	0.08	-7505.899	134.849	{4.6^2}2{4^14.6^12.8^2}{4^4.6^10.8}{4^4.6^2}2
MOF74_43_Fdd2_50sfLeis	2.436	79.6	0.03	-7505.895	135.230	sqc/I 41/a m d->F d d 2 (a-b,a+b,c; 0,3/4,1/4);Bond sets: 2,3,4:sqc
MOF74_12_C2_m_EFUIkL3Y	2.946	91.4	0.00	-7505.894	135.384	flu; sqc169
MOF74_15_C2_c_q6KYSGUG	3.036	93.5	0.00	-7505.891	135.631	tcj-4,6-Cccm-1
MOF74_15_C2_c_SfPU8hEh	2.096	68.7	0.21	-7505.890	135.756	flu; sqc169
MOF74_15_C2_c_XYvY4lz4	2.724	84.7	0.00	-7505.889	135.809	urj
MOF74_11_P21_m_BDYL0puM	2.699	85.5	0.03	-7505.886	136.118	kgd
MOF74_43_Fdd2_CN92ntYx	2.419	75.4	0.03	-7505.882	136.504	ant
MOF74_20_C2221_1GfdjSRJ	3.011	92.3	0.00	-7505.876	137.039	{4^3.6^3}{4^5.6}{4^8.6^18.8^2}
MOF74_4_P21_CuVPDKbP	2.826	90.3	0.00	-7505.875	137.160	{4^3.6^3}{4^3}{4^6.6^12.8^3}

Structure name	Density / g cm^{-3}	Packing coefficient / %	Void fraction	Energy per f. u. / eV	Relative energy / kJ mol^{-1}	Topology
MOF74_5_C2_KGS9Jkko	2.921	90.9	0.00	-7505.874	137.264	fse
MOF74_2_P-1_enZMbQ11	3.002	92.6	0.00	-7505.872	137.507	{3^2.4^6.5^6.6}{3^4.4^8.5^8.6^8}{4^12.6^16}{4^4.6^2}{4^5.6}
MOF74_2_P-1_iUixlXfW	2.757	87.2	0.00	-7505.867	137.932	{4^2.6}2{4^3.6^2.8}2{4^4.6^6.8^5}{4^6.6^15.8^6.10}
MOF74_2_P-1_sGdlkvCj	2.747	86.6	0.00	-7505.866	138.025	{4^14.6^12.8^2}{4^14.6^13.8}{4^4.6^2}6{4^8.6^12.8^7.10}
MOF74_11_P21_m_k8XRGnbp	2.500	78.6	0.10	-7505.858	138.795	fsc; sqc11
MOF74_14_P21_c_9Try0ykM	2.882	89.5	0.00	-7505.857	138.954	{4.6^4.8}{4^4.6^2}{4^8.6^19.8}
MOF74_9_Cc_ELV1ZXmx	2.425	77.1	0.12	-7505.855	139.157	{4^3.6^3}{4^3}{4^6.6^11.8^4}
MOF74_2_P-1_OZbCnE4T	2.839	88.3	0.00	-7505.849	139.707	{4^12.5^4.6^8.7^3.8}{4^2.5^6.6^2.8^5}{4^3.6^3}{4^4.5.6}2
MOF74_148_H-3_4fnzEOcm	1.336	44	0.50	-7505.846	140.006	3,6T18
MOF74_11_P21_m_tGdR1KwJ	2.180	70.4	0.19	-7505.837	140.821	kgd
MOF74_2_P-1_nZ3TcrC4	2.810	86.6	0.00	-7505.836	140.907	{4^14.6^13.8}{4^14.6^14}{4^3}2{4^4.6^2}4{4^4.6^6.8^4.10}
MOF74_13_P2_c_hcYuHaix	2.930	91.6	0.00	-7505.832	141.294	fsc; sqc11
MOF74_2_P-1_76Dur7Kb	3.142	95.1	0.00	-7505.827	141.789	flu; sqc169
MOF74_36_Cmc21_W3FeVllu	2.714	87.8	0.00	-7505.826	141.868	4,8T11
MOF74_2_P-1_u9HbqF8j	2.550	79.8	0.09	-7505.826	141.881	{4^2.6}4{4^4.6^4.8^5.10^2}{4^5.6}2{4^7.6^8.8^6}2
MOF74_2_P-1_PTAlGmJr	2.735	85.3	0.00	-7505.825	141.970	{4^2.6^3.8}{4^2.6}2{4^4.6^2}{4^4.6^7.8^4}{4^6.6^16.8^6}
MOF74_13_P2_c_l6IcapKY	2.780	84.4	0.04	-7505.823	142.216	scu; sqc170

Structure name	Density / g cm^{-3}	Packing coefficient / %	Void fraction	Energy per f. u. / eV	Relative energy / kJ mol^{-1}	Topology
MOF74_7_Pc_ayXrsUkh	2.546	80.5	0.02	-7505.823	142.240	{4^2.6^4}{4^2.6}{4^4.6^15.8^2}
MOF74_43_Fdd2_gYFx3eHz	2.507	77.8	0.14	-7505.822	142.273	{4^16.6^12}{4^4.6^2}2
MOF74_148_H-3_PDSLxmGN	1.204	37.8	0.60	-7505.822	142.319	4,8T1
MOF74_43_Fdd2_Dd7CGHOG	2.676	85	0.02	-7505.820	142.500	sqc-3,6-Fdd2
MOF74_2_P-1_LrM0BIV9	3.000	89.4	0.03	-7505.818	142.669	{4^18.6^10}{4^2.6^4}{4^4.6^2}
MOF74_146_H3_1NOBy9dk	2.805	85.3	0.05	-7505.815	142.936	{4^3.6^3}{4^3}{4^6.6^13.8^2}
MOF74_7_Pc_BLLDjxLC	2.681	84.1	0.00	-7505.814	143.069	{5^10.6^5}{5^6}
MOF74_152_P3121_LScegsKX	2.750	86.5	0.03	-7505.812	143.248	alb/P 6/m m m->P 32 2 1 (a,b,3c);Bond sets: 1,2,6:alb
MOF74_147_P-3_Cpf4x1U6	2.144	68.2	0.24	-7505.806	143.801	csq/P 6/m m m->P -3/Final structure;Bond sets: 2,3,4:csq
MOF74_20_C2221_vbXt7BEZ	3.074	91.6	0.00	-7505.805	143.923	{4^11.6^4}{4^32.6^13}{4^6}
MOF74_2_P-1_5SkaS6ra	2.649	82.2	0.04	-7505.804	144.073	{3.4.5}2{3^2.4^3.5.6^3.7^4.8^2}2{4^2.6^2.8^2}
MOF74_82_I-4_ttygiqcr	2.922	89.5	0.00	-7505.800	144.444	{4^12.6^13.8^3}2{4^2.6^4}{4^4.6^2}{4^5.6}2
MOF74_2_P-1_0HnpzZ4O	2.845	88.6	0.00	-7505.793	145.132	{4^12.6^16}{4^4.6^2}{4^5.6}
MOF74_2_P-1_wxHwLOHn	2.397	75.9	0.13	-7505.791	145.255	{4.6.8}2{4.6^2}2{4^2.6^2.8^9.10^2}{4^2.6}2{4^2.8^3.10}{4^4.6^6.8^11.10^6.12}
MOF74_13_P2_c_OhhydARY	2.787	85.3	0.04	-7505.790	145.395	scu; sqc170
MOF74_3_P2_1raROTjV	2.839	86	0.04	-7505.788	145.599	scu; sqc170
MOF74_152_P3121_0RT225et	2.757	85.5	0.04	-7505.787	145.692	alb/P 6/m m m->P 32 2 1 (a,b,3c);Bond sets: 1,2,5,6:alb
MOF74_2_P-1_N2eOc0d9	2.681	84.3	0.06	-7505.779	146.461	{4^2.5^4.6^4.8^5}{4^2.5^4}2{4^2.5^5.6^4.7^3.8}

Structure name	Density / g cm^{-3}	Packing coefficient / %	Void fraction	Energy per f. u. / eV	Relative energy / kJ mol^{-1}	Topology
MOF74_148_H-3_teiYFTch	1.765	53.6	0.44	-7505.777	146.676	4,8T1
MOF74_2_P-1_lTeaVkWl	2.560	81	0.00	-7505.776	146.693	{4.6.8}2{4.6^2}2{4^2.6^4.8^6.10^3}{4^2.6^4.8^7.10^2}{4^2.6}2{4^4.6^7.8^3.10}
MOF74_14_P21_c_tXPC9T2J	3.471	97.4	0.00	-7505.776	146.736	{4^22.6^22.8}{4^7.6^3}2
MOF74_148_H-3_3X2piMso	2.521	80.1	0.09	-7505.772	147.143	{4.6^2}2{4^2.6^8.8^3.10^2}
MOF74_4_P21_VrGJC4Hw	2.852	89.5	0.00	-7505.772	147.165	{4^2.6^4}{4^2.6}{4^4.6^16.8}
MOF74_2_P-1_Ay4tJWpz	3.061	92.3	0.00	-7505.771	147.178	{4^10.5^5.6^9.7^3.8}{4^2.5^4.6^7.7^2}{4^4.5^2}2{4^4.6^2}{4^6.5^4.6^5}{4^6.5^8.6^11.7^2.8}
MOF74_15_C2_c_vWdYtFDm	2.709	85.9	0.00	-7505.767	147.561	tcj-4,6-Cccm
MOF74_2_P-1_ABMx3zMO	2.776	87.7	0.00	-7505.766	147.653	{4^3}2{4^4.6^2}{4^5.6^9.8}2
MOF74_13_P2_c_0VK04VjF	2.935	90.3	0.00	-7505.762	148.077	{4^2.6^4}{4^2.6^8.8^5}
MOF74_2_P-1_8cHetWyk	2.861	89.7	0.00	-7505.759	148.366	flu; sqc169
MOF74_9_Cc_Saz2HEFf	2.709	85.5	0.00	-7505.759	148.410	{4^2.6}{4^4.6^2}{4^6.6^11.8^4}
MOF74_80_I41_3cy2XG0z	2.286	71.1	0.23	-7505.755	148.714	{4^16.6^12}{4^4.6^2}2
MOF74_5_C2_O8SVWdcU	2.928	92.5	0.00	-7505.753	148.915	alb/P 6/m m m->C m c 21 (-a+b,-a-b,2c);Bond sets: 2,4,5,6:alb
MOF74_144_P31_D9YUPbJu	2.818	87.7	0.00	-7505.753	148.934	flu; sqc169
MOF74_58_Pnnm_bo1UBntJ	2.749	84.6	0.06	-7505.750	149.230	rtl
MOF74_152_P3121_EufnTIxU	2.339	75.3	0.15	-7505.748	149.481	flu/fluorite ;F m -3 m->P 32 2 1 (-1/2a+1/2b,-1/2b+1/2c,a+b+c;2/3,0,1/3);Bond sets: 1,2,4:flu

Structure name	Density / g cm^{-3}	Packing coefficient / %	Void fraction	Energy per f. u. / eV	Relative energy / kJ mol^{-1}	Topology
MOF74_7_Pc_VrzD92kr	2.794	87.9	0.00	-7505.745	149.688	{4.6^2}{4^3.6^3}{4^4.6^15.8^2}
MOF74_9_Cc_0Z9DNMGo	3.086	93.8	0.00	-7505.745	149.717	4,8T6
MOF74_14_P21_c_4kqoO06k	2.961	92.8	0.00	-7505.743	149.963	alb-4,8-P21/c-1
MOF74_2_P-1_bQAPgMaR	2.714	85.7	0.00	-7505.742	149.997	{5^10.6^3.8^2}{5^4.6^2}
MOF74_146_H3_X3v5LjaU	2.057	65.3	0.29	-7505.742	150.041	{4.6^2}2{4^2.6^10.8^3}
MOF74_152_P3121_1Ns4tJeo	2.103	68.5	0.23	-7505.741	150.118	{4.6^2}2{4^2.6^6.8^7}
MOF74_15_C2_c_B3L473gM	2.719	85.8	0.00	-7505.736	150.600	seh-4,6-C2/c
MOF74_8_Cm_PgPTv79q	3.033	92.4	0.00	-7505.733	150.926	{4^14.6^22}{4^6}{4^8.6^2}
MOF74_8_Cm_wfJa36TF	2.984	91.9	0.00	-7505.731	151.066	{4^3}{4^6.6^4}{4^9.6^19}
MOF74_11_P21_m_FJLhz5sB	2.956	93.1	0.00	-7505.725	151.652	{4.6^2}{4^4.6^2}{4^8.6^13}
MOF74_14_P21_c_fQtHn02Q	2.962	92.9	0.00	-7505.723	151.806	{5^10.6^3.7.8}{5^4.6^2}
MOF74_2_P-1_Qad7xVe8	2.845	88.2	0.04	-7505.723	151.883	{4^12.6^14.8^2}2{4^2.6^4}{4^4.6^2}{4^5.6}2
MOF74_15_C2_c_hf6UjaTO	2.873	87.4	0.00	-7505.722	151.980	{4^12.6^14.8^2}{4^4.6^2}{4^5.6}
MOF74_4_P21_9rgBmiY5	3.049	92.7	0.00	-7505.721	152.057	{4^5.6}2{4^7.6^20.8}
MOF74_14_P21_c_1YiUujE7	2.975	93.1	0.00	-7505.721	152.076	{5^10.6^3.7.8}{5^4.6^2}
MOF74_151_P3112_E3A5l2M1	1.736	56.6	0.40	-7505.720	152.096	{3.4^2.5^2.6}{3^2.4^2.5^2.6^3.7^5.8}
MOF74_11_P21_m_20lQGYCh	2.449	76.3	0.14	-7505.718	152.298	flu; sqc169
MOF74_2_P-1_3UHSaU5L	2.765	87.1	0.02	-7505.716	152.525	{4^4.6^2}{4^4.6^3.7^8}{6^4.8^2}
MOF74_14_P21_c_X9DSguFM	2.436	79	0.03	-7505.709	153.215	alb-4,8-Cmce

Structure name	Density / g cm^{-3}	Packing coefficient / %	Void fraction	Energy per f. u. / eV	Relative energy / kJ mol^{-1}	Topology
MOF74_144_P31_1ZJSFlMI	2.599	81.6	0.05	-7505.709	153.231	{4.6^2}{4^3.6^3}{4^4.6^12.8^5}
MOF74_12_C2_m_P2HkyS4n	2.974	93.7	0.00	-7505.704	153.725	kgd
MOF74_152_P3121_G53b2AFG	1.192	37.4	0.61	-7505.700	154.029	4,8T68
MOF74_43_Fdd2_UMFyNiFh	2.740	87.4	0.00	-7505.699	154.146	3,6L66
MOF74_15_C2_c_3FBoLrzI	2.729	83.8	0.00	-7505.696	154.450	{4^14.6^12.8^2}{4^2.6^4}{4^4.6^2}
MOF74_14_P21_c_R9NPPxFd	2.642	84.5	0.00	-7505.696	154.488	flu; sqc169
MOF74_36_Cmc21_6jnUZa3W	2.701	80.8	0.10	-7505.694	154.599	flu; sqc169
MOF74_2_P-1_1ikIw0lP	2.795	84.5	0.00	-7505.692	154.817	{4^10.6^2.8^16}{4^12.6^10.8^6}{4^4.6^2}{4^5.6}3
MOF74_2_P-1_4oJFGdif	2.704	86.4	0.00	-7505.691	154.976	{4^2.5^2.6.7}{4^2.5^4.6^2.7^2.8^5}{4^2.5}2{4^4.5^2.8^7.9^2}
MOF74_15_C2_c_3QNKCrgr	2.792	87.1	0.00	-7505.689	155.135	{4^2.5^3.7}{4^2.5^5.6^4.7^4}
MOF74_2_P-1_9o9TIuoc	2.903	90.7	0.00	-7505.686	155.437	{3.4^6.5^3}2{3^4.4^6.5^7.6^5.7^4.8^2}{4^10.5^2.6^3}{4^10.5^7.6^9.7.8}{4^4.6^2}{4^6.5^12.6^8.8^2}
MOF74_2_P-1_HJQHxNPF	2.941	89.6	0.00	-7505.679	156.098	scu; sqc170
MOF74_7_Pc_FldZQwXM	2.484	78.9	0.06	-7505.678	156.153	sit
MOF74_14_P21_c_1ZBOCuVz	2.756	82	0.00	-7505.678	156.172	{4^12.6^3}{4^26.6^18.8}{4^5.6}
MOF74_43_Fdd2_34hOxsZj	2.501	80	0.00	-7505.675	156.476	5,10T3;F d d d->F d d 2 (b,c,a;0,3/8,3/8);Bond sets: 2,3,5
MOF74_15_C2_c_EQWe6Bpt	2.375	76.7	0.07	-7505.673	156.645	{4^12.6^14.8^2}{4^4.6^2}{4^5.6}
MOF74_13_P2_c_IUH0scuN	2.641	83.8	0.04	-7505.666	157.330	cds; 4/6/t4; sqc5

Structure name	Density / g cm^{-3}	Packing coefficient / %	Void fraction	Energy per f. u. / eV	Relative energy / kJ mol^{-1}	Topology
MOF74_4_P21_7KxzMwqL	2.675	82.8	0.02	-7505.666	157.393	{4^5.6}2{4^7.6^20.8}
MOF74_15_C2_c_GPlZql5P	3.368	97	0.00	-7505.663	157.615	5,10T4
MOF74_2_P-1_8ixOoCPb	2.737	88.3	0.00	-7505.663	157.658	sql
MOF74_151_P3112_IWoL2ran	1.970	62.2	0.32	-7505.660	157.936	{4^10.6^5.8^13}{4^5.6}2
MOF74_2_P-1_ln6RWE7N	2.502	80	0.02	-7505.659	157.991	{4^12.6^8.8^8}{4^2.6}2{4^3}2{4^4.6^2}2{4^4.6^8.8^3}2
MOF74_4_P21_uXMOwOfB	2.671	80.8	0.12	-7505.658	158.087	sql
MOF74_2_P-1_SEwdNamn	2.896	90.1	0.00	-7505.652	158.734	{4^2.5^3.7}{4^4.5.6}{4^4.6^2}{4^8.5^2.6^4.7}{4^8.5^6.6^12.7.8}
MOF74_144_P31_m5PUHGIn	2.751	88.2	0.00	-7505.647	159.213	{6^3}2{6^7.8^8}
MOF74_20_C2221_PDNxeVky	2.684	84.7	0.02	-7505.647	159.221	fse
MOF74_15_C2_c_JMLDoSQZ	2.905	87.4	0.00	-7505.643	159.549	seh-4,6-C2/c
MOF74_15_C2_c_1MOmajZf	2.803	89.6	0.00	-7505.638	160.036	4,6L57
MOF74_41_Aba2_9pxL8yBD	2.847	90.6	0.00	-7505.634	160.408	alb/P 6/m m m->C m c 21 (-a+b,-a-b,2c);Bond sets: 2,4,5,6:alb
MOF74_2_P-1_VY70VPtU	2.417	77	0.08	-7505.631	160.747	{3.4^2.6^2.8}2{3^4.4^6.5^4.6^7.7^4.8^3}{4.6^2}2{4^2.6^10.8^3}{4^4.5.6^7.8^3}{4^4.6^2}
MOF74_14_P21_c_Ng211FaQ	2.756	85.6	0.00	-7505.631	160.750	alb-4,8-Cmce
MOF74_15_C2_c_Bxy4P2Ta	2.558	80.8	0.02	-7505.630	160.808	{4^2.5^3.7}{4^2.5^6.6^7}
MOF74_144_P31_UKqeFnll	2.928	90	0.00	-7505.630	160.818	{4^11.6^14.8^3}{4^3}{4^8.6^2}
MOF74_43_Fdd2_8lDKb1jH	2.650	81.6	0.11	-7505.629	160.929	sqc1964

Structure name	Density / g cm^{-3}	Packing coefficient / %	Void fraction	Energy per f. u. / eV	Relative energy / kJ mol^{-1}	Topology
MOF74_32_Pba2_qaMSgPgM	2.991	94	0.00	-7505.627	161.083	alb/P 6/m m m->P b a 2 (-a+b,-a-b,c);Bond sets: 2,4,5,6:alb
MOF74_144_P31_dnmon1dv	2.434	77.1	0.08	-7505.624	161.378	flu/fluorite ;F m -3 m->P 32 2 1 (-1/2a+1/2b,-1/2b+1/2c,a+b+c; 2/3,0,1/3);Bond sets: 1,3,4:flu
MOF74_20_C2221_ecc89uTs	2.929	87.8	0.00	-7505.624	161.445	seh/P 63/m m c->C 2 2 21 (-a-b,a-b,c);Bond sets: 2,3,4:seh
MOF74_31_Pmn21_1aM6UdW2	2.952	93.4	0.00	-7505.623	161.493	3,5L52
MOF74_18_P21212_aqtWbkQV	2.893	87.9	0.00	-7505.621	161.643	flu; sqc169
MOF74_2_P-1_pPC3CGMb	2.886	90.3	0.00	-7505.619	161.905	{3.4.5^3.6}2{3^4.4^4.5^4.6^13.7^2.8}{4^2.5.6^8.8^4}{4^2.6^4}{5^4.6^2}{5^8.6^4.7.8^2}
MOF74_13_P2_c_O5lRxJMn	2.772	87.5	0.00	-7505.618	161.937	4,6L57
MOF74_15_C2_c_JhISfKv3	2.876	87.8	0.00	-7505.614	162.333	{4^16.6^12}{4^4.6^2}2
MOF74_2_P-1_9qKtJaeG	2.921	90.9	0.00	-7505.613	162.432	{3.4.5^3.6}2{3^4.4^4.5^4.6^13.7^2.8}{4^2.5.6^8.8^4}{4^2.6^4}{5^4.6^2}{5^8.6^4.7.8^2}
MOF74_2_P-1_jxjNUlVn	2.783	87.4	0.00	-7505.610	162.786	{4^2.5^2.6^2}2{4^2.5^7.6^4.7.8}{4^2.5^8.6^2.7^2.8}
MOF74_2_P-1_JdVY42Yv	2.842	89.4	0.00	-7505.609	162.847	{4^10.6^17.8}{4^10.6^5}{4^14.6^27.8^4}{4^4.6^2}3{4^5.6}2{4^8.6^16.8^4}
MOF74_7_Pc_fgS0egWv	2.586	81.4	0.00	-7505.609	162.868	{4^3.6^3}{4^3}{4^6.6^13.8^2}
MOF74_39_Abm2_BooRrudx	2.907	92.2	0.00	-7505.606	163.163	flu; sqc169
MOF74_148_H-3_bt8uqNWV	1.352	42.7	0.54	-7505.602	163.536	3,6T18

Structure name	Density / g cm^{-3}	Packing coefficient / %	Void fraction	Energy per f. u. / eV	Relative energy / kJ mol^{-1}	Topology
MOF74_2_P-1_YZibXUUK	3.043	93.6	0.00	-7505.597	163.986	{4^2.6^2.7.8}{4^2.6^4}{4^2.6^7.7^4.8^2}{4^2.6}2{4^4.6^2}{4^4.6^5.8^5.10}{4^6.6^10.7^2.8^9.10}
MOF74_2_P-1_2EulfOYW	2.730	85.7	0.00	-7505.595	164.242	fsc; sqc11
MOF74_2_P-1_NRH4UFEr	2.809	86.7	0.00	-7505.594	164.333	{4^13.6^15}2{4^2.6}2{4^4.6^2}2{4^4.6^4.8^5.10^2}{4^6}2
MOF74_2_P-1_Tw6UJjX3	3.030	90.2	0.00	-7505.590	164.707	kgd
MOF74_4_P21_0BgkYt4v	2.835	87.5	0.00	-7505.590	164.711	{4.6^2}{4^3.6^3}{4^4.6^12.8^5}
MOF74_144_P31_xbT5mJnK	2.478	77.5	0.12	-7505.583	165.372	{4.6^2}2{4^2.6^10.8^3}
MOF74_2_P-1_pd6qKNxB	2.679	86.2	0.00	-7505.580	165.595	sql
MOF74_13_P2_c_InqDHwY9	2.853	91.2	0.00	-7505.580	165.613	alb/P 6/m m m->P 2/c (-a-2b,c,2b);Bond sets: 2,3,5,6:alb
MOF74_14_P21_c_5Es9Grs3	3.121	95.9	0.00	-7505.580	165.652	alb-4,8-Cmce
MOF74_146_H3_bsicn5uo	2.402	77.1	0.12	-7505.577	165.957	{4^2.6^4}{4^2.6}{4^4.6^15.8^2}
MOF74_2_P-1_oLztbPtO	2.754	85.5	0.02	-7505.575	166.089	{4^2.6^2.8^2}{4^2.6}2{4^3}2{4^4.6^2.8^7.10^2}{4^4.6^2}{4^6.6^6.8^16}{4^6.6^6.8^3}
MOF74_31_Pmn21_0OmJrfmX	2.962	93.1	0.00	-7505.575	166.091	{4^14.6^22}{4^6}{4^8.6^2}
MOF74_9_Cc_PtCTNfyp	1.604	51.1	0.45	-7505.571	166.467	3,4,7T10
MOF74_2_P-1_GloQ0Uda	2.796	88	0.03	-7505.567	166.945	{4.5^2}2{4^2.5^2.6.7}2{4^2.5^4.6^7.7.8}{4^4.6^6.8^4.9}{5^6.6^6.7^3}
MOF74_147_P-3_P5fmKRea	2.480	76.8	0.16	-7505.565	167.109	csq/P 6/m m m->P -3/Final structure;Bond sets: 2,3,4:csq

Structure name	Density / g cm^{-3}	Packing coefficient / %	Void fraction	Energy per f. u. / eV	Relative energy / kJ mol^{-1}	Topology
MOF74_2_P-1_CyFHQwbj	2.938	91.2	0.00	-7505.565	167.128	{3.4^3.5^2}2{3^4.4^6.5^4.6^7.7^4.8^3}{4^2.5^2.6^2}{4^2.5^6.6^5.8^2}{4^6.6^9}{4^8.5^3.6^10.7.8^6}
MOF74_20_C2221_gaSBt3S0	2.660	84.7	0.00	-7505.564	167.147	3,6L66
MOF74_41_Aba2_lqlJJIXk	2.829	90.8	0.00	-7505.563	167.253	alb/P 6/m m m->C m c 21 (-a+b,-a-b,2c);Bond sets: 2,4,5,6:alb
MOF74_4_P21_2nJx2H92	2.603	82.3	0.08	-7505.563	167.258	{4^10.6^16.8^2}{4^4.6^2}{4^6}
MOF74_144_P31_JRWDAAwB	2.569	81.8	0.02	-7505.559	167.688	anh; flu-3,6-P6222
MOF74_146_H3_GshRiSe8	2.719	83.4	0.00	-7505.559	167.713	{4^3}5{4^4.6^9.8^8}3{4^9.6^6}
MOF74_11_P21_m_JSnA1jC7	3.125	93.8	0.00	-7505.555	168.030	alb/P 6/m m m->C m c m (-a-b,a-b,2c; 0,0,1/2);Bond sets: 1,2,4:alb
MOF74_15_C2_c_ONPIVSHg	2.932	90.3	0.00	-7505.555	168.030	flu; sqc169
MOF74_2_P-1_SMWsM7Ug	2.873	88.4	0.00	-7505.555	168.083	{3.4^7.5^2}2{3^4.4^12.5^8.6^14.7^4.8^3}{4^10.6^16.8^2}{4^10.6^5}{4^12.5^3.6^12.8}{4^4.6^2}2
MOF74_2_P-1_mBTvgiOL	2.856	88	0.01	-7505.555	168.083	{4^2.5^3.7}{4^4.5.6}{4^4.6^2}{4^8.5^2.6^4.7}{4^8.5^6.6^12.7.8}
MOF74_8_Cm_WseNmSku	2.961	90.9	0.00	-7505.554	168.179	{4^12.6^15.8}{4^3}{4^6.6^4}
MOF74_13_P2_c_sYUBPsPy	2.795	86.5	0.03	-7505.552	168.387	fsc; sqc11
MOF74_7_Pc_Dt6QNkDv	2.664	83.5	0.00	-7505.550	168.556	{4^3}{4^5.6^16}{4^5.6}
MOF74_2_P-1_65bl2wYC	2.801	85.3	0.00	-7505.544	169.077	{4^12.6^3}{4^14.6^12.8^2}{4^22.6^21.8^2}{4^4.6^2}{4^6}2

Structure name	Density / g cm^{-3}	Packing coefficient / %	Void fraction	Energy per f. u. / eV	Relative energy / kJ mol^{-1}	Topology
MOF74_2_P-1_dBn1TZ49	3.083	93.3	0.00	-7505.543	169.183	{4^10.6^24.8^10.10}{4^2.6^3.8}{4^2.6^4}{4^4.6^2}2{4^4.6^9.8^2}{4^5.6}2{4^8.6^17.8^3}
MOF74_148_H-3_rTYRTjNU	2.288	72.3	0.21	-7505.542	169.286	3,6T18
MOF74_14_P21_c_7Ajcm9hW	3.096	95.3	0.00	-7505.535	170.018	alb/P 6/m m m->P b c n (-a+b,-a-b,2c; 0,0,1/2);Bond sets: 2,3,4,6:alb
MOF74_14_P21_c_I0R9CxIl	2.715	87	0.00	-7505.532	170.298	rtl
MOF74_7_Pc_hvSxyV1I	3.187	95.2	0.00	-7505.531	170.384	{4^14.6^22}{4^6}{4^8.6^2}
MOF74_144_P31_NkakvNCX	2.724	84.7	0.02	-7505.527	170.804	{4^2.6}{4^3.6^3}{4^8.6^9.8^4}
MOF74_5_C2_3uBX4Rel	2.602	82.3	0.09	-7505.525	170.930	{4.6^2}2{4^2.6^11.8^2}{4^4.6^2}2{4^5.6^22.8}
MOF74_146_H3_4wxzbEti	2.843	85.5	0.07	-7505.522	171.203	{4^2.6}{4^3.6^3}{4^8.6^10.8^3}
MOF74_144_P31_YtCKLN4F	2.957	92.9	0.00	-7505.521	171.383	{4^4.6^2}2{4^8.6^16.8^4}
MOF74_148_H-3_FuJ1fD22	2.038	66.5	0.25	-7505.520	171.422	{4.6^2}2{4^2.6^8.8^3.10^2}
MOF74_152_P3121_4U9JZzJt	2.172	71.2	0.14	-7505.519	171.489	{4.6^2}2{4^2.6^10.8^3}
MOF74_2_P-1_uJ4UZNde	3.008	89.6	0.00	-7505.518	171.615	{4^14.6^10.8^4}{4^4.6^2}{4^6}
MOF74_8_Cm_DQdn5dpr	3.000	93	0.00	-7505.511	172.317	3,4,7T50
MOF74_148_H-3_BZyoSOg4	2.243	71.4	0.20	-7505.510	172.351	3,6T18
MOF74_144_P31_lbVrmc68	2.415	78.1	0.09	-7505.508	172.599	anh; flu-3,6-P6222
MOF74_15_C2_c_3t0js24g	1.647	51.3	0.46	-7505.504	172.999	{4^10.6^2.8^16}{4^5.6}2
MOF74_34_Pnn2_hZdNrRNn	2.924	92	0.00	-7505.502	173.187	{4^2.6}2{4^4.6^10.8}

Structure name	Density / g cm^{-3}	Packing coefficient / %	Void fraction	Energy per f. u. / eV	Relative energy / kJ mol^{-1}	Topology
MOF74_36_Cmc21_OOPVNg58	3.013	91.9	0.00	-7505.495	173.887	alb/P 6/m m m->C m c m (-a-b,a-b,2c; 0,0,1/2);Bond sets: 1,2,4:alb
MOF74_2_P-1_7B1cmLnw	2.761	82.9	0.12	-7505.483	175.048	scu; sqc170
MOF74_4_P21_yaSJphtN	2.951	93.3	0.00	-7505.480	175.257	flu; sqc169
MOF74_11_P21_m_6II8Ylxz	2.367	74	0.21	-7505.478	175.522	scu; sqc170
MOF74_11_P21_m_dbzm60N2	3.155	96.2	0.00	-7505.468	176.497	{4.6^2}{4^4.6^2}{4^8.6^13}
MOF74_13_P2_c_oOx4ZadF	2.788	83.2	0.11	-7505.453	177.944	{4^16.6^12}{4^4.6^2}2
MOF74_13_P2_c_cFuUiWok	2.679	80.9	0.11	-7505.449	178.306	sql
MOF74_148_H-3_uP0sqfiO	2.400	77.7	0.04	-7505.426	180.546	4,8T11-3,6-R-3m
MOF74_2_P-1_LIUpVwKt	2.590	82.6	0.05	-7505.424	180.718	3,4,6T77
MOF74_144_P31_RSKyQYqL	2.635	82.8	0.04	-7505.424	180.723	{4^2.6}{4^3.6^2.8}{4^8.6^6.8^7}
MOF74_5_C2_6pHlu2Ko	2.682	87.7	0.00	-7505.422	180.906	{4^2.6}2{4^4.6^10.8}{4^5.6}2{4^7.6^16.8^5}
MOF74_11_P21_m_LYACoXJF	3.175	93.2	0.00	-7505.415	181.606	{4^11.6^4}{4^32.6^13}{4^6}
MOF74_58_Pnnm_eZPoKSm3	2.264	73	0.20	-7505.407	182.353	rtl
MOF74_14_P21_c_yFRiR7UC	2.890	88.7	0.00	-7505.397	183.323	kgd
MOF74_4_P21_1YSAFSh9	2.940	93	0.00	-7505.318	190.941	4L4
MOF74_32_Pba2_KqLmQBfp	2.652	85.9	0.00	-7505.275	195.070	{4^2.6}2{4^4.6^10.8}
MOF74_148_H-3_Hsx7d5Br	2.194	69.2	0.26	-7505.156	206.581	3,6T18
MOF74_174_P-6_8mSKkkAD	2.430	73.8	0.22	-7504.985	223.051	csq

Table **S8**. Calculated parameters for the predicted hydrated structures of Zn_2**DHTA** after geometry optimization with PBE+MBD* method. The relative energies are provided with respect to lowest energy hydrated structure (see section 1.5 for details).

Structure name	Density / g cm^{-3}	Packing coefficient / %	Void fraction	Energy per f. u. (corrected for water) / eV	Relative energy / kJ mol^{-1}	Topology
MOF74_14_P21_c_8ykFjmN5	2.860	91.7	0.00	-7507.297	0.000	flu; sqc169
MOF74_43_Fdd2_gYFx3eHz	2.865	91.8	0.00	-7507.057	23.156	4,8T209
MOF74_9_Cc_ouBwFZkd	2.272	75.4	0.13	-7506.887	39.549	{3.4^2.5^2.6}{3^2.4^2.5^5.6^4.7.8}
MOF74_34_Pnn2_g64zCePU	2.549	85.4	0.00	-7506.882	40.051	rtl
MOF74_15_C2_c_JErmYMZW	2.002	72.4	0.09	-7506.817	46.244	1D
MOF74_13_P2_c_hcYuHaix	2.478	81.1	0.06	-7506.724	55.281	{3^2.4^4.5^4.6^3.7^2}{3^2.4^4.5^4.6^4.7}{3^2.6^2.7^2}
MOF74_11_P21_m_6II8Ylxz	2.556	83.8	0.03	-7506.622	65.084	scu; sqc170
MOF74_147_P-3_5YRSbNhe	2.023	67.9	0.19	-7506.600	67.183	csq/P 6/m m m->P -3/Final structure;Bond sets: 2,3,4:csq
MOF74_147_P-3_6N8uMV7L	1.984	68.1	0.23	-7506.580	69.164	csq/P 6/m m m->P -3/Final structure;Bond sets: 2,3,4:csq
MOF74_2_P-1_jHOzVFNo	2.351	75.5	0.15	-7506.523	74.673	{3.4^3.6^2}2{3^4.4^6.5^4.6^6.7^4.8^4}{4^4.6^2}{4^6.5.6^5.8^3}
MOF74_15_C2_c_wkeUitAg	2.541	82.5	0.06	-7506.400	86.565	4,6T5
MOF74_148_H-3_7uDQl7X0	1.809	63.0	0.22	-7506.262	99.839	nbo; 4/6/c2; sqc35

Structure name	Density / g cm^{-3}	Packing coefficient / %	Void fraction	Energy per f. u. (corrected for water) / eV	Relative energy / kJ mol^{-1}	Topology
MOF74_15_C2_c_LHGO4Cpr	2.502	80.3	0.09	-7506.206	105.278	{4^2.5^2.6^2}{4^2.5^6.6.7^2.8^4}{5^4.6.8}
MOF74_148_H-3_PDSLxmGN	1.326	44.2	0.52	-7506.106	114.933	4,8T1
MOF74_2_P-1_GloQ0Uda	2.722	87.2	0.00	-7506.006	124.563	{4^2.6}2{4^3.6^2.8}2{4^4.5^7.6^2.7^2}{4^4.6^2}{4^4.6^6.8^4.9}{4^6.5^8.6^5.7^4.8^5}
MOF74_143_P3_pAlrmY1w	2.141	70.9	0.18	-7506.002	124.906	3,6L66
MOF74_148_H-3_4fnzEOcm	1.520	53.8	0.35	-7505.994	125.714	3,6T18
MOF74_152_P3121_G53b2AFG	1.317	43.8	0.52	-7505.989	126.177	4,8T68
MOF74_80_I41_3cy2XG0z	1.600	56.0	0.33	-7505.971	127.929	dia; 4/6/c1; sqc6

4. References

1. Ong, S. P. *et al.* Python Materials Genomics (pymatgen): A robust, open-source python library for materials analysis. *Comput. Mater. Sci.* **68**, 314–319 (2013).
2. Togo, A. & Tanaka, I. Spglib: a software library for crystal symmetry search. *arXiv* (2018). doi:arXiv:1808.01590
3. Aroyo, M. I. *et al.* Crystallography online: Bilbao crystallographic server. *Bulg. Chem. Commun.* **43**, 183–197 (2011).
4. Aroyo, M. I. *et al.* Bilbao Crystallographic Server: I. Databases and crystallographic computing programs. *Z. Kristallogr.* **221**, (2006).
5. Aroyo, M. I., Kirov, A., Capillas, C., Perez-Mato, J. M. & Wondratschek, H. Bilbao Crystallographic Server. II. Representations of crystallographic point groups and space groups. *Acta Crystallogr.* **A62**, 115–128 (2006).
6. Clark, S. J. *et al.* First principles methods using CASTEP. *Z. Kristallogr.* **220**, 567–570 (2005).
7. Perdew, J. P., Burke, K. & Ernzerhof, M. Generalized Gradient Approximation Made Simple. *Phys. Rev. Lett.* **77**, 3865–3868 (1996).
8. Grimme, S. Semiempirical GGA-type density functional constructed with a long-range dispersion correction. *J. Comput. Chem.* **27**, 1787–1799 (2006).
9. Chisholm, J. A. & Motherwell, W. D. S. COMPACK : a program for identifying crystal structure similarity using distances. *J. Appl. Crystallogr.* **38**, 228–231 (2005).
10. Spek, A. L. Structure validation in chemical crystallography. *Acta Crystallogr.* **D65**, 148–155 (2009).
11. Blatov, V. A., Shevchenko, A. P. & Proserpio, D. M. Applied Topological Analysis of Crystal Structures with the Program Package ToposPro. *Cryst. Growth Des.* **14**, 3576–3586 (2014).
12. Blatov, V. A. & Proserpio, D. M. ToposPro Version 5.0 Practical Manual 1.1.4. (2017). Available at: topospro.com/download/manuals/topos_practical_manual_5.0_1.1.4.pdf.
13. Friščić, T. New opportunities for materials synthesis using mechanochemistry. *J. Mater. Chem.* **20**, 7599–7605 (2010).
14. Friščić, T. *et al.* Ion- and Liquid-Assisted Grinding: Improved Mechanochemical Synthesis of Metal-Organic Frameworks Reveals Salt Inclusion and Anion Templating. *Angew. Chem. Int. Ed.* **49**, 712–715 (2010).
15. Altomare, A. *et al.* New techniques for indexing: N-TREOR in EXPO. *J. Appl. Crystallogr.* **33**, 1180–1186 (2000).
16. Altomare, A. *et al.* EXPO2013 : a kit of tools for phasing crystal structures from powder data. *J. Appl. Crystallogr.* **46**, 1231–1235 (2013).
17. Wang, X. *et al.* Syntheses, Crystal Structures, and Luminescent Properties of Three Novel Zinc Coordination Polymers with Tetrazolyl Ligands. *Inorg. Chem.* **44**, 5278–5285 (2005).
18. Le Bail, A., Suroy, H. & Fourquet, J. L. Ab-Initio Structure Determination of $LiSbW0_8$ by X-ray Powder Diffraction. *Mat. Res. Bull.* **23**, 447–452 (1988).

AB INITIO PREDICTION OF METAL-ORGANIC FRAMEWORK STRUCTURES

James P. Darby,[1†] Mihails Arhangelskis,[2†] Athanassios D. Katsenis,[2] Joseph M. Marrett,[2] Tomislav Friščić,[2] and Andrew J. Morris[3]*

[1]TCM Group, Cavendish Laboratory, 19 JJ Thomson Avenue, Cambridge, CB3 0HE, UK.

[2]Department of Chemistry, McGill University, 801 Sherbrooke Street W., Montreal H3A 0B8, Canada.

[3]School of Metallurgy and Materials, University of Birmingham, Edgbaston, Birmingham B15 2TT, UK.

[†]These authors contributed equally to this work

Abstract

Metal-organic frameworks (MOFs) have emerged as highly versatile materials with applications in gas storage and separation, solar light energy harvesting and photocatalysis. The design of new MOFs, however, has been hampered by the lack of computational methods for *ab initio* crystal structure prediction, which could be used to direct experimental synthesis. Here we report the first *ab initio* method for MOF structure prediction, and test it against a diverse set of MOFs, with differences in topology, metal coordination geometry and ligand binding sites. In all cases our calculations produced structures which match experiment, proving the versatility of our procedure for MOF structure prediction. With our new methodology for *ab initio* structure prediction, current approaches to MOF design are set to change towards a more systematic, theory-driven, materials development.

Introduction

Metal-organic frameworks (MOFs) are one of the most rapidly developing and recently commercialised classes of modern materials, based on combining diverse metal-based nodes with differently substituted organic linkers. They provide the chemist and the materials scientist with a unique opportunity to couple high levels of microporosity with other types of functional behaviour in a single material. Such modular nature has enabled the development of MOFs[1,2] for a wide range of applications, including gas sorption[3,4] and separation,[5] sequestration of greenhouse gases,[6] light harvesting[7] and photocatalysis,[8] capture of harmful volatile agents[9] and more. Currently the majority of MOFs are developed *via* experimental screening guided by an empirical node-and-linker approach[10] and isoreticular design,[11] which enable precise metric engineering of structures based on rigid building blocks with robust connection geometry. These approaches are not sufficient to address the design of MOFs based on more complex building blocks, for example rod-like secondary building units (SBUs), or the design of highly attractive but topologically diverse materials, including metal azolates and zirconium carboxylate systems.[12] The design of such materials would involve high-level computational modelling and structure prediction, allowing for the prediction of one-, two- and three-dimensional motifs (1-D, 2-D and 3-D motifs) from a given set of metals and linkers.

However, whereas the computational prediction of physical properties for MOFs with known structures has been accomplished,[13,14] the development of computational methods for truly *ab*

initio crystal structure prediction (CSP) of new MOF materials remains a key challenge. This is in stark contrast with the general progress of CSP, which has been used, for example, to predict the high pressure phases of minerals found in the Earth[15] or other planetary systems,[16] new allotropes of elemental solids,[17,18] porous molecular materials,[19] high-temperature superconductors[20] and the structure of battery electrodes.[21] In case of MOFs, computational methods have been utilised to optimise gas sorption performance[22] and study host-guest binding interactions.[6] Periodic density-functional theory (DFT) calculations have recently been deployed to evaluate the stability of MOF topological polymorphs,[14,23] simulate gas sorption behaviour[6] and study mechanisms of MOF-based chemical reactions.[24] Topology-based structure predictions were performed for zeolitic imidazolate frameworks (ZIFs)[25] and polyoxometalate MOFs (POMOFs).[26] We have recently utilised such calculations, aided by crystallographic database searches, to study and anticipate the structural landscapes of previously unreported MOF materials.[27,28] None of these studies, however, performed *ab initio* structure searching but instead relied on databases[13] as an initial source of structures. The limitations of such an approach are evident: by drawing the structures from a database we exclude the possibility of finding new MOF topologies, which are most likely to lead to materials with unprecedented properties.

Here, we report a method for true *ab initio* crystal structure prediction of MOF materials, that is the prediction of three-dimensional (3D) crystal packing and topological connectivity starting from a molecular diagram of nodes and linkers. Our approach is based on a highly successful *ab initio* random structure sampling (AIRSS) algorithm.[29] We refer to our herein outlined approach as Wyckoff Alignment of Molecules (WAM).

Wyckoff Alignment of Molecules

Central to the WAM methodology is the ability to impose symmetry on trial structures, which accelerates the AIRSS search by reducing the dimension of the search space and speeds up the relaxation process. For MOFs this decision is experimentally justified, as 99.5% of MOFs in the Cambridge Structural Database (CSD) are reported with a space group other than *P1*.[30] Having decided to impose symmetry, trial structures can be generated by randomly decorating the Wyckoff sites of a random unit cell commensurate with a random space group. Wyckoff sites are orbits of symmetry-equivalent positions under the action of the space group, where the number of such positions within a site is its multiplicity. For each position within a Wyckoff site some of the space group operators will leave it invariant. These form the site symmetry group of the position, which is isomorphic to the site symmetry group of all other positions within the same site. There are two types of Wyckoff sites: the general site which has no symmetry, and special sites which have symmetry. Very importantly, it is not possible for an object to move from one Wyckoff site to another during a geometry optimisation, which means that a space group cannot be effectively sampled by decorating only general Wyckoff sites.

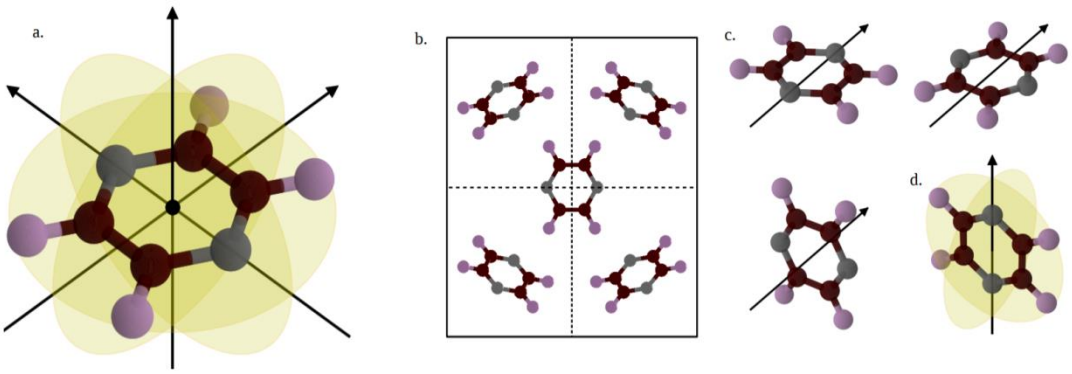

Figure 1. a) A molecule of pyrazine, with symmetry elements shown. Carbon, Nitrogen and Hydrogen atoms are in brown, grey and pink respectively. Yellow planes, black arrows and the black dot represent mirror planes, two-fold rotation axes and a centre of inversion respectively. b) A five molecule *Pmm2* cell, viewed down the *c*-axis. The dotted lines are mirror planes. Four of the molecules are on the general site, whilst the central molecule is on a special site. c) Three distinct ways of orienting a pyrazine molecule on a two-fold rotation axis: each orientation has one degree of freedom corresponding to the rotation of the molecule about the two-fold axis. d) One of the six orientations of a pyrazine molecule on an *mm2* site. This orientation has no rotational degrees of freedom.

The herein presented WAM approach overcomes this obstacle by allowing the placement of molecules onto special Wyckoff sites, as illustrated by Figure 1b which depicts a structure with a *Pmm2* space group and five molecules per unit cell, which cannot be generated using only the general site. In fact, it is only possible to make a structure with space group *P1* using five molecules per cell, as *P1* is the only space group where the general site multiplicity is a factor of five. To place a molecule onto a special Wyckoff site it must possess at least as much symmetry as the site itself (the site symmetry group must be a subgroup of the point group of the molecule). Additionally, the molecule must be oriented to respect the symmetries of the site. In general, there are multiple, symmetry distinct, alignments for a molecule, each of which may have associated rotational degrees of freedom. We consider alignments to be symmetry distinct if it is impossible to convert smoothly between them whilst preserving the site symmetry, as illustrated in Figure 1c where the three symmetry distinct ways of placing a pyrazine molecule on a two-fold rotation axis are shown. Further details and an outline of the algorithm used to align the molecules are contained in the Supporting Information.

Using this AIRSS+WAM approach has enabled us to demonstrate the first *ab initio* prediction of the lowest-energy structure and exploration of phase landscape for MOF structures. In this study we have restricted ourselves to the prediction of MOF structures based on zinc. Zinc is by far the most commonly used metal in MOF chemistry and, from a computational point of view, its closed shell d^{10} electronic configuration relieves the need to consider magnetic interactions between the metal centres, while being able to demonstrate the full power of WAM in sampling the MOF structural space.

As our initial foray into demonstrating the potential of the WAM method, we performed *ab initio* structure prediction for several distinct, progressively more challenging, types of MOFs. Specifically, we addressed the popular SIFSIX-3-Zn framework which is based on two types of linkers: the anionic hexafluorosilicate (**SiF_6^{2-}**) and the neutral pyrazine (**pyr**) unit; the topologically flexible metal azolate frameworks (MAFs)[31] based on tetrazolate (**ttz**$^-$) and 1,2,4-triazolate (**trz**$^-$) linkers, as well as the popular MOF-74 (also known as CPO-27)[32]

framework containing 2,4-dihydroxyterephthalate (**DHTA^{4-}**) ligand, which is an archetypal example of a framework based on a rod-like SBU and a framework exhibiting open metal sites, renowned for its applications in sorption properties and catalytic activity.[33] The diversity of MOF structures that are herein shown to be amenable to WAM method illustrates the generality of this method as a ground-breaking development in the design of future MOFs.

Prediction of the SIFSIX-3-Zn framework of zinc, pyrazine and hexafluorosilicate

As an introductory example to demonstrate the capabilities of WAM, we performed a CSP calculation for a zinc-based representative of the SIFSIX-3-M family of MOFs that was found to be particularly attractive in the context of carbon dioxide capture.[34,35] The framework comprises **pyr** and **SiF_6^{2-}** linkers, with an overall formula Zn(**pyr**)$_2$**SiF_6**. A total of 2000 randomly-generated structures containing one MOF formula unit per crystallographic primitive cell were generated by WAM. The trial structures were geometry-optimised using the CASTEP plane-wave periodic DFT code.[36] The optimised structures were ranked in terms of overall lattice energy and the duplicate structures were removed. Initial energy ranking was achieved using the LDA functional, while the final set of unique lowest energy structures was re-ranked using the PBE functional combined with many body dispersion (MBD*) correction scheme. The latter method has been previously demonstrated to offer highly accurate energies of MOF polymorphs.[28] Finally, the topological connectivity and framework packing density was evaluated for the remaining structures. The calculated energy landscape is shown on Figure 2.

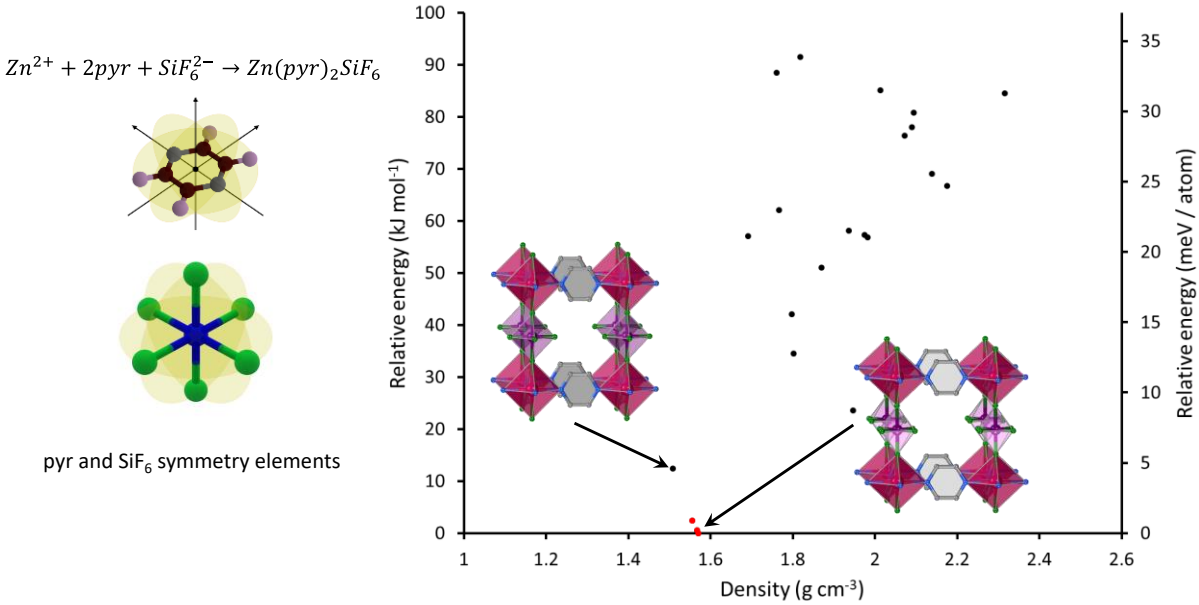

Figure 2 Ligand structure and calculated crystal energy landscape of SIFSIX-3-Zn. Each black dot represents a crystal structure. The low energy structures marked with red dots match with the experimental structures of ***pcu*** topology, found in CSD (FUDQIF, KEDZAX). Further on, a closely related *pcu* structure is found at an energy of +12.4 *kJ mol^{-1}*. The two low energy structures having ***pcu*** topology are highlighted. The principle difference between these *pcu* structures is the orientation of the **SiF_6^{2-}** linker with respect to unit cell axes, as seen on the structure diagrams.

Gratifyingly, the lowest energy predicted structure was identified as a match to the experimentally reported structure (CSD code FUDQIF[37]). In FUDQIF, each Zn^{2+} ion is coordinated by four **pyr** molecules that interconnect metal ions to form two-dimensional (2D)

square sheets. The sheets are, in turn, interconnected by $\mathbf{SiF_6^{2-}}$ anions acting as linkers between neighbouring sheets through Zn-F bonds, resulting in a three-dimensional (3D) primitive cubic (*pcu*) topology net.[37,38] Interestingly, structures matching the experimental lattice of SIFSIX-3-Zn were found in multiple space groups, reflecting varying degrees of structural order. In particular, the highest symmetry structure was found in the space group *P4/mmm*. Under the constraints of this space group the **pyr** linkers were constrained to lie in the (100) and (010) crystallographic planes, while the Si-F bonds of each $Zn^{2+}\cdots\mathbf{SiF_6^{2-}}\cdots Zn^{2+}$ unit were constrained to align at 45° with respect to the crystallographic lattice vectors. In addition, a closely related structure of *P*4/*mmm* symmetry with Si-F bonds aligned along the lattice vectors was located 9.0 *kJ mol*$^{-1}$ higher in energy. Going down the symmetry ladder, two structures with *C2/m* and *P-1* symmetries were found to be 3.6 *kJ mol*$^{-1}$ lower in energy, on the grounds of allowing the $\mathbf{SiF_6^{2-}}$ and **pyr** linkers to deviate from the crystallographic lattice planes. We believe that the symmetry distortions observed in our predicted structure signify the possibility of disorder in the SIFSIX-3-Zn structure and, indeed, rotational disorder of pyrazine linkers has been observed experimentally (crystal structure KEDZAX[38]) and also rationalised using molecular dynamics (MD) simulations.[38]

The herein demonstrated ability to generate the structures with varying degree of symmetry highlights the flexibility of WAM method in exploring all symmetry options, rather than bluntly going with the highest possible symmetry warranted by the point groups of the molecular fragments. Consequently, we expect the WAM functionality on top of AIRSS to become a powerful method for systematically exploring the effect of structural disorder on MOF stability.

Beyond those matching the experimentally observed *pcu*-topology structure, the other predicted structures of $Zn(\mathbf{pyr})_2\mathbf{SiF_6}$ composition were found to be at least 20 *kJ mol*$^{-1}$ higher in energy than the experimentally observed disordered structure. This lets us conclude that the *pcu*-topology lattice maximises the number of metal-linker interactions. Moreover, a careful examination of the higher energy predicted structures reveals sub-optimal lattice connectivity, where certain binding sites of **pyr** and/or $\mathbf{SiF_6^{2-}}$ linkers remained unutilised.

Prediction of metal azolate framework (MAF) structures

Metal azolate frameworks (MAFs)[31] are a class of MOFs based on azolate linkers, namely 5-membered carbon/nitrogen aromatic rings. The MAF family of materials, including zeolitic imidazolate frameworks,[39] have emerged initially as metal-organic topological analogues of zeolites. However, the diversity of available metals and azolate linkers has led to materials with a wide range of topologies previously not seen in the zeolite domain. A particularly remarkable feature of MAFs is their topological diversity, demonstrated by their ability to form true framework polymorphs, *i.e.* framework materials of identical chemical composition but different topologies. While such polymorphism provides an opportunity to generate different structures from the same set of building blocks, it is also a major challenge in materials design: for many MAFs the topological landscape remains incompletely explored, with new phases still being discovered even for well-studied systems, and it is currently not possible to predict from first principles what the preferred topology of a framework will be for a particular combination of nodes and linkers.

Here, we focused on two systems: zinc tetrazolate, $Zn(\mathbf{ttz})_2$ and 1,2,4-triazolate, $Zn(\mathbf{trz})_2$. Both materials have been experimentally found to form interpenetrated diamondoid (*int-dia*)

structures,[40,41] while a second polymorph with *tsa* topology has been recently reported for Zn(**trz**)$_2$.[42] Consequently, this pair of frameworks provides an excellent opportunity to validate the ability of WAM calculations to reproduce the experimentally observed structures, and investigate the possibility of yet unreported topological polymorphs.

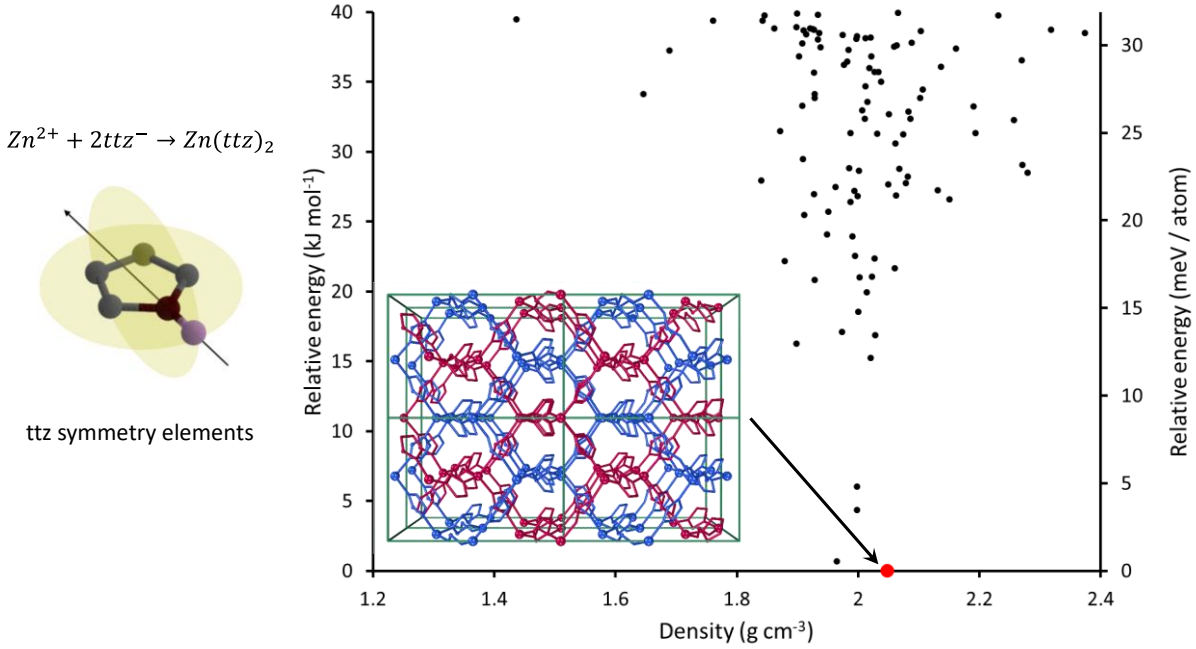

Figure 3. Ligand structure and calculated crystal energy landscape of Zn(**ttz**)$_2$. Each black dot represents a crystal structure. The lowest energy predicted structure, having *int-dia* topology, which closely matches with the experimental structure (CSD WAQRAI), is shown in red. The crystal packing diagram of the lowest energy predicted structure is provided on the inset, with the two interpenetrated diamondoid nets shown in red and blue.

Calculations for the Zn(**ttz**)$_2$ system resulted in a dense, highly populated energy landscape (Figure 3), with around 35 distinct crystal structures within a 30 *kJ mol^{-1}* energy window above the most stable predicted structure. This is in stark contrast to the structure prediction in the Zn(**pyr**)$_2$**SiF$_6$** system, where the lowest-energy structure was separated by over 20 *kJ mol^{-1}* from the closest alternative crystal packing. The majority of predicted Zn(**ttz**)$_2$ polymorphs exhibit very small solvent-accessible voids or none at all. Importantly, such dense structures cannot be efficiently stabilised by guest inclusion, a factor known to drive the experimental formation of high-energy structures of low framework density (*i.e.* number of nodes per unit volume).

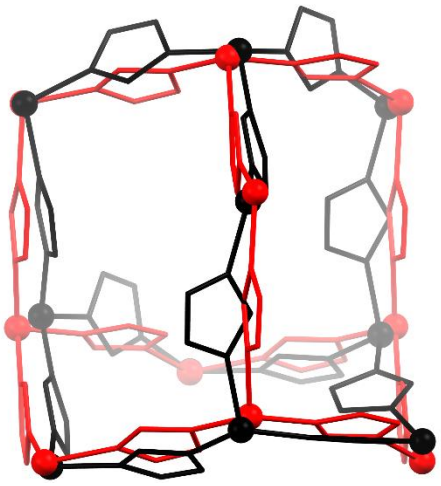

Figure 4. Overlay of the lowest energy predicted (red) and experimental (black) structures of Zn(**ttz**)$_2$. Topological equivalence of both structures is evident, the only difference being the rotational orientation of the **ttz** linkers.

We were pleased to find that the lowest energy predicted structure of Zn(**ttz**)$_2$ adopts an $I4_1cd$ space group with *int-dia* topology, matching that of the topology of the experimentally determined structure. The second lowest structure with *Fddd* symmetry, just 3.5 $kJ\ mol^{-1}$ higher than the global energy minimum, shares the same topology as well. The overlay of the predicted lowest energy structure and observed structures shows extensive similarity, both in unit cell parameters and atomic arrangement. Nonetheless, the structures are not entirely identical, the primary difference being the orientation of **ttz**$^-$ linkers with respect to the Zn$\cdots$Zn axis (Figure 4). The experimental Zn(**ttz**)$_2$ crystal structure adopts a *Pbca* space group with eight formula units (Z=8) per crystallographic unit cell (CSD code WAQRAI[40]). The herein predicted lowest energy structure exhibits the $I4_1cd$ space group. The predicted structure also has eight formula units per crystallographic body-centred unit cell, so four in its primitive unit cell. The crystallographic asymmetric unit of the experimental structure contains two symmetry-independent **ttz**$^-$ linkers, while the predicted structure has only one. Clearly, the lower symmetry found in the experimental structure allows for greater conformational flexibility and, indeed, the unique linker orientation within the predicted structure may be regarded as the average of two orientations found in the experimental structure. While a theoretical structure perfectly matching the experimental one might be accessible by increasing the search space to Z=8, this would come at a considerably higher computational cost. As such, the *ab initio* search limited to Z=4 search has provided us with a clear match with the experiment, both in terms of topology and crystal packing, which we regard as a successful prediction.

The predicted energy landscape of Zn(**trz**)$_2$ was noticeably similar to that of Zn(**ttz**)$_2$. Both **ttz** and **trz** linkers evidently favour formation of dense structures, which is in stark contrast with the imidazolate linkers renowned for the formation of highly-porous framework structures.[43] The lowest energy structure of Zn(**trz**)$_2$ was found to exhibit the *int-dia* topology. Similar to the Zn(**ttz**)$_2$ landscape, a pair of *int-dia* structures of similar energies with *Fddd* and $I4_1cd$ symmetries were predicted, this time the *Fddd* structure being the global energy minimum. An overlay of the two structures (Figure 5) revealed the difference in the

mutual orientation of the neighbouring **trz** linkers with regards to C/N atoms at the 2- and 3-positions of the azolate ring. Based on our prediction, we would expect Zn(**trz**)$_2$ to form an *int-dia* framework structure, similar to that of Zn(**ttz**)$_2$. Such a structure is, in fact, found in CSD under the entry LIHQUP.[41] Our predicted *int-dia* structure is, once again, a good match to the experimental structure found in CSD, signifying yet another successful prediction performed with WAM method.

The CSD also reports a polymorph of Zn(**trz**)$_2$ with *tsa*-topology (CSD JINRIK),[41] crystallising in *Pnma* symmetry and eight formula units per primitive unit cell. We briefly ran a heavily symmetry restricted search which found a four formula unit counterpart to JINRIK for Zn(**trz**)$_2$ and Zn(**ttz**)$_2$. Both crystallised into C2/m symmetry (see SI) lying 13 *kJ mol^{-1}* and 19 *kJ mol^{-1}* respectively above the predicted *int-dia* topology. This indicates, in the AIRSS spirit, that if searches give incomplete coverage, experimentally-led and more targeted searches are highly fruitful.

Looking at the reported experimental *int-dia* structure of Zn(**trz**)$_2$, we noticed that both **trz** linkers are protonated, seemingly violating the charge balance. In order to resolve this ambiguity in the reported *int-dia* structure, we decided to synthesise the material and redetermine its crystal structure. In doing so, we have performed a polymorph screening of Zn(**trz**)$_2$ using solid-state mechanochemical methods which, based on powder X-ray diffraction (PXRD) analysis, persistently led to the formation of the *int-dia* structure, in agreement with its expected stability. The structure of *int-dia* polymorph was re-determined from powder X-ray diffraction (PXRD) data, and the composition was also confirmed *via* thermogravimetric analysis (TGA), correcting the reported structure by ruling out any protonation of the **trz** linkers.

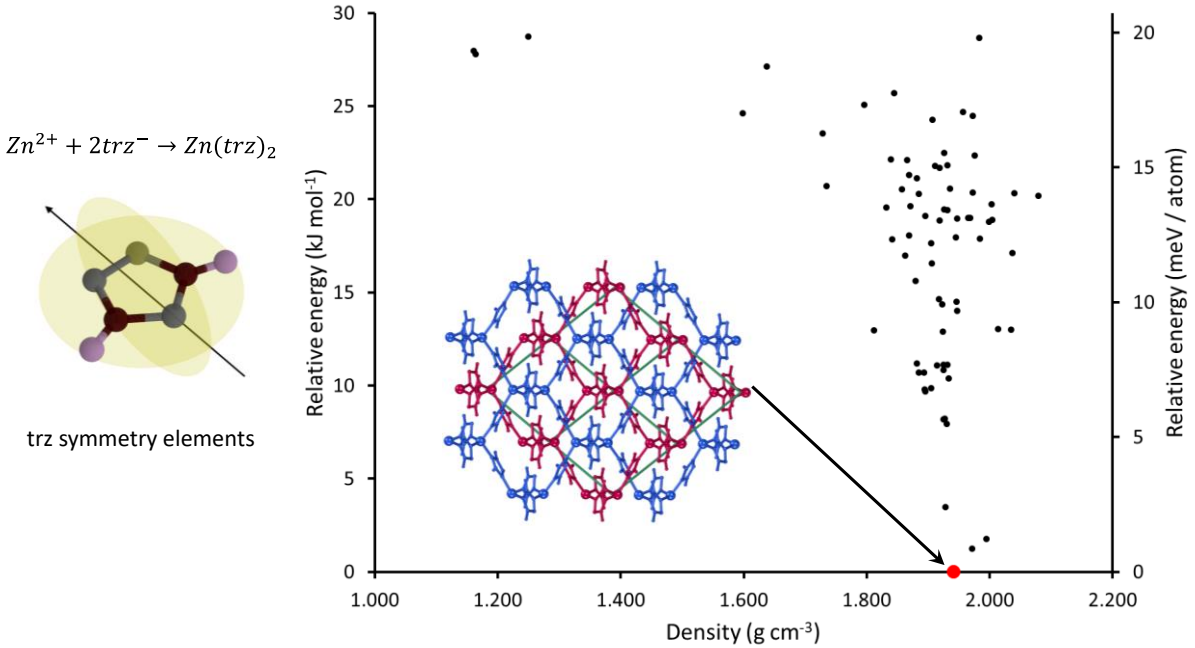

Figure 5. Ligand structure and calculated crystal energy landscape of Zn(**trz**)$_2$. Each black dot represents a crystal structure. The lowest energy predicted structure, matching the experimental structure, is shown in red. The crystal packing diagram of the lowest energy predicted structure is provided on the inset, with the two interpenetrated diamondoid nets shown in red and blue.

Overall, the WAM method has been successful in predicting the *int-dia* topologies as the most stable forms of both Zn(**ttz**)$_2$ and Zn(**trz**)$_2$ frameworks. Furthermore, our predictions have pointed at a possible error in the assignment of proton positions in the reported structure of Zn(**trz**)$_2$ and led us to redetermine the structure experimentally, thus resolving the ambiguity.

Prediction of the MOF-74 structure

The final case study framework for WAM is the MOF-74 (also known as CPO-27) structure, based on rod-like SBUs that can involve a wide range of metal centres, including Mn^{2+}, Fe^{2+}, Co^{2+}, Ni^{2+}, Cu^{2+}, Zn^{2+}, Cd^{2+}, Mg^{2+}, Ca^{2+} and Ba^{2+}, crosslinked via 2,4-dihydroxyterephthalate (**DHTA^{4-}**) linkers into a one-dimensional (1D) channel structure of a honeycomb cross-section. Unlike other herein explored systems, the MOF-74 framework exhibits a 2:1 ratio of metal ions and linkers. The metal centres in MOF-74 have an entirely oxygen-based square pyramidal coordination geometry, leaving an open coordination site which may interact with guest molecules and engage in catalytic activity.

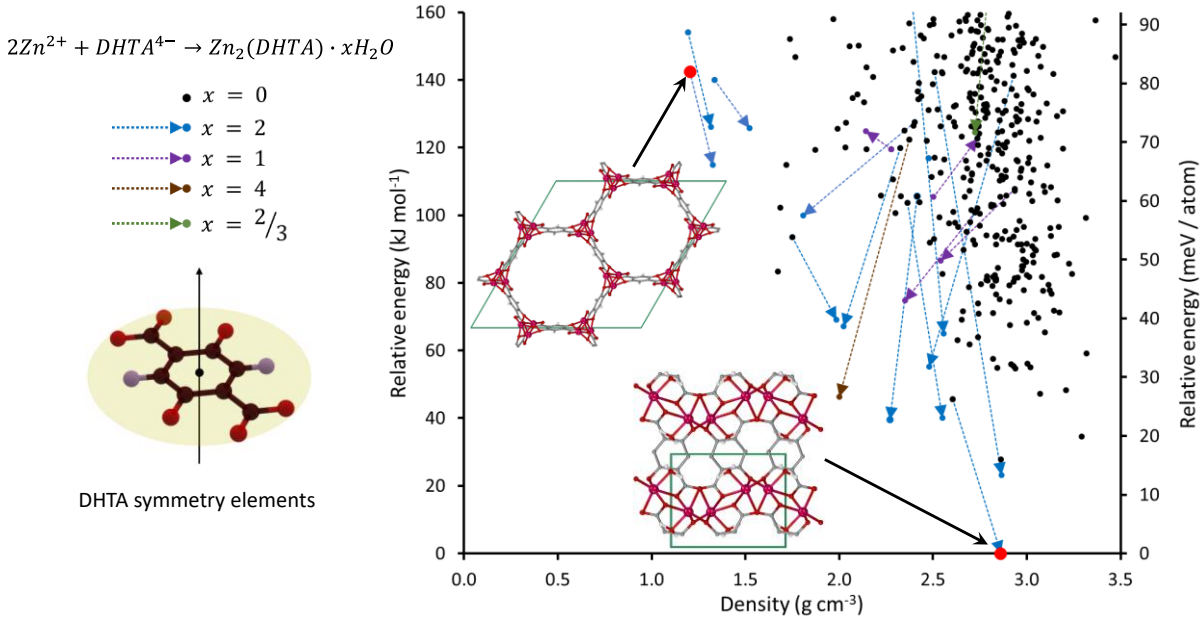

Figure 6. Ligand structure and calculated crystal energy landscape for zinc-based MOF-74 (black dots). The red circles mark the experimentally known porous structure of MOF-74 and the lowest energy structure stabilised by water inclusion. The latter structure is isomorphous with the CSD structure IQISEH. The blue arrows represent the contribution to the hydration enthalpy from structural H_2O bound to open metal sites, showing, on a MOF-by-MOF basis, how structural water enhances the stability and changes the density. (Care should be taken when comparing relative energies of structures with different stoichiometries).

We have focused our WAM effort on the zinc-based (Zn-MOF-74) structure. Analysis of the calculated energy landscape verified that the experimentally observed open MOF-74 structure had indeed been found by WAM, signifying that the algorithm is capable of locating highly complex MOF structures with unusual metal coordination geometries. Unlike the previous examples, where the experimental crystal structures matched the lowest energy predicted structures, in this case a number of structures with an energy lower than the energy of the experimental honeycomb structure was found. However, all predicted structures purported to be more stable than the experimentally observed MOF-74 one, have a higher framework density, and anticipated lower solvent-accessible void volume. Due to the large void volume present in MOF-74 (134 $Å^3$ per Zn atom for the DFT-optimised structure), the experimentally

observed structure of honeycomb cross-section is expected to be extensively stabilised by solvent inclusion in MOF channels. Indeed, the effect of solvent stabilisation has been recognised in the CSP studies of porous molecular materials, where the energies of the predicted porous polymorphs appeared artificially enhanced relative to their non-porous counterparts.[44]

Currently, there is a lack of reliable computationally tractable techniques to assess the thermodynamic effect of solvent inclusion on MOF stability, most notably due to disordered nature and poor structural understanding of the distribution and dynamic of solvent molecules in MOF pores. Consequently, we will not attempt to quantify the energetic effects of dynamic solvent inclusion in this exploratory study of *ab initio* MOF structure prediction. We will, however, investigate the possibility of solvent molecules coordinating to open metal sites.

Analysis of the calculated energy landscape revealed the presence of 19 structures with open metal coordination sites, which can form covalent interactions with solvent molecules. We have investigated the effect by attaching water molecules and calculating the thermodynamic stabilisation resulting from this structural modification (see SI for details). It was found that water coordination stabilises MOF structures (Figure 6). In particular, the experimental MOF-74 structure is stabilised by 27 kJ mol^{-1}, outperforming other structures of similar energy and density. Evidently, solvent coordination to an open metal site facilitates the formation of experimentally-observed MOF-74 structure in preference to other potential candidate structures.

Another interesting effect of solvent inclusion can be found by exploring the low energy part of the structure landscape. Coordination of water to the lowest energy structure containing solvent-accessible voids results in a structure more stable than all the predicted structures, *i.e.* new global minimum. What is more, the new hydrated structure is remarkably similar to the experimentally reported structure $Mn_2(H_2O)_2$**DHTA** (CSD IQISEH[45]), which is essentially a non-porous polymorph of Mn-MOF-74. Our calculations, therefore, suggest that a similar dense polymorph may exist for Zn-MOF-74, something that remains to be investigated experimentally.

Conclusions

We have demonstrated the application of the recently developed WAM algorithm in a first ever report of *ab initio* structure prediction of MOFs. While the field of porous molecular crystals has been enjoying the benefits of CSP calculations for nearly 10 years, the computational design of MOFs has been relying on the limited subset of topological space that had previously been discovered. With the introduction of WAM method we are now able to generate putative MOF structures starting from a 2D molecular diagram of the constituent nodes and linkers, without any inherent restriction on topological connectivity.

We have deliberately chosen our examples from a diverse range of MOFs of varying structural complexity, in order to demonstrate the complete generality of the WAM algorithm towards *ab initio* structure prediction of MOFs. Specifically, this included MOFs based on more than one type of linker (SIFSIX-3-Zn), MOFs with particularly rich topology landscape (Zn(**trz**)$_2$ and Zn(**ttz**)$_2$) and MOFs based on rod-like SBUs and containing open or hydrated metal centers (zinc-based MOF-74/CPO-27). The versatility of the WAM approach to crystallographic symmetry was best manifested in the prediction of the SIFSIX-3-Zn structure, where the experimental structure had been generated in multiple space groups,

reflecting the varying degrees of structural disorder. Our calculations have reproduced all experimentally occurring structures and helped resolve ambiguity over the reported structure of Zn(**trz)**$_2$. The efficiency of WAM approach with regard to symmetry has been demonstrated for the prediction of *int-dia* polymorphs of Zn(**ttz**)$_2$ and Zn(**trz**)$_2$, where the predicted structures have topology and crystallographic parameters that agree with experimental *int-dia* polymorphs. Additional, symmetry-restricted searches, also produced the structures with *tsa*-topology, closely related to the second known polymorph of Zn(**trz**)$_2$ (CSD JINRIK).

Finally, we have predicted the important MOF-74 structure, demonstrating the ability of WAM method to generate highly porous structures with rod-like SBUs and non-standard metal coordination geometries. While a number of structures potentially more stable than the experimental honeycomb-cross section structure had been predicted, all of these possessed inferior solvent-accessible void volumes, implying lower ability to be stabilised under solution-based synthesis. We have also established that the stability of experimental MOF-74 structure is, in part, attributable directly to the interaction of solvent molecules with open metal coordination sites. In addition, we envisage a possibility of synthesizing a dense polymorph of Zn-MOF-74, analogous to an already reported structure of $Mn_2(H_2O)_2$**DHTA.**

Beyond pure *ab initio* predictions, we anticipate WAM being useful when partial experimental data is known *e.g.* number of formula units per cell and space group but not structure. In this situation, running a structure search restricted to the experimental space group and number of formula units would be desirable. As objects cannot move onto higher symmetry sites within a given space group during structural optimization, it is of paramount importance to generate trial structures with molecules on special sites, else these possibilities will be excluded.

We expect that WAM method will open a new chapter in MOF design by enabling a rapid and reliable approach to structure prediction similar to the successes in the past 20 years by CSP for denser crystal and cluster structures. The advantage of our AIRSS-based approach is that is also uncovers metastable structures of varying densities. Hence our method will be used to guide the synthesis of new MOFs, reducing the cost and manual effort of experimental screening. In addition, WAM can be used to assist in crystal structure determination of polycrystalline MOFs, for which single crystals suitable for X-ray diffraction measurement cannot be grown, in a similar manner that CSP was used for elucidating structures of organic molecular crystals.[46] Finally, coupled with already available computational techniques for predicting mechanical properties,[47] gas sorption efficiency[6] and catalytic activity of MOF structures,[24] this method should lead a path towards a true, full *in silico* design of these exciting materials.

Methods

Crystal structures were generated with WAM+AIRSS method, using metal atoms and ligand molecular fragments as structure building blocks. The generated structures were geometry-optimised using plane-wave DFT code CASTEP 19.1.[36] Initial calculations were performed using LDA functional (Zn(**pyr**)$_2$**SiF$_6$**, Zn(**trz**)$_2$ and Zn(**ttz**)$_2$) or PBE[48] functional combined with Grimme D2[49] dispersion correction (Zn_2**DHTA**). The plane-wave cut-off was set to 400 eV and the ultrasoft pseudopotentials from CASTEP internal QC5 library were used. The Brillouin zone was sampled with a 0.07 Å^{-1} Monkhorst-Pack k-point grid. The following

convergence criteria were applied for geometry optimization: maximum energy change $2x10^{-5}$ eV/atom, maximum force on atom 0.05 eV/Å, maximum atom displacement 0.001 Å and residual stress 0.1 GPa.

The optimised structures were ranked by energy. The set of structures falling within a certain energy window above the global minimum (50 kJ mol^{-1} per formula unit for Zn(**pyr**)$_2$**SiF$_6$**, Zn(**trz**)$_2$ and Zn(**ttz**)$_2$; 200 kJ mol^{-1} for Zn$_2$**DHTA**) were selected for further analysis. First duplicate structures were removed (see SI section 1.4 for details), then the remaining structures were once again geometry-optimised using a more reliable energy model and more stringent convergence criteria. This time we used PBE functional combined with many body dispersion (MBD*) correction scheme. Convergence testing with respect to plane wave cutoff and Brillouin zone sampling was performed separately for each MOF system (see SI), and the converged parameters were used for refining the energy landscapes. The resulting set of low energy structures was again checked for duplicates.

Finally, the solvent-accessible void volumes and packing coefficients were calculated for all predicted structures using the software PLATON.[50] Topologies of the structures were determined using the program ToposPro.[51]

References

1. Eddaoudi, M. *et al.* Modular Chemistry: Secondary Building Units as a Basis for the Design of Highly Porous and Robust Metal−Organic Carboxylate Frameworks. *Acc. Chem. Res.* **34**, 319–330 (2001).

2. Kitagawa, S., Kitaura, R. & Noro, S. Functional Porous Coordination Polymers. *Angew. Chem. Int. Ed.* **43**, 2334–2375 (2004).

3. Sung Cho, H. *et al.* Extra adsorption and adsorbate superlattice formation in metal-organic frameworks. *Nature* **527**, 503–507 (2015).

4. Bourrelly, S. *et al.* Different Adsorption Behaviors of Methane and Carbon Dioxide in the Isotypic Nanoporous Metal Terephthalates MIL-53 and MIL-47. *J. Am. Chem. Soc.* **127**, 13519–13521 (2005).

5. Bloch, E. D. *et al.* Hydrocarbon Separations in a Metal-Organic Framework with Open Iron(II) Coordination Sites. *Science* **335**, 1606–1610 (2012).

6. Nandi, S. *et al.* A single-ligand ultra-microporous MOF for precombustion CO_2 capture and hydrogen purification. *Sci. Adv.* **1**, e1500421 (2015).

7. Lee, C. Y. *et al.* Light-Harvesting Metal–Organic Frameworks (MOFs): Efficient Strut-to-Strut Energy Transfer in Bodipy and Porphyrin-Based MOFs. *J. Am. Chem. Soc.* **133**, 15858–15861 (2011).

8. Fateeva, A. *et al.* A Water-Stable Porphyrin-Based Metal-Organic Framework Active for Visible-Light Photocatalysis. *Angew. Chem. Int. Ed.* **51**, 7440–7444 (2012).

9. Montoro, C. *et al.* Capture of Nerve Agents and Mustard Gas Analogues by Hydrophobic Robust MOF-5 Type Metal–Organic Frameworks. *J. Am. Chem. Soc.* **133**, 11888–11891 (2011).

10. Deng, H. *et al.* Large-Pore Apertures in a Series of Metal-Organic Frameworks. *Science* **336**, 1018–1023 (2012).

11. Eddaoudi, M. *et al.* Systematic design of pore size and functionality in isoreticular MOFs and their application in methane storage. *Science* **295**, 469–72 (2002).

12. Cavka, J. H. *et al.* A New Zirconium Inorganic Building Brick Forming Metal Organic Frameworks with Exceptional Stability. *J. Am. Chem. Soc.* **130**, 13850–13851 (2008).

13. Nazarian, D., Camp, J. S., Chung, Y. G., Snurr, R. Q. & Sholl, D. S. Large-Scale Refinement of Metal-Organic Framework Structures Using Density Functional Theory. *Chem. Mater.* **29**, 2521–2528 (2017).

14. Baburin, I. A. & Leoni, S. The energy landscapes of zeolitic imidazolate frameworks (ZIFs): towards quantifying the presence of substituents on the imidazole ring. *J. Mater. Chem.* **22**, 10152–10154 (2012).

15. Zhu, L., Liu, H., Pickard, C. J., Zou, G. & Ma, Y. Reactions of xenon with iron and nickel are predicted in the Earth's inner core. *Nat. Chem.* **6**, 644–648 (2014).

16. Zhu, Q., Oganov, A. R. & Lyakhov, A. O. Novel stable compounds in the Mg–O system under high pressure. *Phys. Chem. Chem. Phys.* **15**, 7696–7700 (2013).

17. Zhao, Z. *et al.* Three Dimensional Carbon-Nanotube Polymers. *ACS Nano* **5**, 7226–7234 (2011).

18. Li, Q. *et al.* Superhard Monoclinic Polymorph of Carbon. *Phys. Rev. Lett.* **102**, 175506 (2009).

19. Jones, J. T. A. *et al.* Modular and predictable assembly of porous organic molecular crystals. *Nature* **474**, 367–71 (2011).

20. Errea, I. *et al.* High-Pressure Hydrogen Sulfide from First Principles: A Strongly Anharmonic Phonon-Mediated Superconductor. *Phys. Rev. Lett.* **114**, 157004 (2015).

21. Mayo, M., Griffith, K. J., Pickard, C. J. & Morris, A. J. Ab Initio Study of Phosphorus Anodes for Lithium- and Sodium-Ion Batteries. *Chem. Mater.* **28**, 2011–2021 (2016).

22. Collins, S. P., Daff, T. D., Piotrkowski, S. S. & Woo, T. K. Materials design by evolutionary optimization of functional groups in metal-organic frameworks. *Sci. Adv.* **2**, e1600954 (2016).

23. Hughes, J. T., Bennett, T. D., Cheetham, A. K. & Navrotsky, A. Thermochemistry of Zeolitic Imidazolate Frameworks of Varying Porosity. *J. Am. Chem. Soc.* **135**, 598–601 (2013).

24. Rosen, A. S., Notestein, J. M. & Snurr, R. Q. Identifying promising metal–organic frameworks for heterogeneous catalysis via high-throughput periodic density functional theory. *J. Comput. Chem.* **40**, 1305–1318 (2019).

25. Lewis, D. W. *et al.* Zeolitic imidazole frameworks: structural and energetics trends compared with their zeolite analogues. *CrystEngComm* **11**, 2272 (2009).

26. Marleny Rodriguez-Albelo, L. *et al.* Zeolitic Polyoxometalate-Based Metal−Organic Frameworks (Z-POMOFs): Computational Evaluation of Hypothetical Polymorphs and the Successful Targeted Synthesis of the Redox-Active Z-POMOF1. *J. Am. Chem. Soc.* **131**, 16078–16087 (2009).

27. Arhangelskis, M., Katsenis, A. D., Morris, A. J. & Friščić, T. Computational evaluation of metal pentazolate frameworks: inorganic analogues of azolate metal–organic frameworks. *Chem. Sci.* **9**, 3367–3375 (2018).

28. Arhangelskis, M. *et al.* Theoretical Prediction and Experimental Evaluation of Topological Landscape and Thermodynamic Stability of a Fluorinated Zeolitic Imidazolate Framework. *Chem. Mater.* **31**, 3777–3783 (2019).

29. Pickard, C. J. & Needs, R. J. Ab initio random structure searching. *J. Phys. Condens. Matter* **23**, 053201 (2011).

30. Groom, C. R., Bruno, I. J., Lightfoot, M. P. & Ward, S. C. The Cambridge Structural Database. *Acta Crystallogr.* **B72**, 171–179 (2016).

31. Zhang, J.-P., Zhang, Y.-B., Lin, J.-B. & Chen, X.-M. Metal Azolate Frameworks: From Crystal Engineering to Functional Materials. *Chem. Rev.* **112**, 1001–1033 (2012).

32. Dietzel, P. D. C., Panella, B., Hirscher, M., Blom, R. & Fjellvåg, H. Hydrogen adsorption in a nickel based coordination polymer with open metal sites in the cylindrical cavities of the desolvated framework. *Chem. Commun.* **1**, 959–961 (2006).

33. Valvekens, P., Vandichel, M., Waroquier, M., Van Speybroeck, V. & De Vos, D. Metal-dioxidoterephthalate MOFs of the MOF-74 type: Microporous basic catalysts with well-defined active sites. *J. Catal.* **317**, 1–10 (2014).

34. Nugent, P. *et al.* Porous materials with optimal adsorption thermodynamics and kinetics for CO_2 separation. *Nature* **495**, 80–84 (2013).

35. Ziaee, A. *et al.* Theoretical Optimization of Pore Size and Chemistry in SIFSIX-3-M Hybrid Ultramicroporous Materials. *Cryst. Growth Des.* **16**, 3890–3897 (2016).

36. Clark, S. J. *et al.* First principles methods using CASTEP. *Zeitschrift für Krist. - Cryst. Mater.* **220**, 567–570 (2005).

37. Uemura, K., Maeda, A., Maji, T. K., Kanoo, P. & Kita, H. Syntheses, Crystal Structures and Adsorption Properties of Ultramicroporous Coordination Polymers Constructed from Hexafluorosilicate Ions and Pyrazine. *Eur. J. Inorg. Chem.* **2009**, 2329–2337 (2009).

38. Forrest, K. A. *et al.* Computational studies of CO_2 sorption and separation in an ultramicroporous metal-organic material. *J. Phys. Chem. C* **117**, 17687–17698 (2013).

39. Park, K. S. *et al.* Exceptional chemical and thermal stability of zeolitic imidazolate frameworks. *Proc. Natl. Acad. Sci.* **103**, 10186–10191 (2006).

40. Wang, X. *et al.* Syntheses, Crystal Structures, and Luminescent Properties of Three Novel Zinc Coordination Polymers with Tetrazolyl Ligands. *Inorg. Chem.* **44**, 5278–5285 (2005).

41. Ouellette, W., Hudson, B. S. & Zubieta, J. Hydrothermal and Structural Chemistry of the Zinc(II)- and Cadmium(II)-1,2,4-Triazolate Systems. *Inorg. Chem.* **46**, 4887–4904 (2007).

42. Yang, X. *et al.* Surfactant-assisted synthesis and electrochemical properties of an unprecedented polyoxometalate-based metal–organic nanocaged framework. *Chem.*

Commun. **55**, 1201–1204 (2019).

43. Huang, X. C., Lin, Y. Y., Zhang, J. P. & Chen, X. M. Ligand-directed strategy for zeolite-type metal-organic frameworks: Zinc(II) imidazolates with unusual zeolitic topologies. *Angew. Chem. Int. Ed.* **45**, 1557–1559 (2006).

44. McMahon, D. P. *et al.* Computational modelling of solvent effects in a prolific solvatomorphic porous organic cage. *Faraday Discuss.* **211**, 383–399 (2018).

45. Gao, Q. *et al.* Crystal structures, topological analyses, and magnetic properties of manganese-dihydroxyterephthalate complexes. *Aust. J. Chem.* **63**, 286–292 (2010).

46. Eddleston, M. D., Hejczyk, K. E., Bithell, E. G., Day, G. M. & Jones, W. Polymorph Identification and Crystal Structure Determination by a Combined Crystal Structure Prediction and Transmission Electron Microscopy Approach. *Chem. Eur. J.* **19**, 7874–7882 (2013).

47. Yang, K., Zhou, G. & Xu, Q. The elasticity of MOFs under mechanical pressure. *RSC Adv.* **6**, 37506–37514 (2016).

48. Perdew, J. P., Burke, K. & Ernzerhof, M. Generalized Gradient Approximation Made Simple. *Phys. Rev. Lett.* **77**, 3865–3868 (1996).

49. Grimme, S. Semiempirical GGA-type density functional constructed with a long-range dispersion correction. *J. Comput. Chem.* **27**, 1787–1799 (2006).

50. Spek, A. L. Structure validation in chemical crystallography. *Acta Crystallogr.* **D65**, 148–155 (2009).

51. Blatov, V. A., Shevchenko, A. P. & Proserpio, D. M. Applied Topological Analysis of Crystal Structures with the Program Package ToposPro. *Cryst. Growth Des.* **14**, 3576–3586 (2014).

Acknowledgements

A.J.M. and J.P.D. would like to acknowledge helpful and insightful discussions with Matthew Cliffe. J.P.D. acknowledges SIMS scholarship and EPSRC for PhD funding. A.J.M. thanks the University of Birmingham for research funding through the Birmingham Fellowship scheme. T.F. acknowledges the support from NSERC Discovery Grant (RGPIN-2017-06467), NSERC E. W. R. Steacie Fellowship (SMFSU 507347-17), NSERC Strategic Grant (STPGP 521582-18)

This work was performed using resources provided by the Cambridge Service for Data Driven Discovery (CSD3) operated by the University of Cambridge Research Computing Service (www.csd3.cam.ac.uk), provided by Dell EMC and Intel using Tier-2 funding from the Engineering and Physical Sciences Research Council (capital grant EP/P020259/1), and DiRAC funding from the Science and Technology Facilities Council (www.dirac.ac.uk). The authors also acknowledge support from the UK national high-performance computing service, ARCHER, for which access was obtained via the UKCP consortium and funded by EPSRC grant ref EP/P022561/1, and the use of the supercomputer Mp2 from the University of Sherbrooke, managed by Calcul Québec and Compute Canada. The operation of this supercomputer is funded by the Canada Foundation for Innovation (CFI), the Ministère de

l'Économie, de la Science et de l'Innovation du Québec (MESI), and the Fonds de Recherche du Québec, Nature et Technologies (FRQ-NT).

Author contributions

J.P.D. wrote the WAM code. M.A. and J.P.D. performed the CSP calculations. A.D.K. performed the topology analysis of all predicted structures. J.M.M. performed experimental synthesis and characterisation of the polymoprhs of Zn(**ttz**)$_2$. M.A. solved the crystal structure of *int-dia* polymorph of Zn(**ttz**)$_2$ from powder X-ray diffraction data. Initial manuscript draft was written by M.A., with revisions made by all co-authors.